VILNIUS GEDIMINAS TECHNICAL UNIVERSITY

Arvydas RIMKUS

EFFECTS OF BAR REINFORCEMENT ARRANGEMENT ON DEFORMATIONS AND CRACKING OF CONCRETE ELEMENTS

DOCTORAL DISSERTATION

TECHNOLOGICAL SCIENCES,
CIVIL ENGINEERING (02T)

VGTU
LEIDYKLA
TECHNIKA
Vilnius 2017

Doctoral dissertation was prepared at Vilnius Gediminas Technical University in 2013–2017.

Supervisor

Dr Viktor GRIBNIAK (Vilnius Gediminas Technical University, Civil Engineering – 02T).

The Dissertation Defense Council of Scientific Field of Civil Engineering of Vilnius Gediminas Technical University:

Chairman

Prof. Dr Juozas VALIVONIS (Vilnius Gediminas Technical University, Civil Engineering – 02T).

Members:

Assoc. Prof. Dr Vladimir POPOV (Vilnius Gediminas Technical University, Civil Engineering – 02T),

Assoc. Prof. Dr Gintautas SKRIPKIŪNAS (Vilnius Gediminas Technical University, Civil Engineering – 02T),

Prof. Dr Habil. Sigitas TAMULEVIČIUS (Kaunas University of Technology, Materials Engineering – 08T),

Dr Carlos ZANUY SANCHEZ (Technical University of Madrid, Spain, Civil Engineering – 02T).

The dissertation will be defended at the public meeting of the Dissertation Defense Council of Civil Engineering in the Senate Hall of Vilnius Gediminas Technical University at **2 p. m. on 18 December 2017**.

Address: Saulėtekio al. 11, LT-10223 Vilnius, Lithuania.
Tel.: +370 5 274 4956; fax +370 5 270 0112; e-mail: doktor@vgtu.lt

A notification on the intend defending of the dissertation was send on 17 November 2017.

A copy of the doctoral dissertation is available for review at VGTU repository http://dspace.vgtu.lt and at the Library of Vilnius Gediminas Technical University (Saulėtekio al. 14, LT-10223 Vilnius, Lithuania).

VGTU leidyklos TECHNIKA 2017-050-M mokslo literatūros knyga

ISBN 978-609-476-077-8

arvydas.rimkus@vgtu.lt

VILNIAUS GEDIMINO TECHNIKOS UNIVERSITETAS

Arvydas RIMKUS

STRYPINĖS ARMATŪROS IŠDĖSTYMO ĮTAKA BETONINIŲ ELEMENTŲ DEFORMACIJOMS IR PLEIŠĖJIMUI

DAKTARO DISERTACIJA

TECHNOLOGIJOS MOKSLAI,
STATYBOS INŽINERIJA (02T)

VGTU
LEIDYKLA
TECHNIKA
Vilnius 2017

Disertacija rengta 2013–2017 metais Vilniaus Gedimino technikos universitete.

Vadovas

dr. Viktor GRIBNIAK (Vilniaus Gedimino technikos universitetas, statybos inžinerija – 02T).

Vilniaus Gedimino technikos universiteto Statybos inžinerijos mokslo krypties disertacijos gynimo taryba:

Pirmininkas

prof. dr. Juozas VALIVONIS (Vilniaus Gedimino technikos universitetas, statybos inžinerija – 02T).

Nariai:

doc. dr. Vladimir POPOV (Vilniaus Gedimino technikos universitetas, statybos inžinerija – 02T),
doc. dr. Gintautas SKRIPKIŪNAS (Vilniaus Gedimino technikos universitetas, statybos inžinerija – 02T),
prof. habil. dr. Sigitas TAMULEVIČIUS (Kauno technologijos universitetas, medžiagų inžinerija – 08T),
dr. Carlos ZANUY SANCHEZ (Madrido technikos universitetas, Ispanija, statybos inžinerija – 02T).

Disertacija bus ginama viešame Statybos inžinerijos mokslo krypties disertacijos gynimo tarybos posėdyje **2017 m. gruodžio 18 d. 14 val.** Vilniaus Gedimino technikos universiteto senato posėdžių salėje.

Adresas: Saulėtekio al. 11, LT-10223 Vilnius, Lietuva.
Tel.: (8 5) 274 4956; faksas (8 5) 270 0112; el. paštas doktor@vgtu.lt

Pranešimai apie numatomą ginti disertaciją išsiųsti 2017 m. lapkričio 17 d.

Disertaciją galima peržiūrėti VGTU talpykloje http://dspace.vgtu.lt ir Vilniaus Gedimino technikos universiteto bibliotekoje (Saulėtekio al. 14, LT-10223 Vilnius, Lietuva).

Abstract

The aim of this work is to investigate the arrangement effect of bar reinforcement to deformations and cracking behaviour of concrete elements subjected to short-term loading. The study experimentally verifies the effective concrete area concept and analyses peculiarities of cracking process of reinforced concrete (RC) members with the emphasis on arrangement of the bar reinforcement. The test results of 9 beams and 119 ties with different reinforcement and loading layouts are reported.

Results of the beam tests do not reveal a clear correlation between the crack widths and the crack spacing when the reinforcement layout changes, while the number of the reinforcement layers correlates with the flexural stiffness.

An iterative procedure has been proposed for localizing the end effect in the ties. This procedure allows identifying the representative geometry for assessing the cracking parameters of RC ties. It was observed that scatter of the experimental outputs increases with the concrete cover.

Specific equipment has been developed for tests of the ties with multiple reinforcement bar. The test results (maximum and average crack spacings) are practically independent of the reinforcement parameters, while the Eurocode 2 and the Model Code 2010 predictions of the maximum crack spacing are dependent on the ratio of the bar diameter to the reinforcement ratio. These results enable formulating a hypothesis that the crack parameters (spacing and width) are mainly dependent on the geometry of the concrete prism and, particularly, the cover depth.

Deformation behaviour of the ties with multiple reinforcement bars was also modelled with nonlinear finite element software ATENA. The results of numerical simulations and physical tests indicate that the strain gradient in the concrete varies not only along the bar, but also within the cover. The outputs support a conclusion that the "effective area" concept has a limited application related with the loading conditions, stress-strain state, cover, and configuration of the unreinforced area.

The thesis is composed of three chapters: literature survey, experimental programs, and discussion of the results. The literature survey is focused on the effects responsible for deformation and cracking performance of reinforced concrete members. The experimental study deals with deformations and cracking of flexural and tensile elements with different arrangement of the reinforcement in the tension zone. The last chapter discusses predominant characteristics of serviceability performance of flexural and tensile reinforced concrete members. The author have published 14 articles on the topic of the dissertation (five of them in the journals with an Impact Factor and three in the conference proceedings reffered by the *Clarivate Analytics Web of Science*).

Reziumė

Disertacijoje nagrinėjama strypinės armatūros išdėstymo įtaka betoninių elementų deformacijoms ir pleišėjimui veikiant trumpalaikei apkrovai. Eksperimentiškai tikrinama efektyviojo tempiamojo betono koncepcija bei, atsižvelgiant į armatūros strypų išdėstymą skerspjūvyje, analizuojami elementų pleišėjimo ypatumai. Pateikta 9 lenkiamųjų bei 119 tempiamųjų armuoto betono elementų deformacijų ir pleišėjimo eksperimentinių rezultatų analizė.

Eksperimentiniai sijų pleišėjimo bei deformacijų rezultatai leidžia teigti, kad armatūros strypų išdėstymas skerspjūvyje, neturi reikšmingos įtakos pagrindiniams pleišėjimo parametrams, t. y. plyšio pločiui ir atstumui tarp plyšių, tačiau armatūros strypų sluoksnių skaičius lemia lenkiamąjį sijų standumą.

Disertacijoje pasiūlyta metodika skirta pakraščio efekto (angl. *end effect*) nustatymui tempiamosiuose elementuose. Eksperimentinio priartėjimo metodika paremta elemento paviršiaus deformacijų matavimo bazės kitimu. Taikant pasiūlytą metodiką nustatyta, kad apsauginio betono sluoksnio storis tiesiogiai proporcingas eksperimentinių armuoto betono elementų rezultatų išsibarstymui.

Siekiant įvertinti armatūros strypų išdėstymo įtaką tempiamųjų elementų deformacijoms bei pleišėjimui, sukurta ir užpatentuota bandymo įranga leidžianti atlikti keletu strypų armuotų elementų tempimo bandymus. Bandymų rezultatai parodė, kad vidutinių ir maksimalių atstumų tarp plyšių dydis nepriklauso nuo armavimo parametrų (armatūros ploto bei strypų išdėstymo), nors norminiuose projektavimo dokumentuose yra aiškiai išreikšta maksimalių atstumų tarp plyšių priklausomybė nuo strypų skersmens ir armavimo koeficiento santykio.

Eksperimentiniai ir skaitinio modeliavimo rezultatai rodo, kad tempiamuose elementuose deformacijos kinta ne tik išilgine elemento kryptimi, bet ir pačiame betono apsauginiame sluoksnyje. Rezultatai patvirtina, kad efektyviojo tempiamojo betono koncepcijos taikomos projektavimo dokumentuose adekvatumas gali būti laikomas priimtinu tik išskirtinais atvejais atsižvelgiant į elementų apkrovimo sąlygas, įtempių ir deformacijų būvį bei nearmuoto betono konfigūraciją.

Disertaciją sudaro trys skyriai – literatūros apžvalga, eksperimentinė dalis bei rezultatų aptarimas. Literatūros apžvalgoje aprašomi veiksniai lemiantys armuotų betoninių elementų deformacijas bei pleišėjimą. Eksperimentinėje darbo dalyje pateikiami lenkiamųjų bei tempiamųjų armuoto betono elementų su skirtingai skerspjūviuose išdėstytais armatūros strypais bandymų rezultatai bei trumpa jų analizė. Paskutiniame skyriuje aptariamos parametrai, lemiantys lenkiamųjų bei tempiamųjų armuoto betono elementų eksploatacines savybes. Disertacijos tema autorius paskelbė 14 publikacijų (5 iš jų žurnaluose, turinčiose cituojamumo rodiklį, bei 3 – konferencijų medžiagose referuojamose *Clarivate Analytics Web of Science* duomenų bazėse).

Notations

Symbols

β – coefficient that accounts for type of the loading;
σ_s – steel stress;
σ_{sr} – maximum stress in reinforcement in a crack;
α_e – modular ratio (=E_r/E_c);
ε – strain;
ε_c – average strain of concrete surface;
ε_{cr} – concrete cracking strain;
ε_r – average strain of reinforcement;
$\varepsilon_{r,ult}$ – ultimate strain of reinforcement;
ε_{sm} – strain of reinforcement at stabilized cracking stage;
κ – curvature;
τ_{bms} – mean bond stress;
$A_{1,2}$ – area of reinforcement in tension (1) and compression (2);
a_2 – concrete cover of reinforcement in compression;
A_c – area of concret cross-section;
$A_{c,ef}$ – effective area of concrete in tension;
A_f – area of FRP reinforcement;
A_s – area of steel reinforcement;
b – overall width of a cross-section;

c – concrete cover;
d – effective depth of a cross-section;
E_c – modulus of elasticity of concrete;
E_r – modulus of elasticity of reinforcement;
f_{cm} – mean value of concrete compressive strength at an age of 28 days;
$f_{cm,t}$ – mean value of concrete compressive strength at an age (t);
f_{ctm} – mean value of axial tensile strength of concrete;
f_u – ultimate tensile strength of reinforcement;
f_y – yield strength of reinforcement;
h – overall depth of a cross-section;
h_{ef} – effective depth of a cross-section;
L – length;
M – bending moment;
M_{cr} – cracking bending moment;
M_{ser} – service bending moment;
M_u – ultimate bending moment;
n – modular ratio ($=E_f/E_s$);
P – perimeter of reinforcement bar;
p – reinforcement ratio ($=A_s/A_c$);
p_{ef} – effective reinforcement ratio ($=A_s/A_{c,ef}$);
P_{ult} – ultimate load;
s_r – distance between cracks;
$s_{r,m}$ – mean distance between cracks;
$s_{r,max}$ – theoretically obtained maximum distance between cracks;
t – the age of concrete;
w_m – mean crack width;
w_{max} – maximum crack width;
x – depth of compression zone;
Ø – diameter of a reinforcement bar.

Abbreviations

CCD – charge-coupled device;
DIC – digital image correlation;
DOF – degrees of freedom;
FE – finite element;
FRP – fiber reinforced polymer;
GFRP – glass fibre reinforced polymer;
LVDT – linear variable displacement transducer;
RC – reinforced concrete.

Contents

[1] The annexes are supplied in the enclosed compact disc.

Introduction

Problem Formulation

Steady increased application of innovative construction materials (high strength reinforcement and concrete) results in longer spans and smaller depths and, consequently, the Serviceability Limit State (limitation of crack width and deformations) becomes the governing criterion in design of structural elements. The design for serviceability, however, is one of the most difficult and unreliable engineering problem. Serviceability behaviour depends primarily on the concrete properties, which are often unknown at the design stage. After the crack initiation, the reinforcement layout plays an important role in deformations and cracking performance of the concrete elements. Although the predictions are in a good agreement with the experimental results of concrete elements with relatively high reinforcement ratios, widely accepted models are often inadequate predicting the cracking behaviour of elements with a specific arrangement of the bars (e.g., distributing bars in several layers, combining bars with different mechanical characteristics). The code provisions implementing semi-empirical methods have a limited ability to predict in-service behaviour of structural concrete.

The application of finite element (FE) simulation techniques has increased due to progressing knowledge and capabilities of computer software and hardware. Commercial FE packages (e.g., ABAQUS, ATENA, DIANA) offer a powerful

tool for analysis of RC structures. The numerical approach enables estimating effects, which are even too complicated to be evaluated experimentally. However, the development and the models should be based on the reliable test data. In order to improve adequacy of the serviceability (deformations and cracking) predictions, the effects related with the arrangement of bar reinforcement require an assessment and consideration for the design. The present study is focused on serviceability characteristics of flexural and tensile reinforced concrete elements. It involves new experimental results (some of them are related with application of innovative testing layout developed within the framework of this work).

Relevance of the Thesis

Structural concrete components exist in buildings and bridges in different forms. Understanding the response of these components during loading is crucial to the development of an overall efficient and safe structure. It is impossible, however, without reference to reliable experimental results, which also could help to develop adequate numerical models for solution of serviceability problems – one of the most complex and difficult tasks in the structural engineering.

Investigation of strain distribution within the concrete cover allows evaluating the cracking phenomena related with cross-section parameters. The reported results enable development of mathematical models (consistent with experimental evidence) that provides a reasonable reliability of the serviceability predictions. The prediction reliability is related with the scatter of the structural responses.

Object of the Research

The object of research is concrete elements with bar reinforcement subjected to short-term loading. The analysis is based on the test results of concrete beams and prisms with different arrangement of tensile reinforcement. The specimens were made of the concrete with 38–56 MPa compressive strength. Diameter, mechanical properties and material of reinforcement, reinforcement ratio and geometry of the specimen as well as depth of the concrete cover are the variables of the study.

Aim of the Thesis

The study is focused on the effect of reinforcement arrangement on deformation and cracking resistance of tensile and flexural elements with the aim of identifying the major parameters, which are responsible for scatter of the structural outputs.

Tasks of the Thesis

In order to achieve the aim of the thesis, the following tasks are formulated:

1. To identify the governing characteristics of the deformation and cracking performance of reinforced concrete members.
2. To perform experimental and numerical analysis of bar reinforcement arrangement effects to deformations and cracking behaviour of concrete elements subjected to short-term loading.
3. To verify the adequacy of the deformation and cracking predictions by design codes.
4. To propose several alternative layouts of reinforcement bars ensuring the control of the stiffness and cracking behaviour of concrete elements under serviceability conditions.

Research Methodology

The present study is exploratory by nature. A qualitative research is based on a relatively small number of carefully selected test specimens. The samples were selected in an iterative manner by following criteria formulated with the help of a comprehensive review of relevant literature. The performed data analysis is descriptive; the corresponding methodological approach is guided by intuition and experience. The data patterns (e.g., correlation of variables) are identified, examined, and interpreted by taking into account the relations between the theoretical and physical nature of the investigated object. The applied research methodology allows identifying the effect of arrangement of reinforcement on deformations and cracking of concrete elements though not every finding of this work can be generalized straightforwardly (owning the limited number of the consided test samples).

Scientific Novelty of the Thesis

1. The fundamental assumption of direct relation between the maximum crack width and the maximum crack distance is not necessarily true. The maximum crack opening is not always adjacent to the maximum distance between cracks or located between two consecutive uncracked blocks of maximum total length. This presumption is supported by the experimental cracking results of nine RC beams.

2. Specific equipment that enables independent variation of each of the key parameters in cracking analysis, i.e. concrete cover, reinforcement ratio and diameter of the reinforcement bars, has been developed. Cracking results obtained using the developed test equipment indicated that crack spacing is practically independent of the reinforcement characteristics (bar diameter and reinforcement ratio) that contradicts the common design assumption. The concrete cover was identified as the key parameter controlling the cracking behaviour.
3. The proposed representativeness condition of a test specimen allows isolating the investigated parameter from uncontrolled effects. For instance, representative shape of the tie (i.e., certain arrangement of reinforcement bar and cover depth) enables minimising the end effect, which is related with different deformations of the reinforcement and concrete surface.
4. On a basis of the regular bond model proposed in the literature, numerical models of the concrete ties with multiple bars tested in this study were developed. This approach is particularly efficient in a numerical sense; furthermore, it ensures to represent an actual distribution of strains in the concrete and to illustrate cracking phenomena in reinforced concrete ties.
5. Both numerical simulation and physical test results indicate that the strain gradient in the tensile concrete varies not only long the bar, but also within the cover. The commonly accepted concept of "area of the concrete effective in tension" has a limited application that is related to the loading conditions, stress-strain state, cover, and configuration of the unreinforced area.

Practical Value of the Research Findings

1. A specific equipment for producing and testing concrete ties reinforced with multiple bars made of any materials was developed. The equipment allows designing ties with independently controlled cross-sectional parameters (i.e. concrete cover, reinforcement ratio and diameter of the bars). The developed equipment was patented in 2016 in the State Patent Bureau of the Republic of Lithuania (Patent No. LT 6275 B).
2. A testing procedure that enables monitoring both deformations of bar reinforcement and concrete surface of the tensile prisms reinforced with multiple bars was proposed. This technique allows obtaining supplementary testing data for control of deformation behaviour of the concrete. Such information is vital for the development of numerical models adequate to the test results.

3. The developed test equipment and the proposed monitoring procedure allow verifying adequacy of cracking predictions by design codes.

The Defended Statements

1. To avoid correlation between the key variables (i.e. concrete cover, reinforcement ratio, and the diameter of reinforcement bars), the traditional equipment for the tensile tests should be modified.
2. The commonly accepted concept of "area of the concrete effective in tension" has a limited application.
3. Increasing the number of reinforcement bars can serve to improve the serviceability properties of elements with moderate (1.4% and 2.0%) reinforcement ratios.
4. Finite element approaches based on concrete fracture and the regular bond models reported in the literature enables estimating effects, which are even too complicated to be evaluated experimentally.

Approval of the Research Findings

A specific equipment for dissertation research was developed and patented in the State Patent Bureau of the Republic of Lithuania. The author have published 14 articles on the topic of the dissertation (five of them in the journals with an Impact Factor and three in the conference proceedings referred by the *Clarivate Analytics Web of Science*). During the PhD study period (2013–2017) the results of the dissertation were published at nine scientific conferences:

- 2017. The 24th International Conference on *Composites and Nano Engineering*. Rome, Italy.
- 2017. The Third International Conference on *Mechanics of Composites.* Bologna, Italy.
- 2016. The 12th International Conference *Modern Building Materials, Structures and Techniques*. Vilnius, Lithuania.
- 2015. The 15th German-Lithuanian-Polish Colloquium and Meeting of EURO Working Group *Sustainable Development and Civil Engineering*. Poznan, Poland.
- 2015. The 18th Conference for Junior Researchers *Science – Future of Lithuania*. Vilnius, Lithuania.
- 2014. The 19th International Conference *Mechanika*. Kaunas, Lithuania.

- 2014. The 17th Conference for Junior Researchers *Science – Future of Lithuania*. Vilnius, Lithuania.
- 2014. The Fourth Conference for Junior Researchers *Interdisciplinary Research of Physical and Technology Sciences*. Vilnius, Lithuania. 2013.
- The 11th International Conference *Numerical Analysis and Applied Mathematics*. Rhodes, Greece.

Structure of the Dissertation

The dissertation consists of an introduction, three chapters, general conclusions, literature reference list (137 publications), list of the author's publications on the research topic (14 publications), LR patent, summary in Lithuanian and 3 annexes. The volume of the dissertation is 143 pages.

Acknowledgements

The author gratefully acknowledge the funding of PhD position provided by the Science Council of Lithuania and covered by the European Union Structural Funds.

The author would like to expresses his sincere gratitude to the supervisor of the scientific work, head of the Laboratory of Innovative Building Structures Dr Viktor Gribniak for his patience, motivation, immense knowledge, and enthusiastic guidance throughout this research.

The author would also like to express appreciation to the staff and PhD students of the Department of Bridges and Special Structures for the help and stimulating discussions about the research. In particular, author would like to thank Dr Aleksandr Sokolov for willingness to help and great assistance during the experimental studies, and Dr Pui Lam NG for valuable comments and remarks on PhD thesis.

Dr Andor Windisch, Dr Lluis Torres Llinas, Dr Alejandro Perez Caldentey and Prof. Dr Joaquim Antonio Oliveira Barros deserve special thanks for valuable insights – their expertise and competence were a significant support improving the quality of the dissertation.

The author would like to express his deepest gratitude to his parents Audronė and Petras, sister Ieva and beloved wife Dovile for encouragement, patience and support throughout his study.

1

Cracking and Deformations of Reinforced Concrete Elements

This chapter reviews material parameters important for analysis of deformation behaviour of reinforced concrete (RC) members. The corresponding test layouts are considered as well. Different approaches in tension-stiffening and methods of deformation analysis of RC members as well as numerical models and design approaches have been observed. This chapter also formulates the main objective and tasks of the present investigation. This chapter includes the material presented in journal publication Rimkus & Gribniak (2016) and conference proceedings Rimkus & Vilėniškytė (2015), Gudonis *et al.* (2014) and Rimkus *et al.* (2014).

1.1. Materials for Reinforced Concrete

1.1.1. Concrete: Structure and Mechanical Properties

Concrete is a heterogenous material that can be considered as a combination of aggregates and hydrated cement paste. The paste, usually composed of cement and water, hardens and binds the aggregates into a rigid structure. In order to improve or to obtain the desired fresh or hardened concrete properties, supplementary cementitious materials and chemical admixtures may also be included in the

paste. The paste constitutes about 25% to 40% while aggregates make up about 60% to 75% of the total volume of concrete. The behaviour of the concrete depends upon the quality of the paste and aggregate and mechanical properties of the transition zone between them (Mehta & Monteiro 1993). Because the transition zone typically has a slightly higher water to cement ratio than is observed in the entire paste (Lowes 1999), this zone is often weaker than the entire paste in normal-weight concrete (Hsu & Slate 1963, Alexander *et al.* 1968).

Defects are the inherent component of the concrete structure. Stale & Olefski (1963) and Stale & Hover (1984) showed that a significant number of micro-defects exists in concrete structure before the application of external load. The defects are governed by curing environment, composition of concrete mixture, consolidation quality, and compatibility of subcomponents of concrete (Soudki 2001). An inappropriate curing environment might increase cement paste hydration temperature that causes thermal expansion of the paste and the development of micro-cracks around the aggregates (Fig. 1.1a). Trigo & Liborio (2014) investigated techniques to improve bond between the hydrated cement paste and aggregates and demonstrated characteristics of micro-cracking (Fig. 1.1b). Discontinuous micro-cracks are not a serious threat to concrete deterioration. Over time, due to mechanical loading, variations in temperature, and changes in environment conditions, they increase in depth, length and width and combine with other micro-cracks (Fig. 1.1c) controlling the overall response of concrete. In case of external loading, the micro-cracks become macro-cracks by bringing together the structural defects (Fig. 1.1d). Although the behaviour of concrete is governed by its heterogeneous composition and stochastic defects, only the macroscopic properties of concrete are considered in practical design applications (Weerheijm 2013).

Concrete properties determined from experiments depend on the particular testing method. In some cases, even the application of standardised testing methods cannot prevent significant scatter of test results (Kaufmann 2013). Bartlett & MacGregor (1996) performed statistical analysis of compressive strength of 3756 cylinder tests representing 108 concrete mixes. It was concluded that coefficient of variation of compressive strength of investigated specimens is 23%.

Typical concrete mixes have high resistance to compressive stresses. However, its tensile strength is only about 8% to 12% of its compressive strength (Nmai *et al.* 2006). The tensile strength of concrete can be determined using either direct or indirect tension tests (Fig. 1.2). Due to the difficultiesof applying tension to the specimen and avoid eccentricity induced by the equipment for the specimen fixing in the testing machine or physical eccentricity due to uneven stiffness of the concrete structure, direct tensile tests (Fig. 1.2a) are complicated and rarely used. Usually, the concrete tensile strength is determined by means of indirect tests such as the split cylinder test, the bending test, or the double punch test, shown in Fig. 1.2b, 2c and 2d, respectively. Compressive strength, tensile strength

and modulus of elasticity of concrete are interrelated mechanical parameters, which govern the elastic behaviour of the concrete. One of the relevant parameters that characterize concrete fracture and allows to perform proper modelling of the initiation and propagation of cracks is the fracture energy G_f (Østergaard & Olesen 2004). The fracture energy is the energy required to form a unit of the cracking surface in the concrete.

Governing characteristics of overall performance of concrete can be identified by various direct and indirect experimental methods. Many researchers have demonstrated that the outputs of aforementioned characteristics are test-method sensitive and can result in significant scatter (up to more than 20%). Therefore, due to inevitable defects and micro-cracks in the heterogeneous composition of concrete, experiments requires great care on specimen size and shape selection.

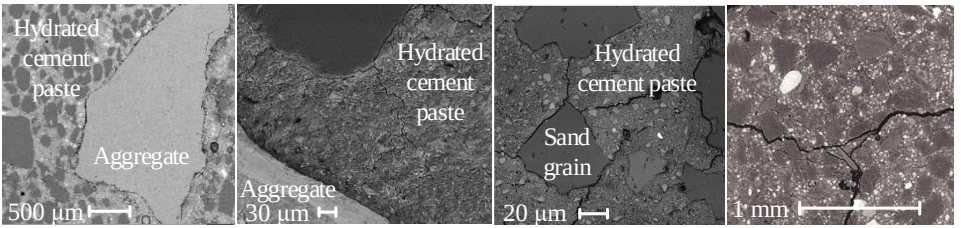

Fig. 1.1. Defects and micro-cracks of the concrete observed by a) and b) Trigo & Liborio (2014), and c) Lima *et al.* (2014), and macro-cracks in a fine-grained concrete under compression observed by d) Landis & Bolander (2009)

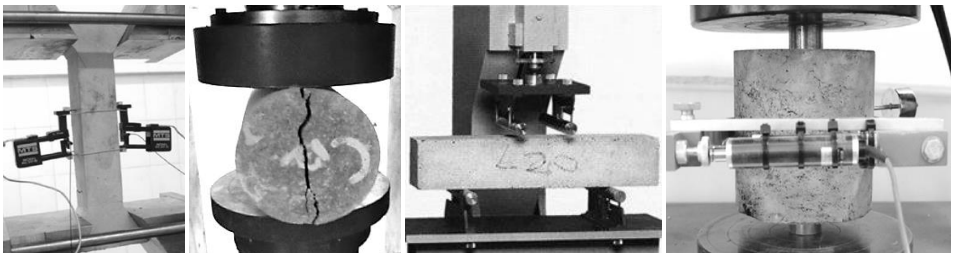

Fig. 1.2. Tensile strength of concrete: a) direct tension test of bone-shaped specimen (Moradian & Shekarchi 2016), b) the split cylinder test (Garg *et al.* 2014), c) the bending test and d) the double punch test (Kim & Lee 2015)

1.1.2. Reinforcement Materials

Various materials in different forms are used as reinforcement for concrete structures. Steel bars with ribs, also known as deformed bars, are the common type of reinforcement for structural concrete. Depending on the desired characteristics,

fibre reinforced polymer (FRP) bars, discrete fibres, welded wire mesh, sheets and plates made of different materials might also be used as a reinforcement.

1.1.2.1. Steel Bars

The steel bars may have plain (round) or deformed surface. Deformed steel bars are the most common type of reinforcement, while plain bars are usually used for non-structural elements, due to its poor mechanical anchorage to the concrete. The deformed shape of the bar enables a mechanical interaction between the ribs of the bar and the surrounding concrete (Hassoun 1985).

The bond strength of reinforcement depends on chemical adhesion, friction resistance and the bearing of the ribs against the surrounding concrete. Mechanical interlock due to bearing action between bar ribs and concrete is the most contributing component to the bond (Chan 2012). Due to variety of the rib shapes and patterns, unified bond modelling becomes hardly possible. In order to solve this problem, European standard EN 10080 (2005) defines technical requirements for the reinforcement bars. Two types of steel based on chemical composition are used for reinforcement bar production: hot-rolled, low-carbon steel and cold-worked, high-carbon steel. The modulus of elasticity and tensile strength are the most important physical parameters of the reinforcement, while a stress-strain diagram (e.g., Fig. 1.3a) describes the overall mechanical response of the reinforcement. Usually this diagram is obtained from direct tension test (Fig. 1.3b). The stress-strain diagram of a hot-rolled, low-carbon steel bar in tension is presented in Fig. 1.3a. The diagram shows several stages of deformation response: linear elastic (segment *Oa*), pseudo-elastic (segment *ab*), yielding (segment *bc*), strain-hardening (segment *cd*) and strain-softening (segment *de*). Unlike a hot-rolled and low-carbon steel, cold-worked and high-carbon steels exhibit a smooth transition from the initial elastic phase to the strain-hardening branch, without a distinct yield plateau. Cold-worked steel is distinguished by its hardness and high strength.

The present study is focused on the application of reinforcement bars made of a hot-rolled steel. For such reinforcement, the modulus of elasticity, E_s, is roughly equal to 205 GPa, while yield strength varies from 400 MPa to 600 MPa.

1.1.2.2. Fibre Reinforced Polymer (FRP) Bars

FRP bars are used as an alternative to steel reinforcement in an aggressive corrosion or electro-magnetic environment. FRP is composed of a polymer matrix reinforced with fibres. The fibres are usually glass, carbon, aramid, or basalt, while the polymer is usually an epoxy, vinylester or polyester thermosetting plastic. The purpose of the matrix in composites is to provide a sufficient bond quality with

concrete as well as the lateral support and protection to the fibres. In order to enhance the bond characteristics of FRP bars in structural concrete, different techniques are used to produce bars in ribbed, wrapped, sand coated, or wrapped and sand coated surfaces (Fig. 1.4). Plain FRP bars are also available.

FRP bars are characterized by a perfectly elastic behaviour up to failure and can develop higher tensile strength than conventional steel in the direction of the fibres. Unlike steel, FRP is nonmagnetic, lightweight (about 25% the weight of steel), and resistant to impact and cyclic loadings (Mufti 2001). However, a brittle failure, low modulus of elasticity, low resistance to high temperatures, and sensitivity to ultraviolet radiation can be identified as the main causes, which limit the application of FRP in civil engineering. Due to the anisotropic structure of the polymer bars, shear resistance of FRP bars is marginal. Due to low buckling resistance, FRP reinforcement is essentially used in tension.

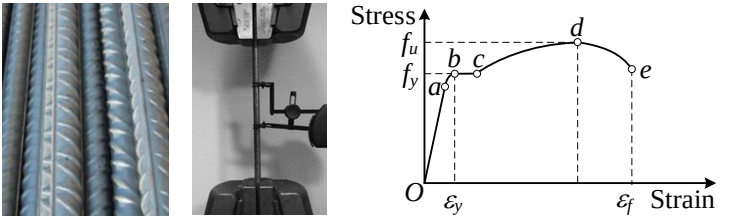

Fig. 1.3. Tension test of reinforcement steel: a) common shape of the surface, b) experimental characterization, c) a typical stress-strain relationship of the steel

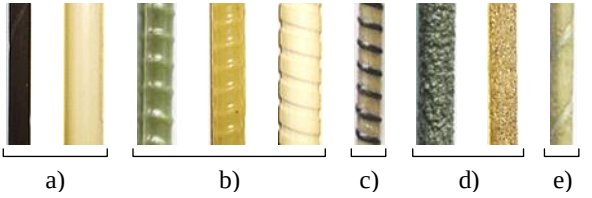

Fig. 1.4. Surface treatment of fiber reinforced polymer bars: a) plain, b) ribbed, c) wrapped, d) sand coated, and e) wrapped and sand coated bars (Quayyum 2010)

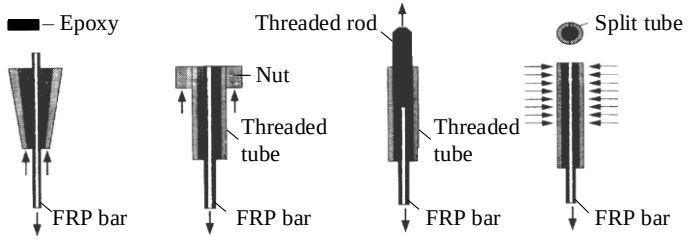

Fig. 1.5. Tensile test fittings for fiber reinforced polymer bars (Castro & Carino 1998)

The principal mechanical properties of FRP bars that need to be specified include tensile strength and modulus of elasticity. These parameters cannot be experimentally determined using the same techniques that are used for the steel bars, since application of the traditional wedge-shaped friction grips (Fig. 1.3b) causes stress concentration following the premature failure of FRP test specimens. To solve this problem, specific bar grip systems should be employed (Fig. 1.5). These anchorage systems involve embedding the bar into tubes filled with a matrix and allow avoiding the compressive clamping.

The mechanical properties of FRP bars differ significantly from steel. Failure brittleness (either tensile reinforcement or compressive concrete zone in flexural elements), high deformability, and low fire resistance are the main aspects, which must be accounted for (Pilakoutas *et al.* 2011).

1.1.2.3. Other Types of Reinforcement

Application of bar reinforcement (steel or FRP) is the most common way to reinforce load bearing concrete structures. However, structures designed for resisting specific loading conditions or installation methods require non-conventional alternatives for reinforcement. Different types of external reinforcement (e.g., sheets, laminates, and profiles), near-surface mounted strips as well as application of steel, synthetic, or natural fibres might help solve various structural problems. In most cases, such reinforcement schemes are combined with internal steel or FRP bars providing additional structural features (Löfgren 2005). At appropriate dosages, the addition of fibres may provide increased resistance to plastic and drying shrinkage cracking, reduced crack widths, and enhanced energy absorption and impact resistance. The major benefit derived from the use of fibre reinforcement is improved concrete durability (Nmai *et al.* 2006, Mesbah & Buyle-Bodin 1999, Larsen & Krenchel 1990). The present study is focused, however, on the application of deformed bars made either of steel or FRP.

1.1.3. Interaction of Reinforcement and Concrete

This subsection is focused on bond behaviour of bar reinforcement. Effectiveness of such reinforcement is related with bond properties of the bars, since they must ensure uniformity of deformations of the reinforcement and concrete.

The bar diameter as well as the shape and geometry of bar ribs have an influence on the bond strength. The diameter of the deformed bars varies from 6 mm to 50 mm. The rib size varies with the bar diameter, thus the bond properties vary as well. Hamad (1995a, 1995b), Darvin & Graham (1993) and Cairns & Abdullah (1996) concluded that bond behaviour of deformed bars is improved by increasing the rib height and decreasing the rib spacing (Fig. 1.6a). The bond stress depends on the cover thickness and deformation range of the reinforcement, the transverse

reinforcement confining effect, concrete strength and type of aggregate used (Williams 2003). Another less obvious but also important parameter is the Poisson ratio, which plays a relevant role for FRP reinforcement (*fib* 2000). Although the individual contributions of these factors are difficult to separate and quantify, interlocking action between ribs and concrete, and the quality of the concrete are considered as major factors, which characterize the bond quality (Williams 2003).

In a plain bar, the bond mechanism is controlled by adhesion, micro-mechanical locking, and friction, while in a deformed bar it is produced by the wedging effect of the bar ribs in the concrete (Tepfers 1979), as shown in Fig. 1.6a. As the concrete tends to slip over the bar, the bearing pressure between the concrete and the ribs increases. The pressure increase causes radial cracking around the ribs, which tends to split the concrete segment. Longitudinal cracks will occur perpendicular to the radial tensile stresses (Fig. 1.6b). Goto (1971) has experimentally demonstrated the bond action between concrete and deformed steel bars. Cracks in the concrete were penetrated by ink and became visible afterwards the tested prisms were axially cut (Fig. 1.7a). The slopes of the internal cracks indicate the trajectories along which the compressive forces leave the ribs of the deformed bar.

The radial bond cracks produced by the ribs bearing on the surrounding concrete tend to propagate to the concrete surface. Brooms (1965), Husain & Ferguson (1968), and Tammo & Thelandersson (2006) demonstrated that widths of the cracks on the surface of RC member might be two to ten times the crack close to the reinforcement bar. Beeby (1978) showed considerable difference between the surface and internal crack width at the very vicinity of the reinforcement (Fig. 1.7b). Husain & Ferguson (1968) concluded that the crack width at the level of the reinforcement is independent from the thickness of the concrete cover, but width of the surface cracks is proportional to the thickness of the concrete cover. Brooms (1965) showed that crack width in the surface is almost linearly proportional to the tensile strain of the reinforcement.

The bond behaviour is often described by the bond stress-slip relationship. The available standards recommend two experimental set-ups to determine the bond strength between reinforcement and concrete. One of them is based on pulling out of a bar reinforcement from the concrete block (Fig. 1.8a). A four point bending test of a concrete beam with a central hinge represents the alternative test setup (RILEM-RC5 1982). Both methods produce quite different results, which complicates assessment of the bond behaviour (Pokorný *et al*. 2015). In the case of the pull-out test, different stress states are characteristic for the concrete and steel: the bar experiences tension, while the concrete is in compression (Ashtiani *et al.* 2013). The results of pull-out test are, therefore, strongly dependent on the strength of the concrete. In case of the beam test, the bond performance is affected by a confining action of the shear reinforcement. Therefore, the results of either tests are not so straightforward and require some arbitrarily interpretations for making a general statement about the bond-strength.

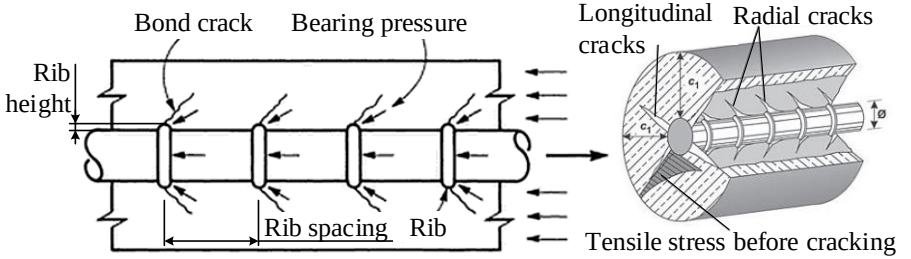

Fig. 1.6. Bond of concrete and reinforcement: a) deformed bar in the concrete (Williams 2003), b) longitudinal and transverse crack development due to the bond (Tepfers 1973)

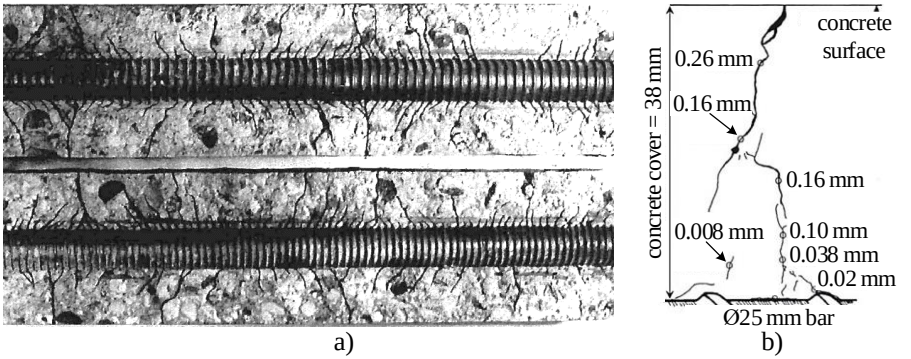

Fig. 1.7. Internal cracking: a) cracks around 32 mm bars with 5.5 mm rib spacing (top) and 7 mm (bottom) (Goto 1971), b) crack width variation within 38 mm cover (Beeby 1978)

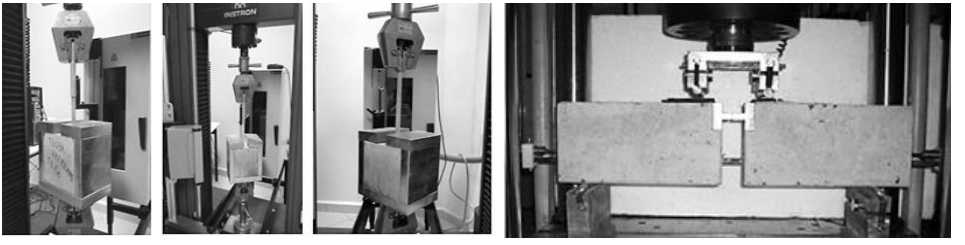

Fig. 1.8. Experimental determination of bond strength: a) pull-out test (Erdem *et al.* 2015) and b) four point bending test of RC beam according RILEM RC-6 (1978)

In case of closely spaced reinforcement bars, the bond strength might be affected by the confining effect due to expansion of concrete caused by the radial bond-stress component. Such confinement leads to an increased bond capacity. This is supported by test data reported by Broms and Lutz (1965), who have

shown that the number of internal cracks between the closely distributed bars might significantly exceed the number of cracks in other areas of RC ties as show in Fig. 1.9a. It can be seen that a large number of internal cracks developed close to the reinforcement and that the spacing of these cracks was approximately constant. Smaller crack distances near reinforcement indicate increased bond capacity. Otsuka and Ozaka (1992) have also illustrated that the confining effect is related to the distance between the reinforcement bars (Figs. 1.9b–1.9d). In case of reduced spacing between the bars (Fig. 1.9c), the tips of radial bond cracks of adjacent bars join together affecting the bond performance of the overall reinforcement (bar group). Gribniak *et al.* (2015) revealed that the elements with a large number of closely distributed reinforcement bars reported by Rostásy *et al.* (1976), Williams (1986), and Purainer (2005) have shown a significantly stiffer behaviour than elements with the same reinforcement area distributed in one bar (or several bars spaced at relatively big distances). This phenomenon might be due to the confining effect of the intact concrete between the closely distributed bars, hampering the expansion of concrete due to secondary cracking (Figs. 1.7a, 1.9). Further studies, therefore, are necessary to investigate the deformational and cracking behaviour of elements with closely distributed reinforcement bars.

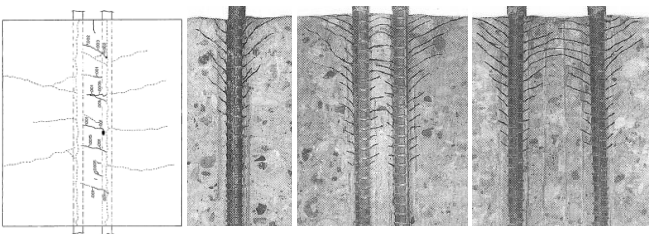

a) b) c) d)

Fig. 1.9. Internal cracking of reinforced concrete elements: a) internal cracking observed by Broms & Lutz (1965), results of elements with b) single Ø22 mm steel bar, c) two Ø22 mm steel bars with 33 mm clear spacing and d) two Ø22 mm steel bars with 89 mm clear spacing obtained by Otsuka and Ozaka (1992)

1.2. Analysing Cracking and Deformation Behaviour

1.2.1. Cracking and Deformation Stages

As noted in Subsection 1.1.1, cracks are intrinsic to concrete structures. This section, however, is focused on development of macro-cracks in concrete elements with bar reinforcement. Cracking and deformation behaviour are explained considering a tensile concrete element reinforced with single steel bar. As can be observed in Fig. 1.10a, the deformation behaviour of a RC tie consists of three

stages. The first stage represents the elastic deformations up to the start of cracking (point *A* in Fig. 1.10a). The second stage refers to the region between the first (point *A*) and the final cracks (point *B*). In the third stage, the deformation behaviour of the member with fully developed cracks is characterized by a gradual degradation of the bond strength. Goto (1971) related this process to the formation of secondary cracks (also known as radial bond cracks) along the deformed bar caused by the transfer of bond stress to the surrounding concrete.

In the cracked state, a stiffness contribution is formed due to the uncracked concrete between the transverse cracks. The total stiffness is found to be higher than the pure stiffness of a reinforcement bar in a cracked section. The stiffness contribution after cracking, referred to as the tension-stiffening effect (Fig. 1.10a), depends on the stresses between the reinforcement bar and the surrounding concrete. Tensile stresses can either be a result of external load acting on the concrete structure or due to restrained deformations. Such deformation could result from thermal strain or drying shrinkage strain, as described in Subsection 1.1.1.

According to CEB-FIP Model Code 90 (CEB 1991), the first crack occurs when the load has reached the theoretical cracking load, N_{cr}, see Fig. 1.10a, and new cracks will appear under small load increase until the element is fully cracked or when the restraint forces decreases below the concrete tensile capacity. When a reinforced concrete member is loaded in tension in the force-controlling manner, the deformation will increase instantaneously for each crack that appears, without increased load. As shown in Fig. 1.10b, the deformation increases rapidly with the cracks. When RC tie is loaded in a deformation-controlled manner, the response is rather different as shown in Fig. 1.10c. With the cracks, the reaction is reduced because of reduced overall stiffness. In any case, the crack appearance reduces the overall stiffness of the element (Figs. 1.10b and 1.10c). The inclination of the dashed line indicates of the stiffness decreases. It is commonly assumed that no new cracks appear in stabilised cracking stage (stage *BC* in Fig. 1.10a). The width of the already existing cracks increases with load until the reinforcement yields.

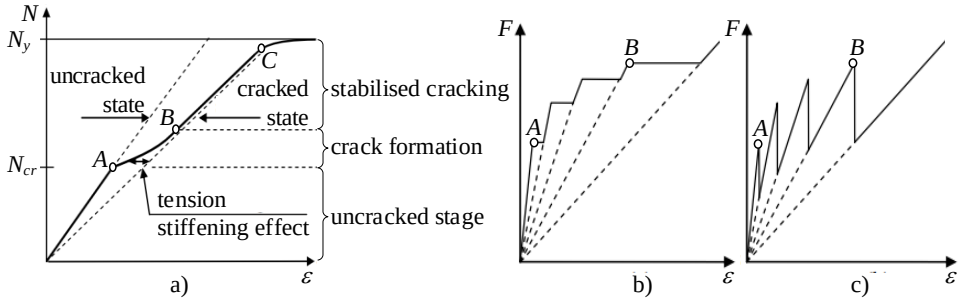

Fig. 1.10. Deformation response of reinforced concrete tensile element: a) cracking stages, b) the force-controlling response, and c) the deformation-controlled loading

1.2.2. Deformations and Cracking: Testing Methods and Layouts

There are two main ways to assess cracking and deformation behaviour of reinforced concrete (Fig. 1.11): 1) flexural tests of RC beams; and 2) direct tension tests of RC ties. The most common way is the beam flexure tests when the beam is subjected to bending by applying either three-point or four-point (Fig. 1.11a) loading scheme. However, interpretation of outcomes of the different tests might lead to different conclusions (Bencardino 2013).

The shear effect can be identified as the major difference between the aforementioned flexural tests. In the three-point bending, the zone of the maximum flexural effect is located under the central bearing, while the four-point bending method brings a much larger portion of the beam (i.e. part between two loading points) subjected to pure flexure action. The latter scheme allows avoiding a premature failure of the beam due to stress concentration under the loading point. This difference is of prime importance when investigating brittle materials, such as reinforced concrete, where the number and severity of defects exposed to the maximum stress is directly related to the flexural strength and crack initiation. Therefore, the three-point bending test is more suitable layout for characterization of the material, while the four-point bending test is often used for assessment of structural parameters of RC elements. The deflection measurement in three-point bending tests is commonly performed using the testing machine's crosshead position sensor, whereas in the four-point bending test it is executed using deflectometers. Due to different distribution of loaded points, the peak load values for four-point bending tests are lower than three-point bending tests of about 12%, while the peak stress values are lower of about 25% (Bencardino 2013). Configuration of test setup is not the only source of scattering results. Due to the shear effect, the response of the beam is highly dependent on the beam geometry, particularly on the length to depth ratio l/h.

a)

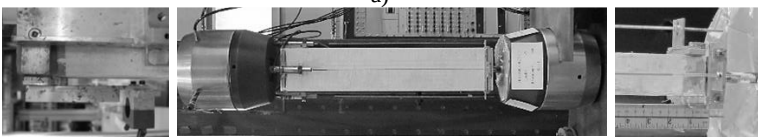

b)

Fig. 1.11. Testing layouts: a) flexural four-point bending test (Gribniak *et al.* 2012) and b) direct tensile test of reinforced concrete tie (Deluce 2011)

Alternatively, deformation and cracking behaviour of RC elements can be determined using the direct tension tests (Fig. 1.11b). A concrete prism reinforced with a single bar in the centre is the most common test specimen for the uniaxial tensile test. As shown in Fig. 1.11, these specimens are commonly instrumented with LVDT (linear variable displacement transducer) sensors on concrete surface (Deluce 2011). Such equipment enables monitoring the average strain of concrete surface. Furthermore, LVDT sensors might also be installed on the reinforcement for monitoring the average deformations of the bar.

In addition to this, the tensile specimen can be equipped with modern monitoring systems such as internal gauging system (Scott & Beeby 2005, Vilanova *et al.* 2014) or optical sensors (Khadour *et al.* 2013, Pinet *et al.* 2007), which are suitable for precise assessment of the bar strains. The digital image correlation (DIC) technique is becoming an increasingly useful tool for tracking deformations at the concrete surface (Michou *et al.* 2015). The modern image back-scattering techniques (X-ray (Landis & Bolander 2009), acoustic emission tomography (Cheng *et al.* 2015), or magnetic resonance imaging (Marfisi *et al.* 2005)), however, are limited to simple specimen geometry and loading cases. Thus, the internal deformations of the concrete can be assessed only in an averaged manner.

1.2.3. Investigating Deformation Behaviour of the Reinforced Concrete

Despite the apparent simplicity of the tensile test setup, interpretation of the test results might be inadequate: the experimental evidence often disagrees with the general assumption of similarity between average strains of the reinforcement and concrete. This discrepancy can be attributed to two well-known, but often neglected issues, namely, the effective area of concrete in tension and the end effect. The bond mechanism and the concrete cover control both these effects, which can be modelled by means of the discrete cracking approach, but cannot be represented within the framework of the smeared (average) cracking models. Accounting for the average deformations of the cracked concrete, the smeared models do not consider development of a particular crack.

Following the load-sharing concept, external load P induces two internal forces associated with the reinforcement N_s and the concrete N_c (Fig. 1.13a):

$$P = N_s + N_c. \tag{1.1}$$

Considering the Navier-Bernoulli hypothesis (the strain profile within a cross-section is represented as a plane), the internal forces in Equation (1.1) are simply related to the average strain of the member, ε_m, assumed the same for both the reinforcement and the concrete (Bischoff 2001):

$$P = A_s E_s \varepsilon_s + A_c E_c' \varepsilon_c = \left(A_s E_s + A_c E_c' \right) \varepsilon_m . \tag{1.2}$$

Here A_s and ε_s, and A_c and ε_c are the area and the strain of the reinforcement and concrete, respectively; E_s is the modulus of elasticity of the reinforcement; E'_c is the secant deformation modulus of the concrete.

Application of the secant modulus allows accounting for reduction of the stiffness of the cracked concrete. However, the exact distribution of the deformations within the concrete as well as the "effective" area in tension (that is characterized by the secant modulus E'_c) is unknown. In general, the total area of the concrete is assumed identically effective in tension though this assumption is adequate only for limited concrete cover ranges. Figure 1.12a illustrates a possible inconsistency of the average deformation model: the average strains of concrete $\varepsilon_{c,m}$ and reinforcement $\varepsilon_{s,m}$ are not equal in a general case.

Figure 1.12b shows an idealized (average) load-strain diagram of a RC tie. Since the average cracking models are valid up to the start of yielding of the reinforcement that is restricted to a single section, the current study considers only the first three loading stages limited by the yielding of reinforcement (point C). The first stage (part OA) covers the elastic deformations up to the start of the cracking that occurs (point A) at the weakest section when the stress in the concrete reaches the local tensile strength. The analysis related to the average tensile strength (a macroscopic material parameter) produces a regular crack pattern. Introducing variation in the strength is only relevant when capturing the best possible experimental crack pattern (Dominguez *et al.* 2005) or the exact crack location (Elfgren & Noghabai 2002).

Under the assumption that all tension at the cracked section is carried by the reinforcement, i.e. neglecting the softening behaviour of the concrete after cracking and considering the idealized crack pattern (regularly distributed fully formed transverse cracks), the predicted crack width would be constant throughout the section depth. Contradicting the experimental evidence (Figs. 1.13a, 1.13b), such an over-simplified assumption does not allow for a difference between the internal and external uncracked blocks (Fig. 1.12a) and, consequently, assessment of the end effect that contributes to an inadequate interpretation of the test results (Husain & Ferguson 1968, Carino & Clifton 1995, Borosnyói & Snobli 2010). At a certain distance from the transverse crack, the concrete continues carrying tensile stresses because of the bond mechanism (Fig. 1.13c). This phenomenon, commonly known as tension-stiffening, is shown by the grey-filled area in Fig. 1.12b.

Deformation behaviour of the tie with fully developed transverse cracks (stage BC) is characterized by the gradual degradation of the bond strength. Goto (1971) related this process with the formation of secondary cracks caused by the transfer of bond stresses to the surrounding concrete between the transverse primary cracks (Fig. 1.13b). Broms (1965) characterized two types of cracks with

different geometry. One type is the primary visible crack attaining the concrete surface, while the secondary cracks do not progress up to the concrete surface. In case of a large cover, a larger number of the cracks will remain as internal cracks at a given level of tensile force. Despite the high amount of experimental and theoretical investigations carried out during the last century, a direct relationship between crack width at the surface and inside the concrete (close to the bar) has not been discovered (Beeby 1983). Moreover, there is no general agreement on the area of the concrete effective in tension (Figs. 1.13c and 1.13d).

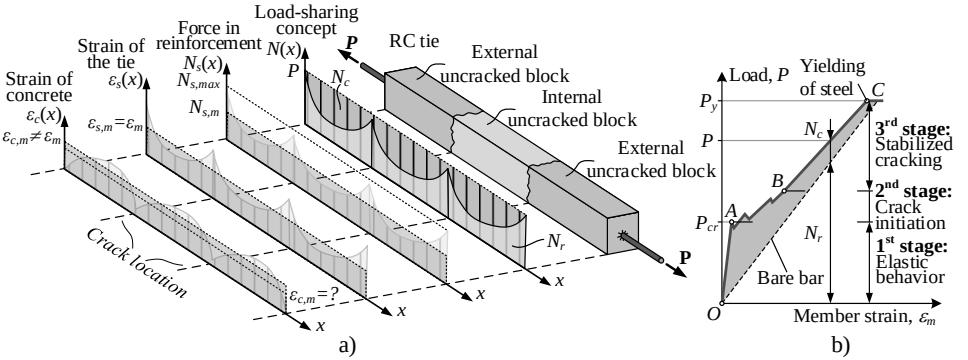

Fig. 1.12. Reinforced concrete tie: a) load-sharing concept, b) average deformation behaviour

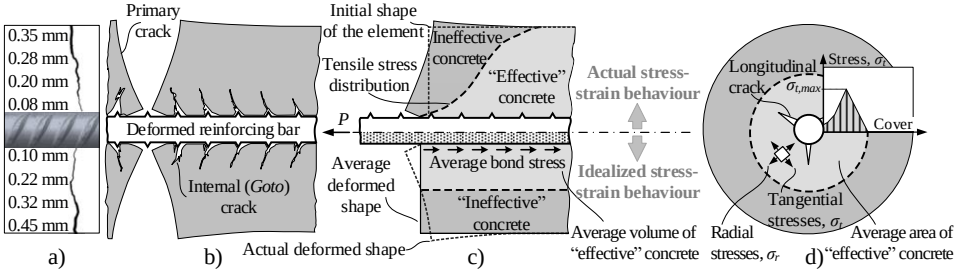

Fig. 1.13. Crack development: a) experimental view, b) Goto cracks, c) actual and averaged stress-strain behaviour of the effective zone, and d) longitudinal cracks

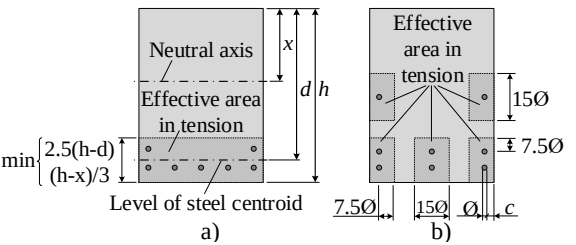

Fig. 1.14. Area of concrete effective in tension: Model Code a) 2010 and b) 1978 issues

Several methods have been proposed to determine effective concrete in tension (Fig. 1.14), however the adequacy of those methods are highly questionable. Consequently, specimens with different dimensions are used for representing the behaviour of structural elements, which naturally increases the scatter of the test results (Gribniak *et al.* 2015, Lee & Kim 2009).

The serviceability analyses described by the Code methods are intended for the stabilized cracking stage (Balázs *et al.* 2013). Unbalanced geometry and material properties, however, might destabilize the cracking process (Debernardi & Taliano 2016). Marginal differences between the cracking and yielding loads (Fig. 1.12b), insufficient number of fully developed primary cracks in relatively short specimens as well as significant tension-softening and crack interlock effects (characteristic for a thick cover) could be associated with the unstable cracking (Base & Murray 1982, Tam & Scanlon 1986, Gilbert 1992, Caldentey *et al.* 2013).

The development of longitudinal cracks can also be identified as a cause of the unstable cracking that is associated with the inability of the cover to resist the splitting stresses (Tepfers 1979, Holschemacher *et al.* 2005). Initiation of longitudinal cracks at extremities of the experimental ties (Tepfers 1979, Jiang *et al.* 1984), significantly contributes to the end effect (Zheng *et al.* 2001, Tammo & Thelandersson 2009). Schematically, the cracking process is shown in Fig. 1.13d. The bond stresses are transferred to the surrounding concrete (particularly, the radial stress component) due to the mechanical interlock of the ribs. The cover controls the longitudinal cracking. Improper arrangement of reinforcement in a cross-section might result in sudden splitting the cover. It is characteristic to large diameter bars (Gambarova & Rosati 1996) and might be associated with the height of the ribs and the stiffness of such reinforcement. Morita & Kaku (1979) concluded that doubling the height of concrete cover (from 3.5 cm to 7 cm) provides a threefold greater bond strength for a tensile element reinforced with a large (51 mm) diameter bar. In structural elements designed in accordance with the minimum cover requirement, the concrete might not be able to resist the forces causing longitudinal cracking (Darwin *et al.* 1992). The resultant stiffness (related to the bond behaviour) might be well below the value predicted by the models derived using test results of samples with relatively large cover (Gribniak *et al.* 2016, Caldentey *et al.* 2017).

Besides, reduction of the cover in the samples (often related to increase of the reinforcement percentage in the ties reinforced with a centre bar) might result in a sudden opening of the longitudinal cracks and the following loss of stiffness. Strain peaks in the boundary zones (Fig. 1.15a) are characteristic to the deformations monitored along the reinforcing bar (Michou *et al.* 2015). These peaks mostly affect average strain measurements within a relatively small deformation range. After the primary cracks open (Fig. 1.13b), the end effect becomes less evident (Fig. 1.14b). It also relies on the geometry (length) of the tie. Considering

the cracking behaviour, experimental results (Gudonis *et al.* 2014, Rimkus & Vileniskyte 2015, Gribniak *et al.* 2016, Carino *et al.* 1995, Borosnyói & Snobli 2010, Caldentey *et al.* 2013, Brooms & Lutz 1965, Base *et al.* 1966, Rostasy *et al.* 1976, Calderón & Fernández 2010) indicated that the crack pattern is dependent on geometry of the specimen and arrangement of the reinforcement.

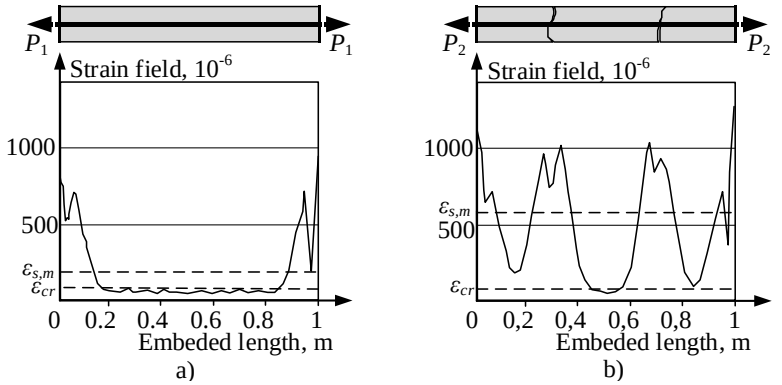

Fig. 1.15. Strain in reinforcement a) before and b) after cracking (Michou *et al.* 2015)

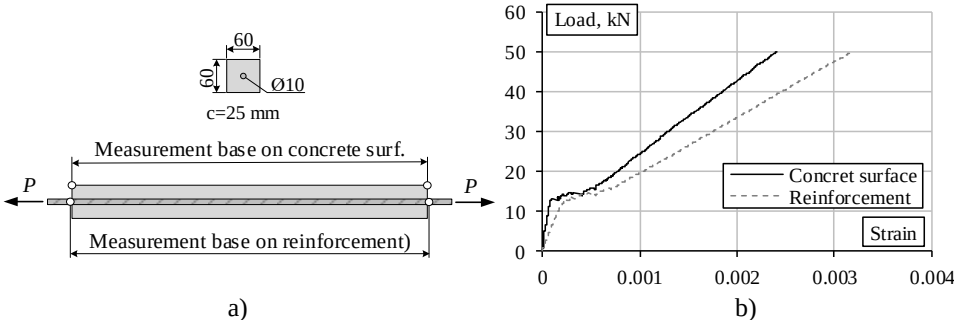

Fig. 1.16. Reinforced concrete tie test: a) test specimen, b) load and average strain relationship of concrete surface and reinforcement

Reinforced concrete tie tests (Fig. 1.16a) performed by Gudonis *et al.* (2014) showed, that average deformations of steel reinforcement and concrete surfaces differs significantly (Fig. 1.16). These results disagree with the general assumption of similarity between average strains of the reinforcement and concrete. Therefore, in order to assess structural behaviour of reinforced concrete, deformation monitoring of concrete surface and reinforcement bar of RC members is essential.

1.3. Numerical Modelling

Structural response of RC elements is an intricate process involving a wide range of effects, such as internal cracking, different strength, deformation and bond characteristics, and time dependent effects. These effects result in a nonlinear behaviour of RC elements. In order to evaluate these effects, one of the most straightforward approach is numerical modelling. The use of finite element (FE) analysis has increased due to progressing knowledge and capabilities of computer software and hardware. Commercial FE packages (ABAQUS, ATENA, DIANA, etc.) now offer a very powerful and general analytical tool for analysis of RC structures (Gribniak *et al.* 2007). In some cases, a numerical approach provides the ability to assess effects, which are even too complicated to be evaluated experimentally.

Common numerical approaches tend to represent reinforced concrete as a continuum media. Cracking of the concrete, however, is a distinctly discontinuous phenomenon. In order to simulate the cracking process, the cracked concrete is modelled as a homogeneous material with degraded mechanical properties. Miglietta *et al.* (2016) introduced a new numerical tool that is capable of predicting the transition between continuum and discontinuum approaches. This tool is based on the assumption that longitudinal cracks propagate around the bar generating a zone where the bond between the reinforcement and the concrete is damaged. In combination with the damage-length model by Maekawa *et al.* (2003), such a modelling approach enables representing the development of the cracks as shown in Fig. 1.17.

Dominguez *et al.* (2005) proposed a numerical model suitable for prediction of the crack patterns. The damage model of the concrete combines two types of the energy dissipation mechanisms: diffused volume dissipation and localized surface dissipation. This approach involves the concrete heterogeneity into the numerical model. The configuration of the crack pattern was changed accordingly. It allows predicting not only mean, but also and maximal crack spacing, even if the exact location of cracks remains unknown. Dominguez *et al.* (2005) also analysed adequacy of bond models by the simulation of concrete tie. The tie was discretized with quadrilateral elements in an axisymmetric formulation: one without interface elements, and the other with non-zero interface elements (Fig. 1.18). For a same imposed displacement, a discretization without joint elements was unable reproducing a realistic crack distribution, while the model with interface elements was found adequate.

Ogura *et al.* (2008) studied the influence of lateral reinforcement, concrete strength and arrangement of the longitudinal bars on the bond splitting failure in RC beams. This study was performed by considering 2D FE model shown in Fig. 1.19a. FE software ATENA was used for this purpose. The tension-softening effect was modelled in the terms of a stress versus crack opening displacement relation. The crack band model (Bažant & Oh 1983) was applied for regularization of the simulated fracture of the concrete. The simulated propagation of the cracks

with load (due to radial stress around the longitudinal reinforcement bars) is shown in Fig. 1.19b. The adequacy of the numerical simulation was proven by using the pull-out tests results.

A remarkable accuracy is characteristic of a meso-scale bond model developed by Michou *et al.* (2015). Unlike other similar approaches, this simplified approach enables modelling different bond stiffnesses due to the rib effect: the reinforcement-concrete interface is modelled as a sequence of constant diameter cylinders with periodic field of regular bond parameters. Bond parameters of a 10 mm deformed steel bar were calibrated by using the pull-out test results. This approach secures the numerical robustness and the convergence of the calculations. It also describes progressive loss of bond stiffness until the maximum bond stress is reached. This allows to obtain inclined cracks at the reinforcement bar ribs and slip between the two materials. Michou *et al.* (2015) successfully validated this model by using experimental results of pull-out tests (Figs. 1.20a and 1.20c). For simplification purposes, the radial stress component (Fig. 1.13d) is neglected in this model. Consequently, it is valid for representing bond behaviour of reinforcement bars, whose diameter is relatively small.

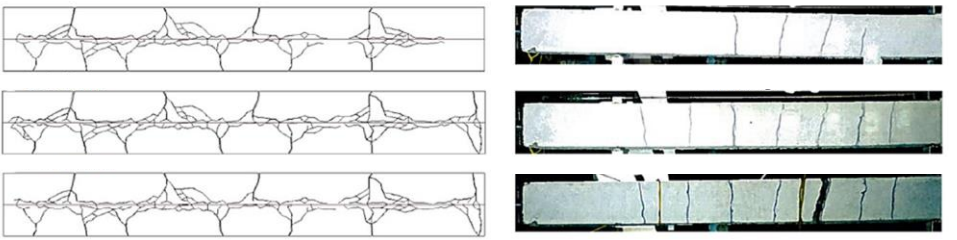

a) b)

Fig. 1.17. Crack patterns: a) numerical simulation and b) experimental view (Miglietta *et al.* 2016)

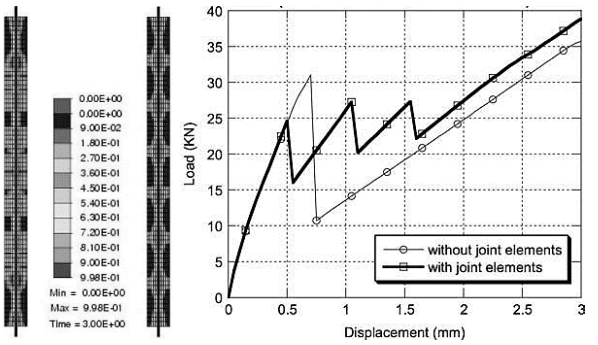

Fig. 1.18. Two discretization types of RC tie: without and with interface elements (Dominguez *et al.* 2005)

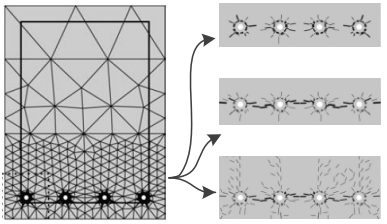

a) b)

Fig. 1.19. Development of the splitting cracks around the reinforcement (Ogura *et al.* 2008): a) finite element model of the cross-section, b) cracking at the different loading stages

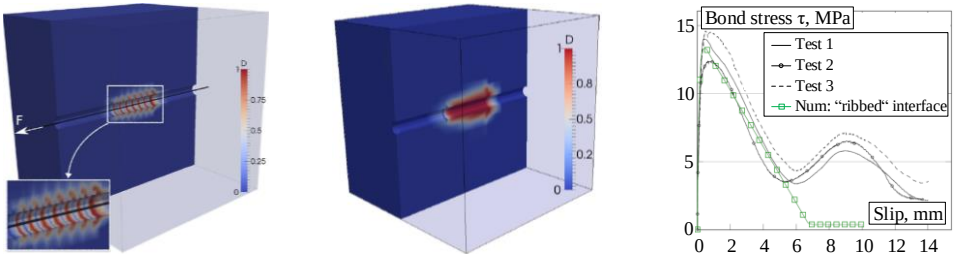

a) b) c)

Fig. 1.20. 3D modelling: damage field of a) the "ribbed" interface, b) classical 3D approach, and c) numerical bond behavior compared to experimental results (Michou *et al.* 2015)

The aforementioned examples demonstrate the potential ability of numerical procedures of performing deformation and cracking analysis of the RC members with intricate internal strain distribution in the concrete. However, numerical approach to the investigation of arrangement effect of bar reinforcement on deformations and cracking of concrete elements requires high performance computing that exceeds the capabilities of the current computer hardware. Therefore, further investigation is necessary to simplify the numerical models (i.e. reduce the calculation demands) and identify the predominant characteristics of the deformation and cracking performance of reinforced concrete members.

Non-linear structural analysis FE software ATENA could be noted as a powerful tool for solution of the deformation and cracking problems. The material model of the cracked concrete, employing the fracture mechanics approach for softening behaviour, is based on the crack band model (Bažant & Oh 1983). The discrete cracks and compression failure zones representing discontinuities are modelled by means of strain localization within bands in FE displacement fields. This model is based on the assumption of equal energy dissipation. A unified approach may be used for tensile and compressive softening (Gribniak *et al*. 2013).

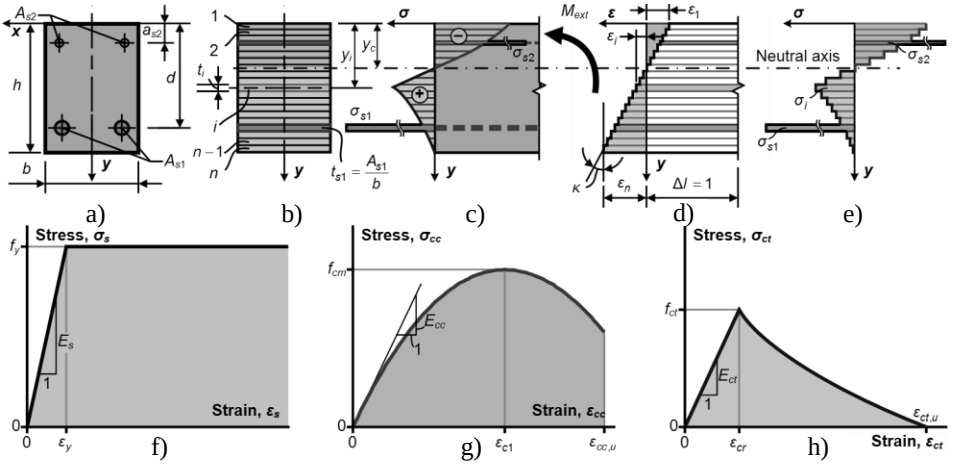

Fig. 1.21. Layer section model: a)–e) the model and constitutive laws for f) reinforcement steel and concrete g) in compression and h) in tension (Gribniak *et al.* 2017)

As an alternative to FE analysis, one of the most straightforward way to investigate deformation behaviour of reinforced concrete member with intricate arrangement of reinforcement bars is the application of layered section model. The modelling aims at predicting the deformation (or average cracking) response for given material laws and sectional characteristics. The deformation (curvature) analysis might be performed based on the model described by Gribniak *et al.* (2017). The calculations are based on the smeared crack approach. The layered section model assumes a linear strain distribution is assumed over the depth of the section.

In order to illustrate the application of the layered section model, a doubly reinforced concrete member subjected to an external bending moment M_{ext} is considered. The cross-section of such a member is presented in Fig. 1.21a. As shown in Fig. 1.21b, the cross-section is divided into n longitudinal layers, corresponding to either concrete or reinforcement. The reinforcement layer thickness t_{s1} (t_{s2}) is taken from the condition of the equivalent area, i.e. relating it to the ratio of respective area A_{s1} (A_{s2}) and the width of the cross-section b_{s1} (b_{s2}) (Fig. 1.21b). The stress-strain state (Figs. 1.21c–1.21e) is approximated using the material models of reinforcement and concrete shown in Figs. 1.21f–1.21h.

Curvature κ and strain ε_i at any layer i (see Fig. 1.21d) are calculated by following formulas:

$$\kappa = \frac{M_{ext}}{IE}; \quad \varepsilon_i = \kappa\left(y_i - y_c\right); \quad y_c = \frac{SE}{AE}; \quad AE = \sum_{i=1}^{n} b_i t_i E_i'; \\ SE = \sum_{i=1}^{n} y_i b_i t_i E_i'; \quad IE = \sum_{i=1}^{n}\left[\frac{t_i^2}{12} + \left(y_i - y_c\right)^2\right] b_i t_i E_i'. \tag{1.3}$$

Here *AE*, *SE* and *IE* are the area, the first and the second moments of inertia of the section multiplied by the secant modulus E'_i. For the given strain ε_i and the constitutive law (Figs. 1.21f–1.21h), the stress σ_i is obtained. The analysis is performed iteratively until equilibrum between the external and internal (calculated) moments is satisfied. The presented numerical approach can be applied for the deformation analysis of plain or fibre reinforced concrete with steel or fibre-reinforced polymer bars. The versatility of this technique is a major advantage with respect to the commonly accepted methods deduced for a separate analysis of each type of the structural reinforcement (Barros & Fortes 2005, Barros *et al.* 2012, 2015, Gribniak *et al.* 2017).

1.4. Design for Serviceability

1.4.1. Deformation Approaches

In the design practice, the deformations of RC members can be predicted by the Eurocode 2 (CEN 2004) and *fib* Model Code 2010 (*fib* 2013) by the equation based on an interpolation between the deformations of uncracked (I state) and cracked (II state) conditions. In state I, both the concrete and reinforcement behave elastically, while in state II the reinforcement carries all the tensile force on the member after cracking. Deformation is expressed as:

$$a = (1-\zeta)\cdot a_I + \zeta \cdot a_{II}. \tag{1.4}$$

Here a is the deformation parameter considered which may be a strain, a curvature, or a rotation (as a simplification, a may also be taken as deflection); a_I and a_{II} are the values calculated for the uncracked and fully cracked conditions, respectively; ζ is an interpolation coefficient (allowing for the effect of tension stiffening at a section). This coefficient indicates how close the stress-strain state is to the condition causing cracking. It takes a value of zero at the cracking moment and approaches unity with increase of load:

$$\zeta = 1 - \beta \cdot (\sigma_{sr} / \sigma_s)^2. \tag{1.5}$$

Here β is a coefficient to account for the influence of the duration of loading or repeated loading on the average strain (= 1.0 for a single or short-term loading and

= 0.5 for sustained loading or multiple cycles of repeated loading); σ_s is the stress in the tension reinforcement calculated on the basis of a cracked elastic section under the load considered; σ_{sr} is the stress in the tension reinforcement calculated on the basis of a cracked elastic section under the loading conditions that cause first cracking. The ratio σ_{sr}/σ_s in Eq. 1.5 may be replaced by M_{cr}/M for flexure and N_{cr}/N for pure tension, where M_{cr} is the cracking moment and N_{cr} is the cracking force. M and N represent the maximum moment and normal force in the load combination considered.

Regarding deformation predictions, Model Code 2010 and Eurocode 2 provide simplified procedures to account for long-term effects due to creep and shrinkage (Balázs *et al.* 2013). In addition to this, simplified method for fully or partially prestressed concrete structures are also provided in RC design provisions.

Gribniak *et al.* (2013) revealed that the accuracy of the Code predictions varied significantly with load intensity and amount of reinforcement. In general, the accuracy improved with increase of load. For the beams with moderate reinforcement ratio (> 0.8%) under service load, the Codes have demonstrated reasonable accuracy acceptable for design purposes. Accuracy significantly decreased for the beams with small reinforcement ratio. A higher prediction variation was observed at early cracking stages, which can be attributed to the random variation of tension strength of concrete. Consequently, there should be a larger safety margin (for the same probability) at low load levels and small reinforcement ratios.

1.4.2. Cracking Approaches

The crack width might be predicted according various international design provisions based on different analytical models. For practical use and design purposes, design codes, such as Model Code 2010 (*fib* 2013) and Eurocode 2 (CEN 2004), provide an explicit formulation of crack spacing and average strain in the steel reinforcement and concrete. For the maximum crack width predictions, the aforementioned provisions account for the average strains of the reinforcement bars and the concrete in tension, modular ratio of reinforcement and concrete, effective area of the concrete in tension, concrete cover, reinforcement bar diameter, bond properties of reinforcement bar, strain distribution along the cross section of the element and loading conditions. Influence of these parameters on the predictions of cracking characteristics according to different design provisions is significantly different; therefore, Model Code 2010 and Eurocode 2 provide contrasting results.

According to Eurocode 2, the maximum crack width can be calculated as following:

$$w_{\max} = s_{r,\max} \cdot (\varepsilon_{sm} - \varepsilon_{cm}). \tag{1.6}$$

Here $s_{r,max}$ is the maximum crack spacing, and ε_{sm} and ε_{cm} are the average strains of the reinforcement bars and the concrete in tension, respectively, over the length $s_{r,max}$. The maximum value of crack width is related to the average value (w_m) by the expression:

$$w_{\max} = \beta \cdot w_m . \tag{1.7}$$

Here β is a statistical coefficient equal to 1.7 (Borosnyói & Balázs 2005, ENV 1991). The difference between the reinforcement and concrete strains (Eq. 1.6) might be calculated by:

$$\varepsilon_{sm} - \varepsilon_{cm} = \sigma_s / E_s - k_t f_{ctm} / (E_s \rho_{s,eff})(1 + \rho_{s,eff} \alpha_e). \tag{1.8}$$

Here α_e is the ratio between E_s and E_c, $\rho_{s,eff}$ is the ratio between A_s, that is the whole area of the longitudinal reinforcement, and A_{ce}, that is the effective area of the concrete in tension. The value of A_{ce} is obtained multiplying the width of the section for $h_{c,eff}$, equal to the minimum value between 2.5(h - d), (h - x)/3 and h/2 (Fig. 1.14). The coefficient k_t is set equal to 0.6 for short-term loading condition and 0.4 for long term or cyclic loading; σ_s is the stress in the tensile reinforcement calculated in a cracked section under the applied external load.

The crack spacing ($s_{r,max}$) can be obtained employing following semi-empirical formulation:

$$s_{r,\max} = k_3 \cdot c + k_1 \cdot k_2 \cdot k_4 \cdot \frac{\varnothing_s}{\rho_{s,eff}}. \tag{1.9}$$

Here c is the cover depth (mm) and $\varnothing_s$ is the bar diameter (mm). The Eurocode 2 suggests to set k_3 equal to 3.4 and k_4 to 0.425; k_1 is a coefficient which accounts for the bond properties of steel bars (= 0.8 for corrugated bars and = 1.6 for smooth bars); k_2 is a coefficient which takes account of the form of strain distribution along the cross section (= 0.5 for bending and = 1 for pure tension).

Model Code 2010 suggests alternative way to obtain maximum crack width:

$$w_k = 2 \cdot l_{s,\max} \cdot (\varepsilon_{sm} - \varepsilon_{cm} - \varepsilon_{cs}). \tag{1.10}$$

Here $l_{s,max}$ is the length (mm) over which slip between concrete and steel occurs. ε_{sm} and ε_{cm} are the average strains of steel bars and concrete, respectively, over the length $l_{s,max}$. ε_{cs} is the strain of the concrete due to free shrinkage. $l_{s,max}$ can be calculated as:

$$l_{s,\max} = k \cdot c + \frac{1}{4} \cdot \frac{f_{ctm}}{\tau_{bm}} \cdot \frac{\varnothing_s}{\rho_{s,eff}}. \tag{1.11}$$

Here k is the empirical parameter to take the influence of the concrete cover into consideration. Balázs *et al.* (2013) referred $k \cdot c$ to the load transfer of bond forces from the rebar surface to the concrete surface. The relative mean strain in Eq. 1.10 can be calculated as:

$$\varepsilon_{sm} - \varepsilon_{cm} - \varepsilon_{cs} = (\sigma_s - \beta \cdot \sigma_{sr}) / E_s + \eta_r \cdot \varepsilon_{sh}. \tag{1.12}$$

Here σ_s is the stress in the reinforcement bar at a cracked section, in which the effect of fibres needs to be taken into account; σ_{sr} is the maximum steel stress in a cracked section at the crack formation stage, which can be calculated according following expression:

$$\sigma_{sr} = f_{ctm} \cdot (1 + \rho_{s,eff} \cdot \alpha_e) / \rho_{s,eff}. \tag{1.13}$$

The stress τ_{bm} is equal to 1.8 f_{ctm} for stabilized cracking in both short and long term loading. β is equal to 0.6 and 0.4, for short and long term loading, respectively. η_r is equal to 0 or 1, for short and long term loading, respectively.

However, the adequacy of Model Code 2010 and Eurocode 2 provisions for the calculation of crack width and crack spacing are questionable in terms of the effects related with the effective area of the concrete in tension, reinforcement bar diameter, and cover depth (Windisch 2016). Regarding the length $l_{s,max}$ over which slip between concrete and steel occurs (Eq. 1.11) or crack spacing $s_{r,max}$ (Eq. 1.9) some researches doubted that $Ø_s/\rho_{s,eff}$ parameter is suitable for these expressions and has sufficient influence (Windisch 2016, 2017, Kaklauskas 2017). Borges (1965) concluded that a very weak correlation between crack spacing and $Ø_s/A_{s,eff}$ parameter is obtained in case concrete cover is disregarded. Moreover, Beeby (2004) complied with this statement, that crack spacing is independent of parameter $Ø_s/\rho_{s,eff}$, and showed that crack spacing depends only on the distance of the crack from the nearest reinforcing bar. These uncertainties encouraged to investigate the influence of cross-section parameters and mechanical properties of RC members (including effects of bar reinforcement arrangement) to cracking and deformation behaviour of reinforced concrete. Therefore, the adequacy of the Codes issue is identified as important for analysis in the present thesis.

1.5. Conclusions of Chapter 1 and Formulation of the Objectives of the Thesis

Based on the literature review, the following conclusions can be drawn:

1. The deformation and cracking response of RC members is governed by the tensile properties of concrete, the elastic properties of reinforcement, the bond characteristics between concrete and reinforcement and the

cross-sectional parameters of RC members. Heterogenity of concrete, external and internal cracks, bond behaviour are responsible for the scatter of test results of reinforced concrete members. However, demand to predict the serviceability properties requires simple and straightforward approach for cracking response. In order to determine part of the concrete surrounding the reinforcement that is considerably influenced by the force transfer, concrete effective in tension is applied.

2. Proper selection of testing layout of RC members might significantly increase the adequacy of interpretation of the structural response. Following the concept commonly accepted in design codes, the area of concrete effective in tension is considered to reperesent an equivalent element with unified material and deformation characteristics contributing in the same average manner.
3. Bond behaviour is an important factor of "effectiveness" of the concrete; however, appearance of multiple bar reinforcement (in the tension zone) complicates the behaviour of the concrete. Therefore, the effect of the arrangement of the bars on the overall stiffness and the cracking behaviour of the tensile zone must be investigated.
4. In order to assess the effect of arrangement of bar reinforcement on the area of concrete effective in tension, deformation monitoring of concrete surface and reinforcement bar of RC members is essential.
5. The numerical modelling might be an appropriate way to perform deformations and cracking analysis of the RC members with elaborate internal strain distribution in the concrete. The numerical approach provides the ability to evaluate intricate load transfer and internal cracking phenomena and assess effects, which are too complex as to be evaluated experimentally.

The object of research is concrete elements with bar reinforcement subjected to short-term loading. The study is dedicated for investigation of effect of arrangement of bar reinforcement on deformations and cracking of concrete elements. In order to achieve the objective, the following tasks are formulated:

1. To identify the governing characteristics of the deformation and cracking performance of reinforced concrete members.
2. To perform experimental and numerical analysis of arrangement effect of bar reinforcement on deformations and cracking behaviour of concrete elements subjected to short-term loading.
3. To verify adequacy of the current design code predictions of deformations and cracking behaviour of reinforced concrete members.
4. To propose several alternative layouts of reinforcement bar ensuring the control of the stiffness and cracking behaviour of concrete elements under serviceability conditions.

2

Experimental Investigation on Deformation and Cracking of Reinforced Concrete Elements

This chapter experimentally investigates bar reinforcement arrangement effect on deformations and cracking behaviour of concrete elements. The chapter presents test results of flexural and tensile elements with various cross-section parameters and loading layouts. Representativness condition of test specimen has been proposed. An iterative procedure of reduction of the concrete surface deformation gauge length has been proposed for localizing the end effect in the ties. Chapter 2 also verifies adequacy of cracking predictions by design codes. This chapter includes the material presented in journal publications Gribniak *et al.* (2016, 2017a), Rimkus & Gribniak (2017a, 2017b), Meškėnas *et al.* (2017), and conference proceedings Rimkus *et al.* (2015, 2016), Rimkus & Vilėniškytė (2015) and Gudonis *et al.* (2014).

2.1. Reinforcement Materials

Due to relatively high strength and good ductility, steel is the most widely used reinforcing material for concrete structures. As a corrosion-resistant alternative to

steel reinforcement, fibre reinforced polymer (FRP) composites have been used in concrete structures quite frequently in recent years. Considering the most common materials of reinforcement, steel and glass fibre reinforced polymer (GFRP) bars were used in present investigation.

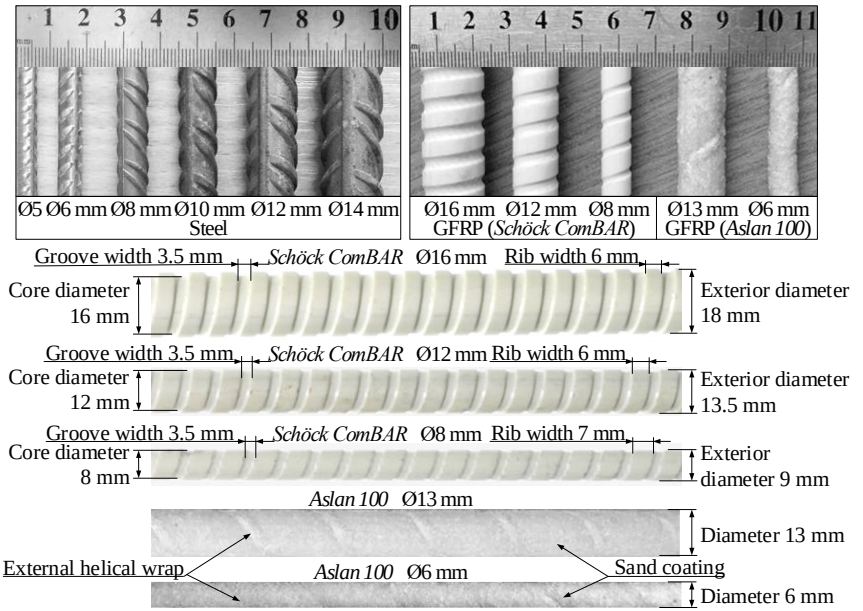

Fig. 2.1. Surface characteristics of the reinforcement bars

Table 2.1. Mechanical properties of the reinforcement bars

Material	Used for	Ø, mm	E_r, GPa	f_y, MPa	f_u, MPa
Steel	Beams	6	223.5	585.4	642.5
		8	209.8	589.0	625.1
		10	209.9	578.1	658.5
		14	210.5	632.3	695.1
		22	199.3	551.1	553.0
	Ties	5	200.7	503.9	600.1
		6	203.6	504.7	606.3
		8	197.1	473.9	621.2
		10	199.5	510.1	650.3
		12	202.8	543.7	639.3
		14	205.3	558.7	625.7
GFRP (*Schöck ComBAR*)	Beams / Ties	8	65.1	–	1491
		12	64.7	–	1468
		16	65.1	–	1491
GFRP (*Aslan 100*)	Ties	6	46.0	–	896
		13	46.0	–	758

All concrete specimens, considered in this investigation, were reinforced using different combinations of deformed 5, 6, 8, 10, 12, 14, 22 mm diameter steel (Fig. 2.1a) and 6, 8, 12, 16 mm diameter GFRP (Fig. 2.1b) bars. To determine mechanical properties of the steel, three samples of each bar diameter were tested. The GFRP bars were not tested assuming the mechanical properties specified by the producers (Weber 2006, Hughes Brothers 2011). The mechanical properties of the reinforcement are presented in Table 2.1. Schöck ComBAR reinforcement are the most commercially used GFRP bars due to the ribbed surface which corresponds the adhesive properties of ribbed steel bars (Fig. 2.1c). On the contrary, the adhesion between Aslan 100 bar and concrete is ensured by the sand coated surface (Fig. 2.1c).

2.2. Flexural Elements

This section investigates the effects of the arrangement of tensile reinforcement to the flexural stiffness and cracking of concrete beams. For the quantification purpose, bending tests of nine specific beams with different arrangements of reinforcement in the tension zone are considered. Test specimens were selected from a large experimental program performed by Gribniak *et al.* (2011). This experimental campaign involved more than 80 RC beams with various cross-section parameters, arrangement and material of the reinforcement bars. The previous study has indicated almost identical deformation behaviour of the twin-specimens. Therefore, the present study involves only one sample of each type of the beams. Selected beams were reinforced with steel or GFRP (produced by *Schöck*) bars using two principal layouts. The first group of specimens had a conventional reinforcement layout – the bars were distributed in a single layer with 20 mm cover. The second group contains specimens with the same reinforcement ratio (as in the conventional beams), but with non-conventional distribution of the tensile reinforcement arranged in three layers. Gribniak *et al.* (2013) and Meskenas *et al.* (2017) investigated the effect of fibre reinforcement to the serviceability properties of RC beams. The previous studies compared serviceability of the beams included in the first group of the present study with the counterparts (with identical arrangement of the bars) made of fibre reinforced concrete. The fibre effect to increase of the cracking resistance was found being very similar to that observed in this study in the beams of the second group (with reinforcement distributed in several layers). This inference allows rising a hypothesis about similar efficiency of increasing number of the bars and the dispersive fibre reinforcement.

The previous study (Gudonis *et al*. 2014) revealed no slip of GFRP bars at the deformation levels characteristic of the service conditions of RC elements. This inference makes possible the comparative analysis of serviceability (cracking and deformation) properties of the beams reinforced with steel and GFRP bars.

For the purpose of comparative analysis, all test specimens had identical concrete cross-sections with a similar concrete strength f_{cm} and two different reinforcement ratios p (0.6% and 1.0%). To evaluate differences in the deformation and cracking behaviour of the selected beams, the predictions by Model Code 2010 (*fib* 2013) were set as the reference assuming that a prediction is safe if the code overestimates the experimental value.

2.2.1. Description of Beam Specimens

The main parameters of the beams are listed in Table 2.2 with sectional notations evident from Figure 2.2. Other parameters presented in the table are the average compressive strength of the concrete Ø150×300 mm cylinder at 28 days ($f_{cm,28}$) and at age (t) of testing (f_{cm}).

The presented data is part of large experimental investigation (Gribniak *et al.* 2011) of concrete shrinkage effect on cracking resistance and deformations of concrete structures. Nine beams with different arrangements of reinforcement were selected from experimental database of aforementioned investigation. The selected specimens were produced using the same concrete grade (C 37) expressed in two concrete mixes given in Table 2.3 and denoted as *Mix A* and *Mix B*. Nomenclature of the specimens characterizes type of the element and composition of the reinforcement, including the reinforcement ratio and material. The letter "S" defines "Beam"; the first number corresponds to the reinforcement ratio p ("2" refers to $p \approx 0.6\%$ and "1" to $p \approx 1.0\%$); "nm" refers to non-metallic (GFRP) reinforcement. The experimental beams were cast using steel formworks. The beams were unmolded in 2–3 days after casting. The specimens were cured at an average relative humidity (*RH*) of 73% and a temperature of 20 °C.

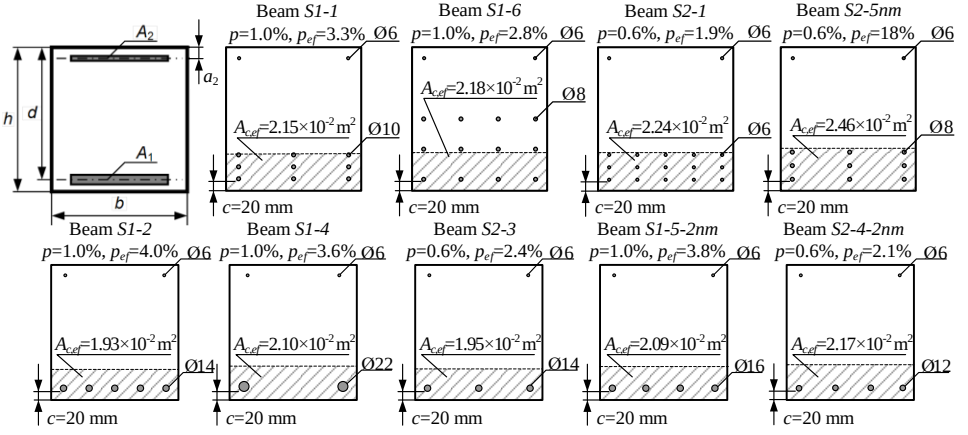

Fig. 2.2. Cross-sections of the beams with different arrangement of reinforcement bars

Table 2.2. Main characteristics of the test specimens

Specimen	h	d(*)	a_2	b	A_1	A_2	np	$f_{cm,28}$	f_{cm}	t	Mix
	mm				mm^2		%	MPa		days	
S1-1	299	248	25	282	695.9	56.6	5.70	45.52	49.7	75	B
S1-6	303	217	37	271	603.2	56.6	5.76	39.55	43.0	256	A
S2-1	301	254	30	279	429.9	56.6	3.60	45.52	49.4	73	B
S2-5nm	302	246	26	276	452.4	56.6	1.12	41.29	56.0	167	A
S1-2	300	273	29	284	776.8	56.6	5.62	45.52	49.4	67	B
S1-4	300	267	24	280	760.0	56.6	5.47	45.52	49.4	68	B
S1-5-2nm	305	275	33	277	804.2	56.6	1.89	38.37	44.6	236	A
S2-3	300	272	29	282	466.1	56.6	3.44	42.51	48.1	66	B
S2-4-2nm	303	272	27	276	452.4	56.6	1.06	47.21	49.4	37	A

(*) The effective depth is given with respect to the centroid of tensile reinforcement.

Table 2.3. Mix proportions, kg/m^3

Material	*Mix A*	*Mix B*
Sand 0/4 mm	910 ± 2%	905 ± 2%
Crushed aggregate 5/8 mm	470 ± 2%	388 ± 1%
Crushed aggregate 11/16 mm	470 ± 2%	548 ± 1%
Cement CEM I 42.5 N	415 ± 1%	400 ± 0.5%
Water	174 ± 5%	124 ± 5%
Concrete plasticizer *Stachement 2067*	3.32 ± 2%	–
Concrete plasticizer *Muraplast FK 63.30*	–	2 ± 2%

The beams with a nominal length of 3280 mm were tested under a four-point bending scheme with 1000 mm shear spans as shown in Figure 2.3 that also gives the strain gauge position. The specimens were loaded with a 1000 kN hydraulic jack in a stiff testing frame. The test was performed with small increments (2 kN) and paused for short periods (about 2 minutes) to take readings of the gauges and to measure crack development. On average, it took 50–80 load increments with a total test duration of 3 hours. The testing equipment acting on the beam weighed 2.3 kN and summed up with the beam's own weight induced a 3.5 kNm bending moment at the mid-span.

Moment-curvature diagrams were obtained in two ways: from deflections and from concrete surface strains, both recorded in the pure bending zone. Concrete surface strains were measured throughout the length of the pure bending zone, using mechanical 200 mm gauges. As shown in Figure 2.3 (view "A"), four continuous gauge lines (with five gauges in each line) were located at different heights. The two extreme gauge lines were placed along the top and the bottom reinforcement whereas two other lines were located 60 mm off these lines. To measure deflections, linear variable differential transducers (*L1–L8*, see Figure 2.3) were placed beneath the soffit of each of the beams. Previous studies (Gribniak *et al.* 2009, 2013, Stramandinoli & Rovere 2008, Caldentey & Peiretti

1999) revealed good agreement between the moment-curvature diagrams obtained from the deflection of the pure bending zone and strain measurements. In the present study, the moment-curvature response of the beams was assessed using the surface strains averaged along each of the gauge lines shown in Figure 2.3. Following the methodology detailed in references (Gribniak *et al.* 2009, 2013), the curvature averaged through the pure bending zone is calculated as:

$$\kappa = \frac{1}{6}\sum_{l=2}^{4}\sum_{k=1}^{l-1}\frac{D_k - D_l}{h_{kl}}. \tag{2.1}$$

Here D_k and D_l are the averaged strains along k and l gauge lines (1st…4th lines, Figure 2.3), respectively; h_{kl} is the distance between the lines (k, $l = 1…4$, $k \neq l$). Figure 2.4 shows the obtained moment-curvature diagrams.

The crack pattern was marked during the tests at the side of the beams, opposite to that where surface deformation measurements were taken (Figure 2.4). At the chosen loading levels, the crack width was measured at the gravity centre of the tensile reinforcement using a 50 magnification (50×) optical microscope. Additionally, development of the visible cracks was located specifying the crack shape under the particular loading level. Figure 2.5 represents the final crack pattern of the beams, indicating the load levels for which the cracks reach a given web depth, thereby obtaining a representation of the crack development with load.

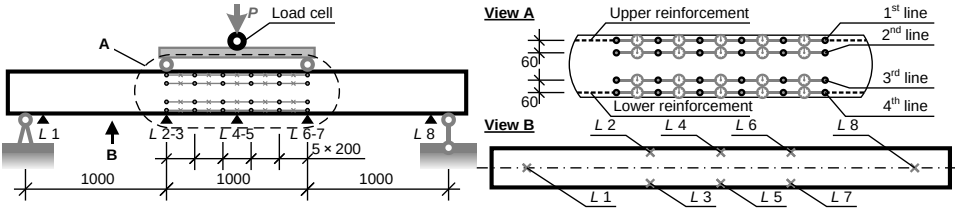

Fig. 2.3. Loading system and arrangement of test devices

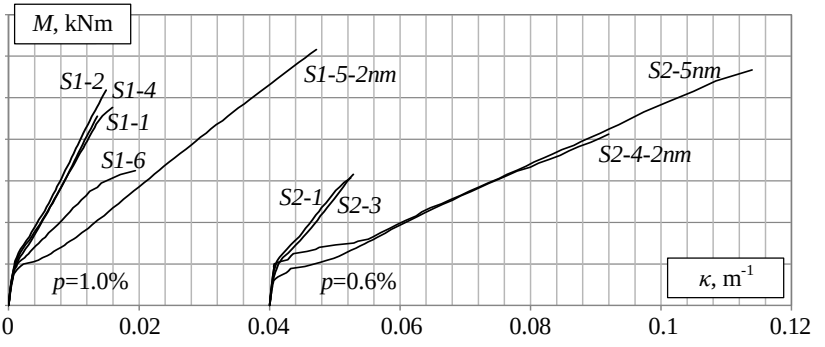

Fig. 2.4. Moment-curvature response of the beams

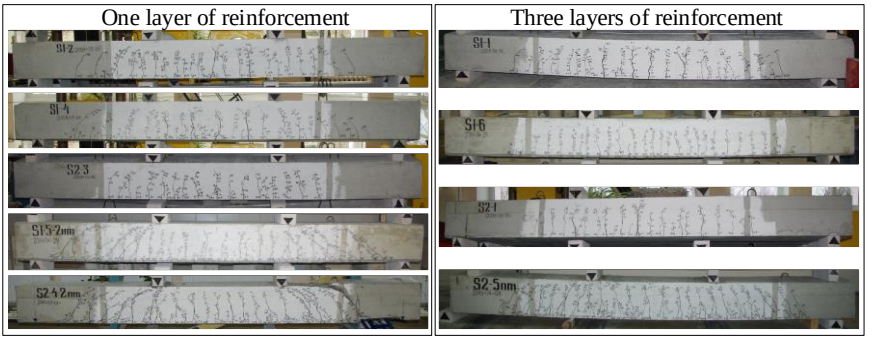

Fig. 2.5. Final crack pattern

To investigate the effects of bar reinforcement on deformation and cracking behaviour of beams made of SFRC, several beams with the same section parameters as shown in Fig. 2.2 were made using steel fibres as additive for the concrete. Meskenenas *et al.* (2017) and Gribniak *et al.* (2013) reported results of the structural tests. The brief discussion of the relevant results in the context of the present research is given in Section 3.1.

2.2.2. Deformation Analysis

In Figure 2.6, Model Code 2010 (*fib* 2013) predictions are compared with the experimental moment-curvature diagrams. Two types of behaviour can be observed comparing the experimental and predicted diagrams: with increasing load, beams with one layer of reinforcement exhibit a progressive degradation of the stiffness, with respect to values predicted by MC 2010, whereas the actual stiffness of the beams with multiple layers of the bars does not exhibit such a degradation until failure. The differences in deformation behaviour of the beams can be explained by decisive difference in the bond characteristics, which are related with an increase of the bonded area and diverse deformations of the bars distributed in several layers. This aspect might be very important at the crack formation stage, where beams with the alternative reinforcement layouts are capable of resisting development of the cracks. As can be observed in Figure 2.2, all beams had a constant nominal cover (c = 20 mm), which did not secure sufficient confinement causing initiation of splitting cracks and, consequently, degradation of overall stiffness. On the contrary, a large number of bars closely distributed in the tensile zone safeguarded high relative stiffness of the cracked specimen throughout all loading stages. Similar results were obtained in the tests of tensile members (Rostasy *et al.* 1976, Purainer 2005, Rizkalla & Hwang 1984, Williams 1986) and beams (Jakubovskis *et al.* 2014, Gribniak *et al.* 2013, Calderón & Fernández 2010, Gribniak *et al.* 2015) reinforced with a large number of closely spaced bars.

Such members have demonstrated significant increase of stiffness of the cracked section (with respect to the specimens with conventional arrangement of the tensile reinforcement).

To assess differences in the stiffness, the curvature predictions by the MC 2010 were used as reference. The curvature results in different specimens were compared using the relative term:

$$\Delta\kappa = \frac{\kappa_{obs} - \kappa_{MC}}{\kappa_{obs}}. \tag{2.2}$$

Here κ_{obs} and κ_{MC} are the observed and calculated (reference) curvatures, respectively.

The deformation behaviour of the test specimens was investigated at four reference levels of loading intensity related to the reference ultimate bending moment M_u. This value was calculated assuming the strength limit of 500 MPa for the bar reinforcement. Table 2.4 shows the characteristic load levels and the corresponding values of the relative curvature, $\Delta\kappa$, from Equation (2.2). Additionally to the reference load levels, the predictions at the service load, M_{ser}, were analysed. This loading level is of vital importance in the design for serviceability (Jakubovskis *et al.* 2014, Debernardi *et al.* 2011). As can be observed from Table 2.4 and Figure 2.6, the service load is within the bounds described by "3" and "4" reference points.

In Table 2.4, the beams are presented in two groups – the first four specimens with three layers of the tensile bars are included in *Group I*. Whereas, *Group II* represents the beams with the reinforcement distributed in one layer (Figure 2.6).

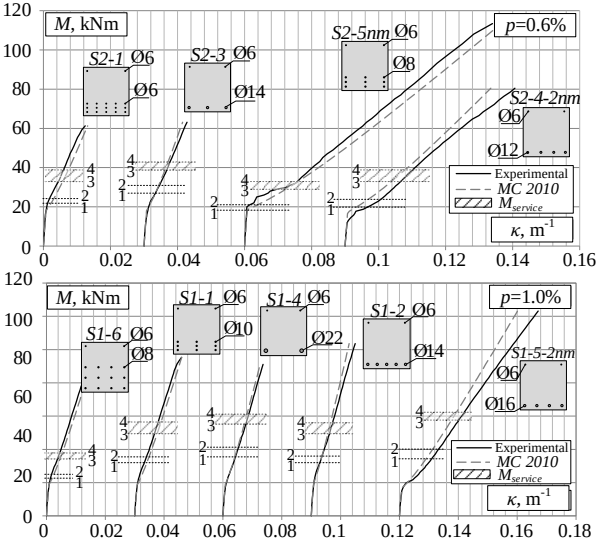

Fig. 2.6. Comparison of experimental and predicted moment-curvature behaviour

It is evident that the deformation behaviour of the beams from these two groups are different. The author's viewpoint is that a prediction is safe, if $\Delta\kappa \leq 0$, since the physical nature of the ratio $\Delta\kappa$ means that the code overestimates the deflection in such cases. MC 2010 overestimated deformations (curvatures) of the elements from the first group at all considered loading levels: at the service load, the overestimation of the predictions (the prediction safety) varies from 14% to 32%. On the contrary, deformations of the beams with conventional distribution of the reinforcement (in one layer with minimal cover) were underestimated almost at all loading stages: at the service loading, deficiency of the predictions was found equal to 7–15%. The obvious differences of the predictions between the groups inspire a modification of the deflection prediction for the specimens with three layers of the reinforcement. The modification is provided in Subsection 3.1.

Table 2.4. Relative curvature prediction percentage, $\Delta\kappa$ (loading levels shown in Figure 2.6)

Group	Beam	M_u, kNm	Loading level				
			1 0.32–0.33·M_u	2 0.36–0.39·M_u	3 0.48–0.54·M_u	4 0.58–0.63·M_u	M_{ser} 0.55·M_u
I	*S1-1*	92.24	–36.3	–23.7	–14.2	–13.0	–13.6
	S1-6	59.95	–92.9	–71.9	–34.6	–30.2	–32.2
	S2-1	60.56	–62.3	–84.6	–35.3	–25.8	–29.7
	S2-5nm	52.74	–15.2	–85.9	–49.2	–4.7	–20.7
II	*S1-2*	122.89	3.0	8.6	10.4	11.1	10.8
	S1-4	103.52	3.7	4.6	6.4	6.9	6.7
	S1-5-2nm	101.48	18.6	16.7	12.3	12.2	12.2
	S2-3	75.71	–2.1	1.4	7.6	7.9	7.8
	S2-4-2nm	58.77	57.1	41.5	18.3	11.9	14.9

2.2.3. Cracking Analysis

2.2.3.1. Crack Distances

The distance between cracks is the governing parameter for the crack width prediction. However, assessment of crack distances in some cases is not so straightforward. At different loading stages, cracks appear with different spacing, length, and width. The crack opening varies not only between the cracks, but it also might vary from zero to w_{max} (maximum width) in the same crack. Furthermore, a complex topology of the crack surface often does not allow identifying a unique value of the crack width (i.e. a small change of the monitoring position might lead to noticeable change of the identified opening).

It should be kept in mind that the general idea of the Codes (MC 2010 and EC2) is to formulate a mathematical model (consistent with experimental evidence) that provides a reasonable reliability of the predictions of the maximum crack spacing that can potentially occur. For both standards, the maximum crack

spacing is related with the transmission length. Since this parameter was not determined experimentally, the observed results might be considered as a rough approximation to the cracking problem. Moreover, experimental estimation of the cracking parameters might be subjective. To avoid subjectivity of the judgement, a numerical procedure for determination of the distances between cracks has been developed. The location of a crack is defined as the centroid of the projection of the crack points on the longitudinal axis of the specimen. The current analysis considers the cracking behaviour in the pure bending zone. Figure 2.7 sketches the procedure for obtaining the crack distances that consists of following steps:

1. At a given loading level, the crack distribution scheme is made using the crack patterns (Figure 2.5).
2. Using horizontal lines spaced at a constant distance (in the considered situation, it was equal to 5 mm), the schematic cracks are "trimmed" generating an array of the cracking points.
3. The origin of the longitudinal axis *x* is associated with the boundary of the pure bending zone. The collection of the projections of the generated array of the cracking projections produces the dataset for further clustering.

The agglomerative hierarchical clustering technique was chosen for identifying the cracking points (projections) that closely resemble one another. The clusters, related with location of the discrete cracks, were formed using the linkage function described as a shortest Euclidean distance between the elements. The 20 mm distance was chosen as a threshold for "cutting" the data into clusters. Application of the clustering technique to the datasets generated at the different loading levels results in the diagram that represents evolution of the crack distance with increasing load. The evolution diagrams of maximum crack distance are shown in Figure 2.8 for all beams. Similar graphs for the average crack distance are presented in Figure 2.9. The delayed crack formation can be observed from both figures. This effect is more evident for the beams with relatively low amount of the reinforcement (p = 0.6%). The delayed cracking is closely related to the increment in stiffness, evidenced in Subsection 2.2.2.

For the assessment of differences in the crack distances in the beams with one and three layers of reinforcement, the predictions by MC 2010 were used as a reference. The distance between the cracks can be obtained as following:

$$s_{r,\max} = 2 \cdot \left(k \cdot c + \frac{f_{ctm} \cdot \varnothing_s}{4 \cdot \tau_{bms} \cdot \rho_{s,ef}} \right). \tag{2.3}$$

Here k is an empirical parameter to take the influence of the concrete cover into consideration; as a simplification, k=1.0 can be assumed; c is the concrete cover; f_{ctm} is the mean axial tensile stress of concrete; τ_{bms} is the mean bond strength between steel and concrete, τ_{bms}=1.8·f_{ctm} for stabilized cracking stage for short term,

instantaneous loading; $Ø_s$ is the nominal diameter of steel bar; $\rho_{s,ef}$ is the effective reinforcement ratio.

The clustered and the calculated, from Equation (2.3), maximum crack distances at the service load are compared in Table 2.5. The service load is assumed as 55% of the theoretical ultimate bending moment of the beam.

As can be observed in Figures 2.6, 2.8 and 2.9 for all beams, the stabilized cracking stage was achieved before the service load (the crack stabilization is represented by vertical lines in Figs. 2.8 and 2.9). In Table 2.5, the relative predictions Δs were calculated by Equation (2.2), where, instead of the curvatures, the corresponding values of the maximum crack distances, i.e. experimental ($s_{r,obs}$) and calculated ($s_{r,MC}$) are considered. Similarly to the curvature analysis, Table 2.5 reveals differences in the relative predictions Δs. From this table, three important observations can be made:

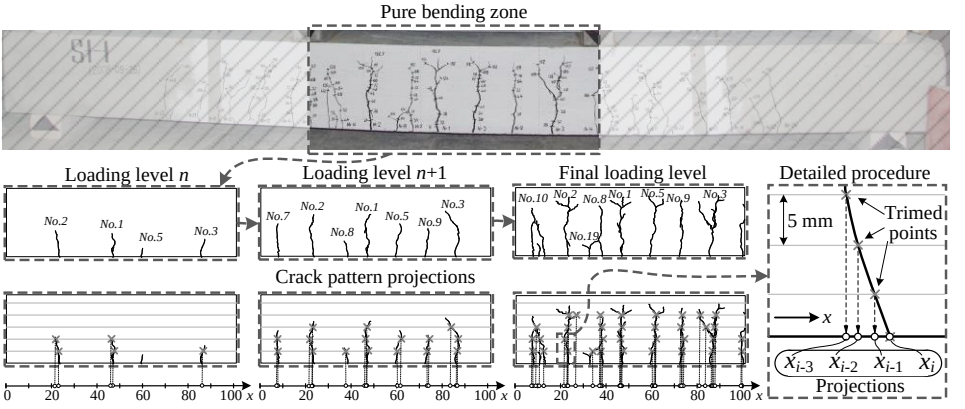

Fig. 2.7. Extraction of the data-points for the crack projections clustering procedure

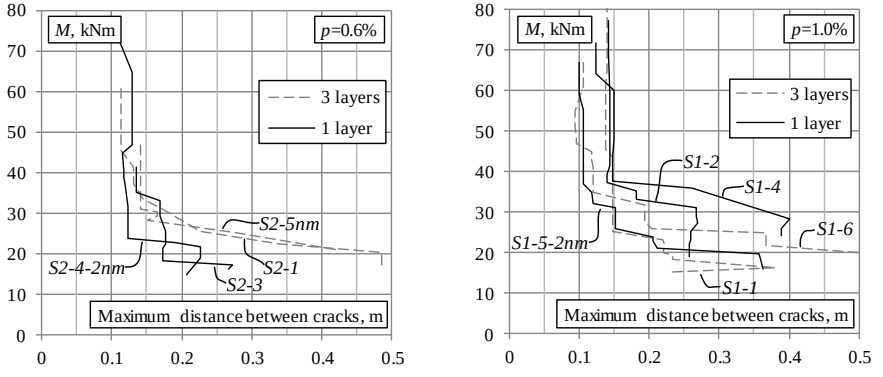

Fig. 2.8. Variation of maximum crack distance with load for the beams with one and three layers of reinforcement

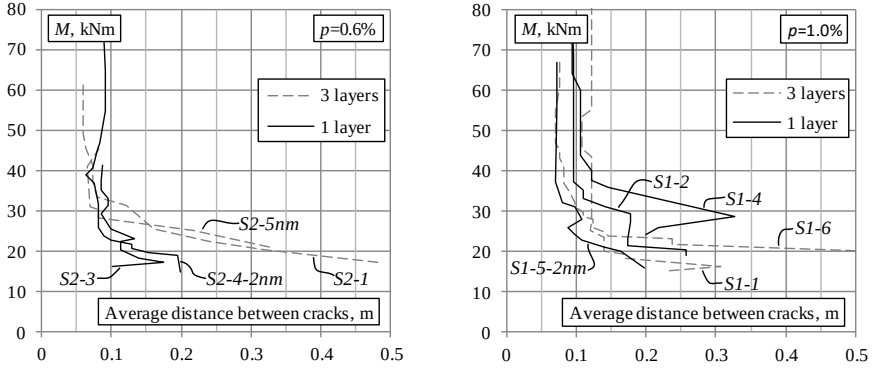

Fig. 2.9. Variation of mean crack distance with load for the beams with one and three layers of reinforcement

1. There is a general tendency that the predicted maximum crack distances are smaller in the beams of the first group having noticeably smaller diameters of the bars compared to the reference beams of the second group. Despite of different area of location of the tensile bars (Figure 2.2), the differences between the effective heights, h_{ef}, are not that significant as they were established from two alternative governing conditions given in Table 2.5. In other words, the introduction of multiple layers of reinforcement does not significantly affect the effective reinforcement ratio. Thus, the predictions by the MC 2010 are mainly controlled by the diameter of the bars.
2. Differences in the experimentally observed maximum crack distances between the beams of the two groups are less significant. In contrast to the predictions, the conventionally reinforced beams displayed smaller crack distances than the ones in the equivalent specimens with three layers of the reinforcement. Providing the total area of the tensile reinforcement is constant, distribution of bars in multiple layers resulted in a delayed stabilized cracking stage. Consequently, the MC 2010 prediction adequacy seems to be dependent on the layout of the tensile reinforcement.
3. The predictions for the conventionally reinforced elements noticeably overestimate the experimental values. The number of the tested specimens, however, is not sufficient to reach a reliable conclusion about the adequacy of the predictions. Further research is needed to investigate the suitability of the equations proposed by the MC 2010.

A relation between the maximum and average crack distances (Figures 2.8 and 2.9) is another important parameter that needs a clarification. The respective values of the crack distances determined using the proposed clustering procedure at loading levels “3” and “4” (Figure 2.6) are given in Table 2.6. In Table 2.6, the experimental data are ranged in accordance with the ratio presented in the last column. In the considered cases, this ratio varies from 1.3 to 2.0 and is equal to

1.5 in average. This result is in agreement with the findings of other studies suggesting the ratio of maximum and mean crack spacing to be between 1.3 and 1.7 (Balázs *et al.* 2013). This ratio differed for the members with different reinforcement ratio, on average being 1.7 and 1.4, respectively for the cases of $p = 0.6\%$ and 1.0%. However, due to a limited number of test specimens and interval of the reinforcement ratio, these observations should be understood more as insights for further research than as general evidence.

It should be also kept in mind that the above results were obtained based on the crack distances that were established using the clustering technique. For sake of illustration, a simple approach was presented in the study that was not taking into account the height of the cracks. Thus, the secondary cracks were not excluded, possibly giving reduced values of crack distances. Future research should include filtering technologies that will be able to suppress minor inputs of the clustered data. In practical terms, it would include accounting for the height of the cracks as well as possibly their width.

Table 2.5. Experimental and calculated maximum distances between cracks, determined at the service load

Group	Beam	Ø, mm	p_{ef}, %	h_{ef}*, mm		$s_{r,max}$, mm		Δs, %
				2.5(h-d)	(h-x)/3	Experimental	Calculated	
I	*S1-1*	9×Ø10	3.3	–	76.3	137.5	124.6	9.4
	S1-6	12×Ø8	2.8	–	80.4	194.1	120.3	38.0
	S2-1	15×Ø6	1.9	–	80.5	168.3	128.2	23.9
	S2-5nm	9×Ø8	1.8	–	89.4	151.4	161.0	-6.3
II	*S1-2*	5×Ø14	4.0	68.0	–	141.7	137.7	2.8
	S1-4	2×Ø22	3.6	–	75.2	125.1	209.0	-67.1
	S1-5-2nm	4×Ø16	3.8	75.6	–	105.7	155.7	-47.3
	S2-3	3×Ø14	2.4	69.0	–	134.1	203.9	-52.0
	S2-4-2nm	4×Ø12	2.1	78.5	–	122.3	199.8	-63.4

*The effective height is associated with the corresponding governing criteria.

Table 2.6. The cracking results (distances) corresponding to the "3" and "4" loading steps highlighted in Figure 2.6

Group	Beam	p, %	p_{ef}, %	Ø/p_{ef}	$s_{r,max}$, mm		$s_{r,m}$, mm		$s_{r,max}/s_{r,m}$	
					Step 3	Step 4	Step 3	Step 4	Step 3	Step 4
I	*S1-1*	1.01	3.28	3.05	137.5	137.5	108.7	108.7	1.26	1.26
II	*S1-4*	1.02	3.61	6.09	125.1	125.1	93.9	93.9	1.33	1.33
I	*S1-6*	1.03	2.77	2.89	192.8	120.3	98.5	89.6	1.96	1.34
II	*S1-5-2nm*	1.06	3.84	4.17	105.7	105.7	69.4	72.6	1.52	1.46
II	*S2-3*	0.60	2.37	5.90	134.1	134.1	85.0	87.0	1.58	1.54
II	*S2-4-2nm*	0.60	2.09	5.75	122.3	119.1	81.8	75.0	1.50	1.59
II	*S1-2*	0.99	3.98	3.52	141.7	142.3	95.0	86.4	1.49	1.65
I	*S2-1*	0.60	1.89	3.17	168.3	130.8	120.4	74.1	1.40	1.77
I	*S2-5nm*	0.67	1.84	4.35	151.4	142.0	81.6	69.4	1.86	2.04

2.2.3.2. Crack Width

Stochastic nature and complex topology of cracks, mentioned in the beggining of this subsection, complicate crack width analysis. Furthermore, flexural cracking is dependent on the level of the measurements (within the height of the section) (Borosnyói & Snobli 2010). In this context, reliability of crack width measurements is rather low in comparison to the experimental data considered in the previous subsections. Therefore, this subsection presents more a qualitative than a quantitative assessment of the results.

The analysis of the location of the maximum crack openings and the corresponding distances between the cracks is the topic of the following investigation. This analysis is performed under the same characteristic loading levels as for the deformation analysis. Due to their time-consuming character, crack measurements were performed for a limited number of loading stages. Thus, the nearest crack width measurement was attributed to the characteristic stage under consideration. This analysis deals with measurements of the cracks located in the pure bending zone. At each loading stage, the five cracks with the maximum crack openings are considered. This experimental data is presented in Table 2.7; the respective crack patterns are shown in Figure 2.10. Characteristics presented in Table 2.7 are following: $w_{(1)–(5)}$ – crack width of five maximum cracks, crack with the largest opening is referred to as $w_{(1)}$; w_m(cracks) – average crack width and the number of considered cracks (provided in the brackets); w_{MC} – maximum crack predictions by the Model Code.

It is important to note that Tables 2.5 and 2.7 indicate contrasting results: although the observed crack distances for the stabilized cracking stage (0.5–0.6·M_u) of the unconventionally reinforced beams are larger, their maximum crack openings are smaller than in the corresponding specimens with one layer of the bars. The maximum crack widths of the paired beams *S1-6* and *S1-4* differ more than twofold at all considered loading stages.

Due to the decreased deformation modulus of GFRP reinforcement (Table 2.1), the paired elements *S2-5nm* and *S2-4-2nm* represent more extreme differences. Such result is a consequence of differences in the levels of crack monitoring – the measurements were associated with the gravity centres of the tensile reinforcement. However, it can be also linked with the fact that a bar controls cracking in its vicinity only with internal cracks closing as distance from the bar increases and deformation concentrating in a decreasing number of wider cracks (Jakubovskis *et al.* 2014, Borosnyói & Snobli 2010, Debernardi *et al.* 2013, Debernardi & Taliano 2016).

Along with the experimental data, Table 2.7 presents crack width predictions obtained by the MC 2010 for the stabilized cracking stage. Although the reported crack width measurements could be analysed only qualitatively, overestimation of the predictions is quite evident. The relative predictions calculated by Equation (2.2) vary between 20% and 120% with exception of the beams *S1-5-2nm* and *S2-4-2nm*. The

specimens, reinforced with GFRP bars distributed in one layer (Figure 2.2), demonstrate crack width overestimation two to four times. These results can be related to a limited predictive capability of the MC 2010 regarding unconventional reinforcement types, though previous research (Gudonis *et al.* 2014) has shown that within the loading stage characteristic to the serviceability analysis bond characteristics of the GFRP bars comparable to ribbed steel reinforcement. Furthermore, the general idea of the MC 2010 is to formulate a mathematical model (consistent with experimental evidence) that provides a reasonable reliability of the predictions of the maximum crack spacing and the maximum crack width that can potentially occur.

Table 2.7. Width (μm) of five maximum, $w_{(1)–(5)}$, and average, w_m, cracks measured at the load stages shown in Figure 2.6 (notation of the cracks corresponds to Figure 2.10)

Loading level	Opening rank	Three layers of reinforcement				One layer of reinforcement				
		S1-1	*S1-6*	*S2-1*	*S2-5nm*	*S1-2*	*S1-4*	*S1-5-2nm*	*S2-3*	*S2-4-2nm*
1 (0.32–0.33·M_u)	$w_{(1)}$	50	30	24	–	50	60	110	40	180
	$w_{(2)}$	40	20	14	–	40	60	100	40	140
	$w_{(3)}$	40	–	14	–	30	38	100	30	140
	$w_{(4)}$	40	–	14	–	24	34	90	30	100
	$w_{(5)}$	40	–	–	–	20	24	70	30	100
	w_m(cracks)	37(7)	25(2)	17(4)	–	31(10)	33(11)	65(10)	24(9)	132(5)
	$w_{(1)}/w_m$	1.35	1.20	1.41	–	1.61	1.82	1.69	1.67	1.36
2 (0.36–0.39·M_u)	$w_{(1)}$	80	30	30	–	62	80	120	60	320
	$w_{(2)}$	70	30	30	–	50	60	110	60	300
	$w_{(3)}$	70	30	24	–	50	54	110	50	26
	$w_{(4)}$	60	20	14	–	40	50	90	40	240
	$w_{(5)}$	60	20	–	–	40	34	70	40	220
	w_m(cracks)	59(7)	26(5)	25(4)	–	39(11)	42(11)	68(12)	29(11)	210(8)
	$w_{(1)}/w_m$	1.36	1.15	1.20	–	1.59	1.91	1.77	2.07	1.52
3 (0.48–0.54·M_u)	$w_{(1)}$	100	60	82	200	102	120	130	100	440
	$w_{(2)}$	94	60	80	200	80	90	120	80	440
	$w_{(3)}$	80	40	80	190	70	70	110	60	440
	$w_{(4)}$	70	40	80	150	62	70	110	60	420
	$w_{(5)}$	70	40	60	100	54	44	110	60	420
	w_{MC}^*	121	101	101	298	179	208	444	191	973
	w_m(cracks)	71(9)	39(11)	59(8)	136(8)	59(11)	61(11)	77(14)	42(12)	350(10)
	$w_{(1)}/w_m$	1.41	1.54	1.39	1.47	1.73	1.96	1.69	2.41	1.26
4 (0.58–0.63·M_u)	$w_{(1)}$	124	60	102	240	142	140	140	120	480
	$w_{(2)}$	120	60	100	230	100	100	120	80	480
	$w_{(3)}$	120	60	100	200	100	100	120	80	460
	$w_{(4)}$	120	50	80	160	100	70	120	80	460
	$w_{(5)}$	100	50	80	140	90	60	110	80	460
	w_{MC}^*	154	131	144	419	223	264	558	248	1233
	w_m(cracks)	93(10)	43(12)	74(9)	142(14)	88(11)	71(12)	81(15)	52(13)	376(11)
	$w_{(1)}/w_m$	1.33	1.40	1.38	1.69	1.61	1.97	1.73	2.31	1.28

*Maximum crack predictions by the Model Code

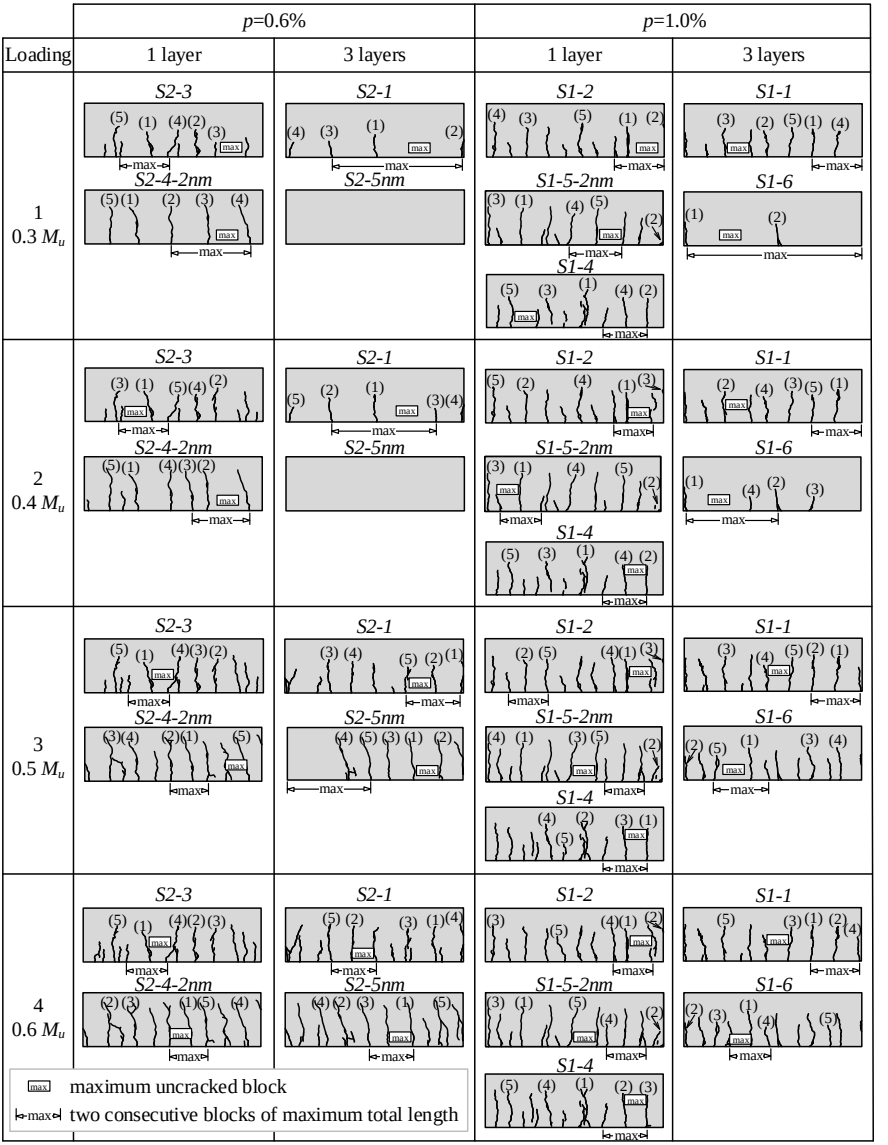

Fig. 2.10. Crack pattern under the reference loading levels indicated in Figure 2.6 – the maximum cracks $w_{(1)}$–$w_{(5)}$ are designated as (1)–(5)

The obtained crack patterns shown in Figure 2.10 illustrate the approximate nature of the assumption of direct relation between the maximum crack width and the maximum crack distance, fundamental for most of the cracking prediction models. The maximum crack opening is not necessarily located near the maximum

uncracked blocks noted as "max" (this is true for 11 of 18 cracked schemes associated with the loading ranges "3" and "4"). However, in the remaining seven cases, one of the five considered maximum cracks is adjacent to the maximum length block. In this regard, it is important to note that in most cases of the latter specimens the differences between the widths of the maximum cracks (Table 2.7) was small.

From the theoretical point of view, in the stabilized cracking stage, the maximum crack should appear between two uncracked blocks of maximum total length (highlighted in Figure 2.10). However, in the considered crack patterns, only 11 cases represent such an "ideal" crack distribution. In reality, the location of the maximum crack is related to the defects in concrete structure and/or local damages of the bond with reinforcement. The latter is important for concrete elements reinforced with a relatively small number of bars. The increase of the number of bars smears out the cracking behaviour. An elaborate discussion of this issue can be found in reference (Jakubovskis *et al.* 2014). Comparison of the results of paired-beams (Figure 2.10) reveals the fact that the number of visible cracks in the specimens with a conventional distribution of the bars is always greater than that observed in the elements with three layers of reinforcement. This observation seems to be in a conflict with the generally accepted concept relating crack widths to the cracking distances. Although the maximum crack distances observed at the stabilized cracking stage ($\approx 0.6 \cdot M_u$) were larger in the beams with the reinforcement distributed in several layers, their maximum crack openings were smaller than in the corresponding conventionally reinforced specimens. Probably, this effect might be related to the development of internal cracks around the multiple layers of the bars that are not visible on the surface.

In the analogy to the crack distances discussed in the first part of this subsection, the ratio between the maximum and average crack widths is of high importance. Thus, Table 2.8 includes this ratio as well as the average crack width. (The table also includes the respective number of cracks, which were averaged for. The loading stages "3" and "4" (Figure 2.6) are characteristic for the cracking analysis related with the stabilized cracking stage. In detail, this loading range is analysed in Table 2.8, where the experimental data are ranged in accordance to the ratio presented in the last column. From the results shown in Tables 2.7 and 2.8, the following observations can be made:

1. The ratio between the maximum and mean crack widths, varying between 1.3 and 2.4, is equal to 1.7 in average. This ratio is about 20% larger compared to the one defined for the crack distances in Subsection 2.2.3.
2. Unlike the crack distances (see Subsection 2.2.3), the ratio $w_{(1)}/w_m$ is dependent on the variation in the total perimeter ΣP of the reinforcement bars and the parameter $Ø/p_{ef}$. An exception serves beam *S2-4-2nm* that was reinforced with a single layer GFRP bars (Figure 2.2). The observed discrepancy could be due to the uncertainties related to the serviceability characteristics of members with low reinforcement ratio and high deformability

of the bars. This issue is discussed in more detail in reference (Jakubovskis *et al.* 2014). If this point is discarded, it is observed that $w_{(1)}/w_m$ increases with decreasing bar perimeter and with increasing $Ø/p_{ef}$ ratio.

Unusual layout of the reinforcement bars in the beam *S1-6* (Figure 2.2) raises the issue of adequacy of the effective reinforcement ratio. In accordance with design regulations (Balázs *et al.* 2013), only the tensile bars being inside the effective area of the concrete are accounted for. Following this rule, only the bottom layer (4 × Ø8 mm bars) of the reinforcement could be taken into account resulting in the height of effective area, h_{ef} = 58.6 mm (compare to 80.4 mm, Table 2.5). Then results of the parametric analysis presented in Tables 2.6 and 2.8 assuming the reduced effective reinforcement ratio, p'_{ef} = 1.26%, become less consistent as compared to the data of other specimens. The same applies to the prediction results of crack distance (Table 2.5) and crack width (Table 2.7).

Table 2.8. Parametric analysis of the crack width results

Group	Beam	Ø, mm	Σ*P*, mm	*p*, %	p_{ef}, %	$Ø/p_{ef}$	$Ø/p'_{ef}$	$w_{(1)}/w_m$	
								Step 3	Step 4
II	*S2-4-2nm*	12	150.8	0.60	2.09	5.75	5.75	1.26	1.28
I	*S1-1*	10	282.7	1.01	3.28	3.05	3.05	1.41	1.33
I	*S2-1*	6	282.7	0.60	1.89	3.17	3.17	1.39	1.38
I	*S1-6*	8	301.6	1.03	2.77	2.89	6.33	1.54	1.40
II	*S1-2*	14	219.9	0.99	3.98	3.52	3.52	1.73	1.61
I	*S2-5nm*	8	226.2	0.67	1.84	4.35	4.35	1.47	1.69
II	*S1-5-2nm*	16	201.1	1.06	3.84	4.17	4.17	1.69	1.73
II	*S1-4*	22	138.2	1.02	3.61	6.09	6.09	1.96	1.97
II	*S2-3*	14	132.0	0.60	2.37	5.90	5.90	2.41	2.31

2.2.4. Concluding Remarks

This section investigates the effect of the arrangement of tensile reinforcement on the flexural stiffness and cracking of concrete beams. Two groups of the beams were considered.

The first, reference group of specimens had a conventional reinforcement layout – the bars were distributed in a single layer with minimum cover. The second group contains specimens with the same reinforcement ratio (as in the conventional beams), but with tensile reinforcement arranged in three layers. The study reveals that the number of the reinforcement layers correlates with the flexural stiffness. At the service load (55% of the theoretical ultimate bending moment), the deflection (curvature) predictions by the Model Code were on the safe side for the beams with three reinforcement layers (the prediction safety varied from 14% to 32%), whereas the predictions for the conventionally reinforced members were deficient by 7–15%. Although the crack spacing predictions by the Model Code for the beams with high concentration of the bars were quite accurate,

the results for the conventionally reinforced elements differed significantly with the experimental values being about 50% larger than the calculated ones.

The present experimental results on cracking do not reveal a clear correlation between crack widths and the crack spacing when the reinforcement layout changes. Although the observed crack distances for the stabilized cracking stage of the beams with three layers of bars were larger, their maximum crack openings were smaller than in the conventionally reinforced specimens with the same reinforcement ratio. Furthermore, the maximum crack opening is not necessarily adjacent to the maximum distance between cracks or located between two consecutive uncracked blocks of maximum total length. In this study, 11 of the considered 18 cracked schemes characteristic for the stabilized cracking stage (i.e. 61% of the cases) are in accordance with the conventional assumption of direct relation between the maximum crack width and maximum crack distance. In general, related to the defects in concrete structure and/or local damages of the bond with reinforcement, the maximum crack localization problem requires elaborate stochastic modelling algorithms.

Experimental results presented in this section cover a wide range of phenomena, caused by interaction between concrete and structural reinforcement and layout of cross-section of the element. One of predominant effects, which is characteristic for flexural elements and governs deformation behaviour, is related to the equivalent area of concrete effective in tension. The effective tension area of concrete has been developed as a computational tool in order to demonstrate the part of the concrete surrounding the reinforcement that is considerably influenced by the force transfer. The definition of the effective depth of the beam is a great issue due to the complexity of the internal stress distribution prior to and after cracking. Intricate nature of flexural elements limits the ability to assess the effect of the arrangement of tensile reinforcement on the serviceability of concrete structures. Analysis of a simplified structure with possibly the most straightforward deformation behaviour is indispensable in evaluation process of concrete damaging effects of structural concrete. The most direct way to isolate uncertainty of area of the concrete effective in tension is to investigate the aforementioned effects on RC members subjected to pure tension: RC tie is considered as equivalent of the efective zone. These tests are discussed in following sections.

2.3. Typical Tensile Tests

Although a standard test setup for tension concrete does not exist, the direct tensile test is the most widely used experimental layout. A concrete prism reinforced with a bar in the centre (Fig. 2.11a) is the common test specimen for the analysis. During the test, the reinforcing bar is fixed by the grips of the testing machine and the test is performed under displacement or force control (Ingraffea *et al.* 1984). This

typical test provides measurements of deformations of the reinforcing bar as well as on the surface of concrete. In order to represent the deformation behaviour of a real structural member, i.e. the case of the inability to monitor deformations of the reinforcement, alternative tensile test might be performed using a bone-shaped specimen (Fig. 2.11b). This specimen has a shoulder at each end and a gauge section in between. The shoulders are wider than the gauge section that causes a stress concentration to occur in the internal part of the sample. This loading layout allows testing specimens reinforced with multiple bars. Unlike the typical tensile test, this alternative method provides measurements of deformations only on the surface of concrete.

Despite the apparent simplicity of the tensile test layouts, a variety of cracking sources are responsible for the noticeable scatter of the test results. The experimental evidence of RC ties often contradicts with the general assumption of similarity of average strains of the reinforcement and of the concrete. Such discrepancy can be mainly associated with the well known, but often neglected issue, namely the end effect. Cover effect is another important issue.

In this study, a representativeness condition is introduced for analysing the aforementioned effects. The representativeness is considered as a property of the test specimen to isolate the investigated parameter (e.g., average deformations) from uncontrolled effects. Following the terminology suggested by Pereira *et al.* (2011) and Lárusson *et al.* (2012), the representative tie would allow obtaining an equivalent deformation of the concrete surface and the bar reinforcement. Therefore, the main idea of this section is to attain the shape of the tie that allows reducing/minimising the end effect.

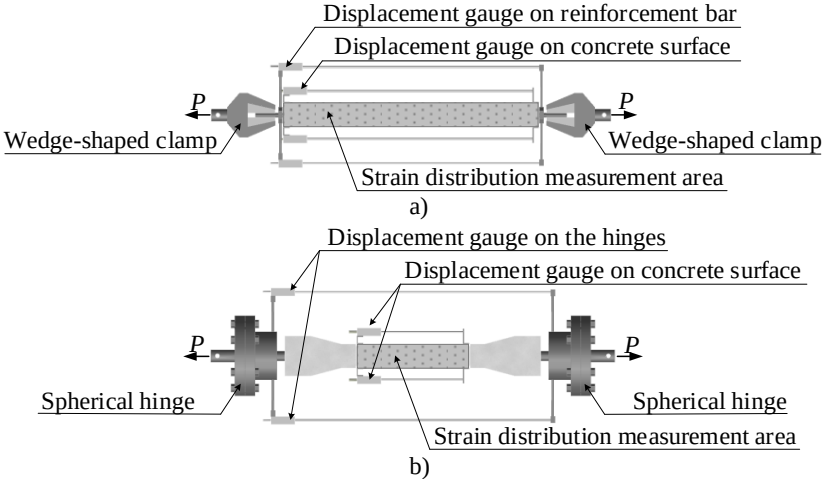

Fig. 2.11. Tensile tests and possible arrangement of the monitoring equipment: a) typical and b) alternative layouts

Reduction of the gauge length, a well-known procedure applied in a number of test programs (Michou *et al.* 2015, Elfgren & Noghabai 2002, Tammo & Thelanderssonm 2009, Ganesan *et al.* 2013), is chosen for implementing the general idea of the research. Average strain of the reinforcement was chosen as the reference for assessing representativeness of the geometry. In contrast with the common practice when the monitoring base is determined in some instance arbitrarily, the present study determines the proper monitoring length experimentally. In order to assess the cover effect in specimens with various cross-section parameters, cumulative deformation criteria is introduced. Relation between the number of cracks and deformation behaviour (tension-stiffening effect) is also investigated.

2.3.1. Description of experimental ties

An experimental campaign on the representativeness of RC ties with various cross-section parameters was carried out. The main aim of this investigation is to attain representative geometry of the tie that allows to account for the uncontrolled effects. The most widely used direct tensile tests (Fig 2.11) were considered for this research. In order to investigate representative geometry of the ties, a number of cross-section compositions, varying the concrete area and reinforcement bar diameter, were designed. The design of specimens is supported by the results reported by Gribniak et al. (2016). The geometry and section parameters of the ties are presented in Fig. 2.12. The ties were tested under two different loading layouts (Fig. 2.13). The first (reference) type, *Specimen A* (Fig. 2.12a), represents a specimen conventionally used for the experimental analysis (Fig. 2.11a). It was tested by applying the load directly to reinforcement (Fig. 2.13a). The rest (specific) types, *Specimen B* and *C* (Fig. 2.12b and c), are designed to represent the deformation behaviour of a real structural member, i.e. the case when the load is applied to the reinforcement indirectly through the surrounding concrete (Fig. 2.13b). In total, 55 RC ties (23 samples of *Specimen* A, 19 – *Specimen B*, and 13 – *Specimen C*) were tested.

Layouts of *Specimen B* and *C* provided the same reinforcement ratio (p=2.2%). The surface geometry of steel bar reinforcement is presented in Fig. 2.1a. The bars were embedded into *Specimen A* and *B* with concrete cover of 25 mm (34 mm and 44 mm for 80×80 and 100×100 specimens, respectively), into *Specimen C* – 15 mm. Originally, the layout of a bone-shaped specimen was designed by Rimantas Kupliauskas only with a single internal reinforcement bar. In considered experimental campaign, bone-shaped specimen was modified by introducing additional confinement frames in the outer regions of the specimens. Modification was made in order to secure the tensile load transfer through the boundary concrete parts (indirectly from testing machine to the main reinforcement). Such a modification was applied for *Specimens B* and *C*. Furthermore, to localize cracking within the inner regions, the *Specimens B* and *C* were notched at the boundaries of the supplemental frames.

All specimens were casted using the concrete grade C30/37 with a maximum aggregate size of 11 mm. To eliminate the shrinkage effect, the elements were stored in water tanks. Before the tests, each element was removed from the water and dried under laboratory conditions at least two hours. Compressive strength of the concrete was determined on the testing day using Ø150×300 mm cylinders resulting in an average value of 39.5 MPa. Main characteristics of the test specimens are shown in Table 2.9.

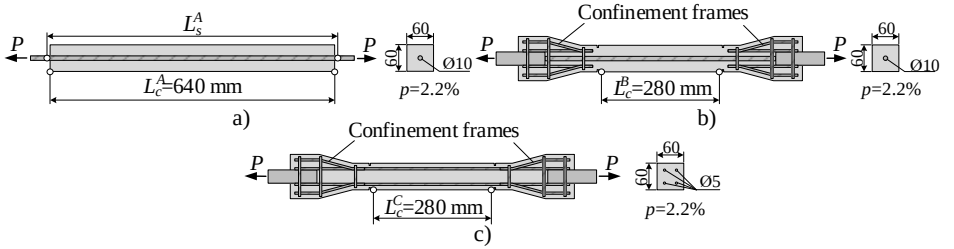

Fig. 2.12. Ties with load transferred to: a) reinforcement bar (*Specimen A*), b) and c) concrete (*Specimens B* and *C*)

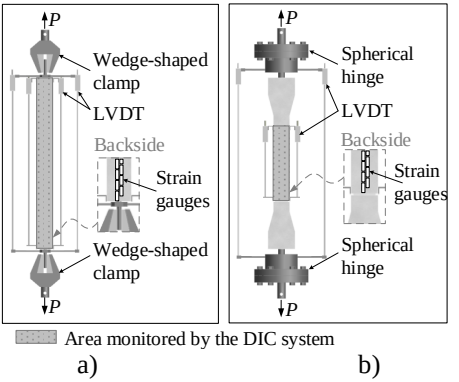

Fig. 2.13. Test setup of the ties: a) *Specimen A* and b) *Specimens B* and *C*

Table 2.9. Main characteristics of the test specimens

Test specimens	Cross-section, mm	Reinforcement, mm	*c*, mm	*p*, %	Number of specimens
Specimen A	60×60	1×Ø10	25	2.2	11
	60×60	1×Ø12	24	3.1	4
	80×80	1×Ø10	35	1.2	2
	80×80	1×Ø12	34	1.8	2
	100×100	1×Ø10	45	0.8	2
	100×100	1×Ø12	44	1.1	2
Specimen B	60×60	1×Ø10	25	2.2	19
Specimen C	60×60	4×Ø5	15	2.2	13

The tests were carried out using an electromechanical machine with capacity of 100 kN under displacement control at 0.2 mm/min loading rate. Due to the different structure of the ties, two types of monitoring systems were used (Fig. 2.13). In both test layouts, linear variable displacement transducers (LVDT) were used to measure the average deformations of the reinforcement and concrete surface.

To avoid possible eccentricity, *Specimens B* and *C* were equipped with spherical hinges (Fig. 2.13b). In order to observe the crack propagation and strain distribution, the front surface of the ties was exposed to a digital image correlation (DIC) system (Fig. 2.14). Images were captured by two digital cameras (Imager E-lite 5M) placed on a tripod at 2.5 m distance from the test specimens. The cameras, incorporating a charge-coupled device (CCD) detector, have a resolution of 2456×2085 pixel at 12.2 fps frame rate. This system allows obtaining strain distribution maps from the digital images of concrete surface using DaVis 8.1.6 software by LaVision – the position of each point of the surface is identified by applying a particular correlation algorithm to the same points from reference image. Precise position of every surface point at every loading step allows tracking the movement of the points for obtaining distribution map of the surface strains. Moreover, DIC method allows attaining relative displacement distribution profile for a linear cut of the surface. These profiles can be collected from the points of the surface cut at every 0.3 mm. For validation of the DIC results, boundary zones of a few samples (*Specimens A, B* and *C*) were additionally equipped with a 20 mm strain gauges (Fig. 2.13).

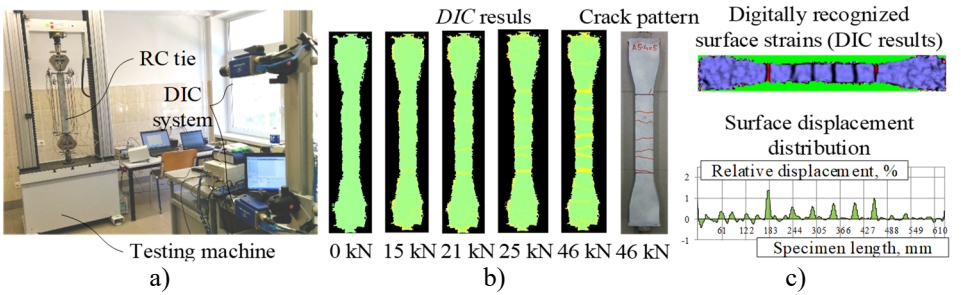

Fig. 2.14. Digital image correlation system: a) test setup, b) obtained crack patterns, and c) digitally recognized displacement distribution of the reinforced concrete tie surface

2.3.2. Eliminating the End Effect

Application of the iterative procedure of the gauge length reduction, is illustrated using the average strain diagrams shown in Fig. 2.15. These diagrams were obtained using measurements of the reinforcement and concrete surface deformations of *Specimens A* with 60×60 mm, 80×80 mm and 100×100 mm cross-sections reinforced with single steel bar.

To localize the end effect, the relative displacements of the concrete surface in the boundary zones were monitored using a digital image correlation (DIC) system at several bases (Fig. 2.16a). The DIC results were verified using 20 mm strain gauges fixed to the concrete in two rows in an overlapping manner (Fig. 2.16b). This allows determining the displacement increments at every 10 mm. The surface strains, determined at the different bases, were compared to each other iteratively identifying the minimum distance (from the edge of the specimen) at which the strain difference of the neighbouring bases is insignificant.

The results of the stepwise implementation of the monitoring base reduction procedure are shown in Figs. 2.15b–d along with the original experimental diagrams. Discrepancies between the original average strains of the concrete surface ("Base 1", Fig. 2.15a) and reinforcement ("Base 2") are characteristic of all considered specimens. As shown in Fig. 2.15b, the strain compatibility condition (implementing the gauge length reduction procedure) was satisfied only for the 60×60×640 mm prism: the averaged concrete strains "Base 3" matched the reference diagram ("Base 1"). The differences (Figs. 2.15c and 2.15d) can be related to limited validity of the Navier-Bernoulli hypothesis. The increased cover most probably delays formation of the transverse crack and makes the crack topology more complicated limiting the adequacy of the plane section assumption. A relatively small length of the ties could also contribute to the observed discrepancies limiting the number of the cracks, thus increasing the impact of formation of each additional crack on the overall response.

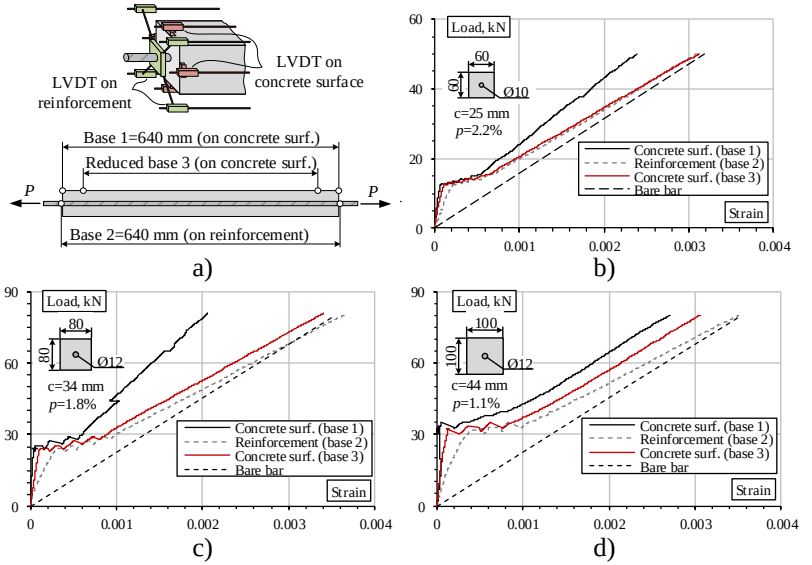

Fig. 2.15. Validation of the representative tie concept: a) arrangement of the LVDT, assessment of the average strains in the ties with b) 60×60 mm, c) 80×80 mm, and d) 100×100 mm cross-section

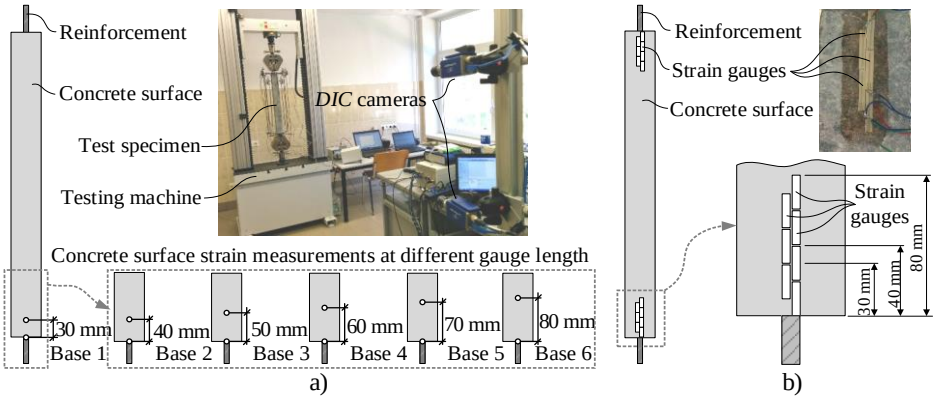

Fig. 2.16. Concrete surface strain monitoring: using a) the digital image correlation system and b) strain gauges

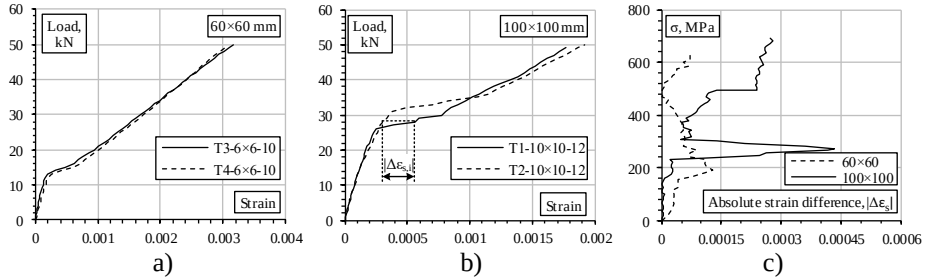

Fig. 2.17. Load-average strain diagrams of twin-ties (Gribniak *et al.* 2016) with a) 60×60 mm and b) 100×100 mm cross-sections, and c) the absolute differences of the strains of reinforcement $|\Delta\varepsilon_s|$ determined for the twin *Specimens A*

Test results (Baena *et al.* 2011, Jakubovskis *et al.* 2014, Gudonis *et al.* 2014, Rimkus & Vileniskyte 2015, Gribniak *et al.* 2016) indicated that the cover correlates with the scatter of average deformations of the ties. An example of such effect is presented in Fig. 2.17 that shows the tensile load-average strain diagrams of twin *Specimens A* with 60×60 mm and 100×100 mm cross-sections. The absolute differences $|\Delta\varepsilon_s|$ of the respective strains are shown in Fig. 2.17c.

The differences $|\Delta\varepsilon_s|$ in Fig. 2.17c are related to the strain level in the reinforcement, therefore results obtained for different bars (i.e. Ø10 and Ø12 mm) can be compared. Most likely, the increased scatter could be related with the inability of some internal cracks to reach the concrete surface in the specimens with enlarged cover and with a complex topology of the crack pattern (in this case, 100×100 mm section). The respective crack patterns are presented in Fig. 2.18.

The aforementioned effects are illustrated by means of the finite element (FE) software ATENA (Cervenka 2002). The external 280 mm parts of RC ties (with

crack patterns shown in Fig. 2.18) are modelled with an exception that both numerical models are reinforced with 10 mm bar. The deformation problem is solved within the 3D formulation. Owning the symmetry conditions, quarter-segments are considered. Due to the limited computation capacity, two different meshes are generated: ties with 60 × 60 mm (Fig. 2.19a) and 100 × 100 mm (Fig. 2.19b) sections are modelled using 3 mm and 5 mm FE size. The triple refinement is used to represent the reinforcement and concrete contact zone. The respective models contain 107,795 and 60,574 FE in total. Isoparametric tetrahedral FE with 12 degrees of freedom are used. It is worth to mention that the fine discretization is used for analysis of strain distribution in the concrete. In general, such discretization is impractical and might inadequate represent meso-structural behaviour of the concrete with relatively large aggregates.

The softening law proposed by Hordijk (1991) is assumed to describe the cracking process. The slipped contact between the reinforcement and concrete is modelled using the segmental bond model proposed by Michou et al. (2015), that is represented by a sequence of cylindrical segments (of same diameters) with different cohesion/strength parameters. The outputs of the simulation are shown in Fig. 2.19 indicating an evident increase of the strain gradient in the concrete with increase of the cover. Concrete strains below the theoretical cracking limit are showen in grey. However, this does not mean that uncracked concrete do not contribute to the force transfer and influence on tension-stiffening of the tie. Since a more uniform strain distribution was obtained for the tie with 60 × 60 mm section, it was chosen for further experimental analysis with the main target of attaining the representative length of the tie eliminating the end effect. Further numerical simulations employing segmental bond model are discussed in detail in Subsection 3.2.3.

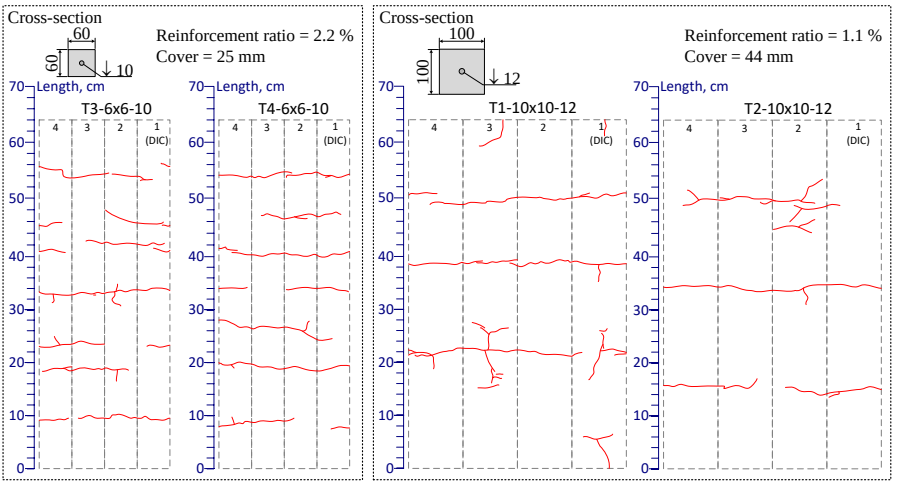

Fig. 2.18. Final crack pattern of RC ties: twin-specimens with 60×60 mm and 100×100 mm cross-sections (Note: the specimens are the same as shown in Fig. 2.15)

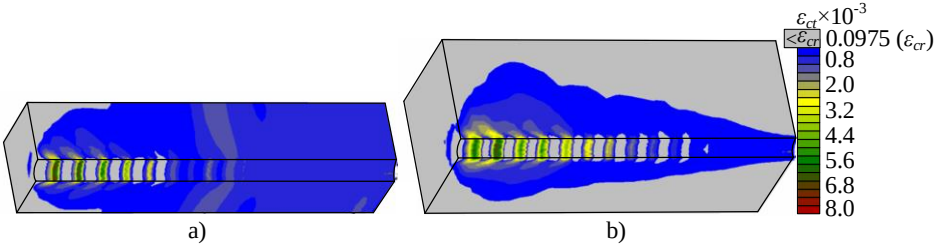

Fig. 2.19. Modelling results (strain distribution) by FE software ATENA of 280 mm external segments of RC ties shown in Fig. 2.12a: a) 60×60 mm and b) 100×100 mm cross-sections. (Note: the strain distribution corresponds to the average strain of the reinforcement equal to 0.77‰, results are shown only for the concrete, strains below the theoretical cracking limit are shown in grey)

Two types of ties with the representative size of the section (i.e. 60 × 60 mm) are considered. The process for assessing the end effect was carried out for both specimen types separately. First, the reference 60×60×640 mm prisms (Fig. 2.12a) were tested. Deformations of the reinforcing bar (gauge length L_s^A) and concrete surface (gauge length L_c^A) were monitored as shown in Fig. 2.13a. The specific ties (*Specimen B*, Fig. 2.12b) were tested at the second step. These tests provide the concrete surface deformation monitoring results (gauge length L_c^B) only. The assessed average strains of the selected *Specimens A* and *B* are presented in Fig. 2.20. In this figure, the reinforcement strain (determined for *Specimen A*) was set as the reference for comparison with the concrete surface strains determined for both specimens. For both specimens, the average strains of the concrete are significantly smaller than the reference one.

The end effect localization procedure consists of five steps outlined in Fig. 2.21. At *Step 1*, the ties are prepared for the testing; the measurement equipment (LVDT) is attached to the concrete surface. The reference *Specimen A* is additionally equipped with LVDT fixed on the reinforcement bar. The load-displacement relationships are determined at *Step 2*. In *Step 3* the average strains determined for the reference tie using the recordings of LVDT fixed on the concrete surface and on the reinforcement are compared. At this stage, two alternative outputs are possible: 1) the difference between the average strains of the reinforcement and concrete surface is greater than the assumed tolerance; and 2) the obtained difference is within the tolerance limits. The first case means that the concrete deformation gauge length (L_c^A, Fig. 2.20a) must be reduced (*Step 4a*, Fig. 2.21). The alternative output indicates that the gauge length is approaching the target gauge length, i.e. localization of the end effect (*Step 4b*); the current reduction in the gauge length ΔL is fixed and the new specimens (with the same material properties and geometry) are tested with the reduced base L_c^B (Fig. 2.20b). The respectively reduced monitoring bases $L^A{}_{c,red}$ and $L^B{}_{c,red}$ enable the identification of the cracking parameters and further comparative analysis. As previously shown (Fig. 2.16), the end effect was localized within the 40 mm boundary zone.

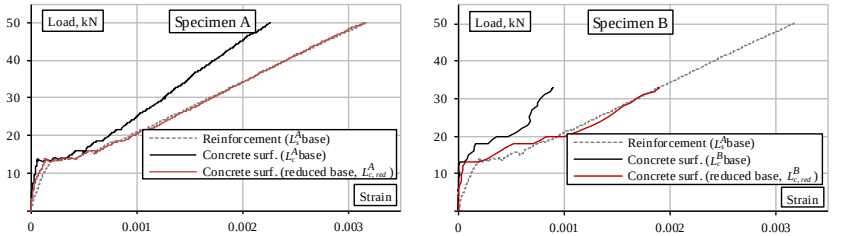

a) b)

Fig. 2.20. Load-average strain diagrams of a) embedded reinforcement bar (*Specimen A*) and b) concrete (*Specimen B*)

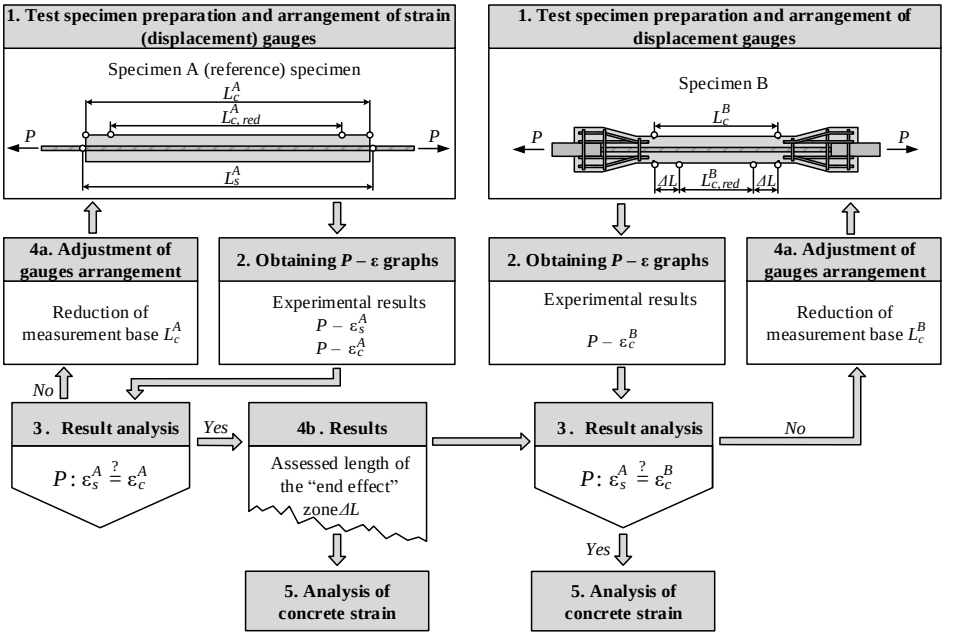

Fig. 2.21. The proposed experimental procedure

Results of the control tests with LVDT located at the initial and the reduced bases (*Step 1*, Fig. 2.21) are presented in Fig. 2.20 along with the original diagrams. The average concrete strains determined using the reduced monitoring bases $L^A{}_{c,red}$ and $L^B{}_{c,red}$ (*Step 3*, Fig. 2.21) practically coincide with the reinforcement strain (of the reference *Specimen A*). An important aspect is that the proposed procedure (Fig. 2.21) is valid only for the cracked ties. Before cracking, the stiffness of the *Specimens A* and *B* is incomparable due to the effect of the uncracked concrete in the pre-notched sections leading to the additional stiffness of *Specimen B* (Fig. 2.20b).

2.3.3. Representative Cracking Parameters

Assessment of the end effect for the bone-shaped specimens represents a real structural analysis when the direct strain measurement of the reinforcement is impossible. Experimental results obtained by the author (Jakubovskis *et al.* 2014, Gudonis *et al.* 2014, Rimkus & Vileniskyte 2015) and other researchers (Broms & Lutz 1965, Borosnyói & Snobli 2010, Caldentey *et al.* 2013) indicated that the crack pattern is dependent on geometry of the specimen and arrangement of the reinforcement. Thus, cracking parameters of the specific ties with different arrangement of reinforcement, *Specimen B* (Fig. 2.12b) and *Specimen C* (Fig. 2.12c), are compared. For illustrative purposes, reference tie, *Specimen A* (Fig. 2.12a), is also included in comparison.

A different crack patterns were observed for the specific ties reinforced with one 10 mm or four 5 mm bars (Fig. 2.12): the cracking schemes of the selected ties are presented in Fig. 2.22. Therefore, a relation between the number of cracks and the deformation behaviour was another object of this research.

Figure 2.23 presents distribution of the surface strain, determined at the service load (determined as 60% of the ultimate load bearing capacity) for the *Specimens A*, *B* and *C* using the DIC system. Digitally recognised surface strain maps represent position of the cracks and can be related to their widths. Figure 2.24 shows that cracks are formed not equally through the section, i.e. crack width varys significantly in single section. This illustrates complexity of the crack topology that complicates crack width identification.

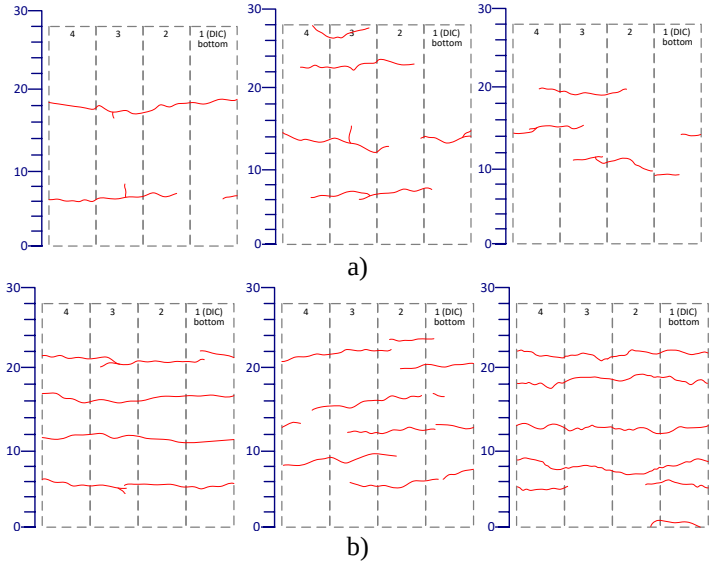

Fig. 2.22. Crack patterns of the selected ties reinforced with a) one and b) four bars

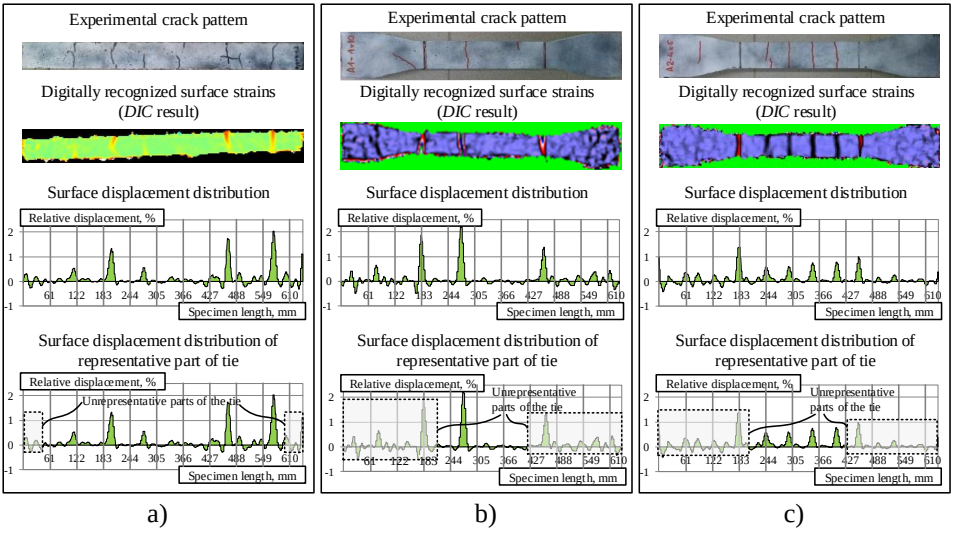

Fig. 2.23. Crack pattern, concrete surface strain distribution and relative displacement determined at the service load (60% of the ultimate theoretical load) for the *Specimens* a) *A*, b) *B*, and c) *C*

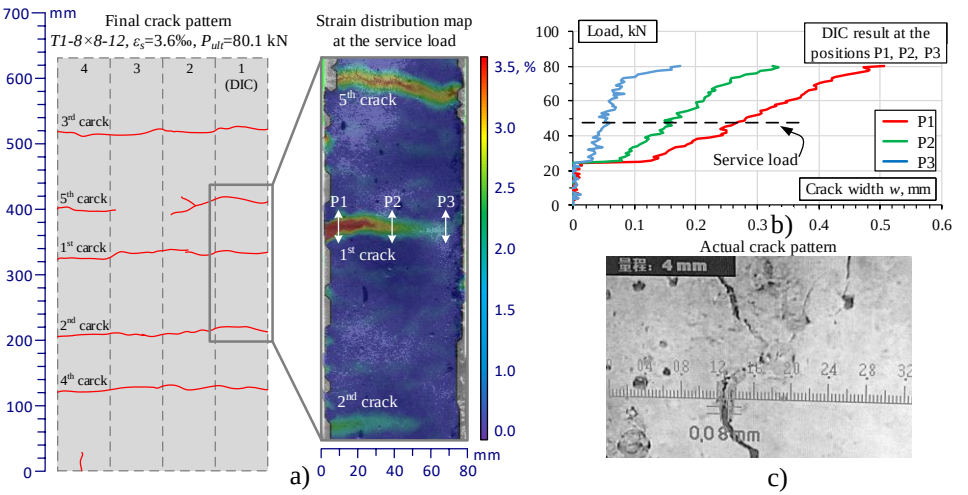

Fig. 2.24. Crack width determination: a) and b) using the strain distribution map of digitally recognised concrete surface, and c) uising a microscope

Figure 2.23 also provides the relative displacement profiles, where the linear surface cuts are associated with the position of the reinforcement bars (Fig. 2.12). It can be observed that the peak displacements correspond to the locations of the

actual cracks. The shaded area under these diagrams is representing the cumulative deformation of the concrete surface. Furthermore, this area can be considered as an equivalent of the total crack opening. Relationship between the cumulative deformations and tension-stiffening is presented in Subsection 3.3.4.

2.3.4. Concluding Remarks

A concrete prism reinforced with a single bar in the centre is the common test specimen for the analysis of the cracking phenomenon. Despite the seeming simplicity of the test layout, a variety of cracking sources (e.g., cover width, height of the ribs) are responsible for the discrepancy of cracking responses of theoretically identical specimens. To solve this problem, a *representativeness* condition has been introduced. The representativeness is considered as a property of the test specimen to isolate the investigated parameter from uncontrolled effects. The main idea was to attain the shape of the tie that allows to minimise the end effect which is related with local differences between deformations of internal reinforcement and concrete surface at the extremities of ties. An experimental procedure has been developed to achieve this objective. The consistency of the excessively simplified average deformation concept was experimentally revealed with the help of the test results of more than 50 ties with different geometry and loading setup. The study reveals that:

- The developed iterative procedure for the reduction of the gauge length allows to localize the end effect and, hence, to validate representativeness of the tie elements.
- Validity of the Navier-Bernoulli hypothesis in combination with the average deformation approach is limited to the stabilized cracking stage when the crack width is relatively large, i.e. the tension softening stresses (in the primary cracks) are practically released. At the pre-cracking stage, the average deformations of the reinforcement and concrete differ due to the end effect: the boundary concrete involved through the bond stress transfer undergoes relatively smaller deformations than the internal part of the tie. This effect increases with cover. Therefore, experimental behaviour corresponded to the relatively small deformations region must be analysed with a particular care.
- The strain gradient in the concrete varies not only along the bar, but also within the cover. Increase in the width of the cover increases scatter of the experimental results related to the stochastic nature of cracking of the "ineffective" concrete. Cases when parameters of the structural response could not be measured directly (e.g., deformations of the reinforcement) and must be assessed indirectly (e.g., using the surface deformations of the concrete) should be treated with particular care.

– The difference in the observed crack pattern (crack spacing) can be attributed to the differences in the concrete cover and variation of bonded surface of the bars with different diameter. Further researches are essential to analyse cracking behaviour of ties with different arrangement of the reinforcement but the similar cover.

The representativeness principle could be extended to various structural problems including verification of the experimental setup. Application of the discussed test layouts, however, does not allow assessing particular effect of characteristic parameters (i.e. concrete cover, reinforcement ratio, diameter of reinforcement bars) on deformation and cracking behaviour of RC. The observed limitations characteristic of traditional test setups have motivated development of specific equipment that makes possible production of the test specimens ensuring independent variation of each of the key parameters, i.e. concrete cover, reinforcement ratio and diameter of the reinforcement bars.

2.4. Ties with Multiple Bar Reinforcement

In accordance with the aforementioned criteria of the independent variation of cross-section parameters (i.e. concrete cover, reinforcement ratio, diameter of reinforcement bars), Gribniak & Rimkus (2016) developed specific equipment (anchorage blocks) for testing ties reinforced with multiple bars. General idea of the setup was to secure uniform distribution of the applied tension in the multiple bars. The capability to monitor the deformation for each of the bars was another goal of the design. The test equipment is shown in Fig. 2.25. As can be observed, the anchorage joints embrace two plates connected by a central bar that is connected to tension device using a spherical hinge. It allows reducing possible imperfection (related to an inhomogeneity of the concrete structure and non-uniform development of the cracks) in applying the tensile load. The plates are perforated to fix and distribute the reinforcement bars within the concrete prism. Steel clamps are used assuring additional confinement of the anchorage joints. The most important benefit of the developed equipment is that it allows testing concrete prisms reinforced with bars made of any materials (e.g., steel, FRP). This equipment was registred in the State Patent Bureau of the Republic of Lithuania (Patent No. LT 6275 B). The most important benefit of the developed equipment is that it allows testing concrete prisms reinforced with bars made of any materials. However, differences in mechanical and bond properties of reinforcement made of different materials may also affect the deformation and cracking behaviour of RC members (Baena *et al.* 2013). Therefore, the present study includes tests of ties with different types of the bar reinforcement into the consideration.

Fibre reinforced polymers (FRP) are considered to be an alternative to steel reinforcement in concrete structures subjected to aggressive environment or to the effects of electromagnetic fields (Torres *et al.* 2012). With high durability, FRP bars have a tensile strength up to 5–6 times higher than structural steel. However, the low elastic modulus of polymer bars (in respect to the steel) generally leads to increased deformations of FRP reinforced concrete elements. This is characteristic of glass fibre reinforced polymer (GFRP) bars as one of the most frequently used types of structural reinforcement (Mias *et al.* 2013, Mahmoud & El-Salakawy 2013). In order to compensate the decrease of sectional stiffness of FRP reinforced concrete elements, additionally, steel bar reinforcement may be introduced. This combination, so called hybrid reinforcement, allows taking an advantage of durability issue. This combination, so called hybrid reinforcement, allows taking an advantage of durability issue related with FRP bars immunity to corrosion in combination with the required ductility and load capacity ensured with the steel reinforcement in case of a fire. Moreover, a high deformation resistance of FRP bars would allow to exploit the structures in the deformation regions exceeded the yielding of the steel bars.

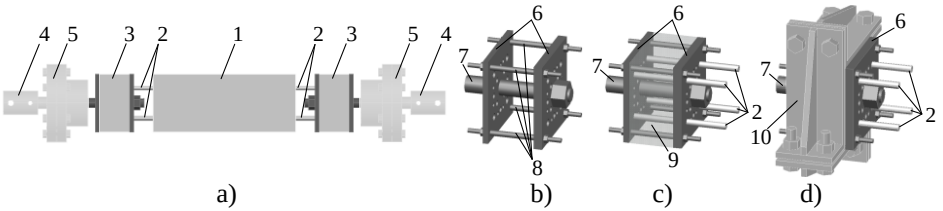

Fig. 2.25. Developed equipment for testing ties reinforced with multiple bars: a) test specimen, b) and c) detailed composition of anchorage joint, and d) anchorage joint with supplemental equipment for shear restrain, where 1 – reinforced concrete element, 2 – reinforcement bars, 3 – anchorage joint, 4 – standard joint of tension device, 5 – spherical hinge, 6 – steel plates of anchorage joint, 7 – central bar of anchorage joint, 8 – supplemental bars of anchorage joint, 9 – concrete, 10 – supplemental equipment for shear restrain of anchorage joint

2.4.1. Experimental Programme

Concrete prisms with 100×100 mm and 150×150 mm cross-section and 25–30 mm cover are considered. Steel, GFRP, and hybrid combination of steel and GFRP bars were used as reinforcement. In total, 64 ties (43 with steel, 13 with GFRP and 8 with hybrid reinforcement) with 24 different reinforcement layouts are considered. The sections are shown in Fig. 2.26. As can be observed, some of the ties with steel reinforcement are grouped regarding reinforcement ratio (Fig. 2.30a), consisting different reinforcement schemes.

The previous tests (Gribniak *et al.* 2016, Gribniak & Rimkus 2016, Rimkus & Vileniskyte 2015) revealed that the effect of different distribution of the bars is evident in ties with a relatively low reinforcement ratio ($p \approx 1.5\%$). Therefore, two different covers (i.e. 30 mm and 50 mm) are considered in the reference ties with the lowest amount of reinforcement (Fig. 2.26a). Characterisctics of the reinforcement have been described in Section 2.1. Length of the test specimens is limited by the capacity of tensile machine (380–500 mm). Thus, the length-to-width ratio of the ties is quite low. However, previous experience (Gribniak *et al.* 2016) indicates that the section area should be related with a number of the reinforcement bars. To assess the adequacy of the cracking results of relatively short specimens, two 1230 mm ties (reinforced with steel and GFRP bars) are also considered.

All specimens were produced using the similar concrete mixture with a target compressive strength class of C30/37. A site-mix concrete with 8 mm maximum aggregate size was employed. Compressive strength of the concrete was determined using Ø150 × 300 mm cylinders. The cylinders were stored under the same conditions and tested on the same day as the tensile elements. During the curing process, all elements were stored in the water to reduce the shrinkage effect. Some of the specimens are shown in Fig. 2.27.

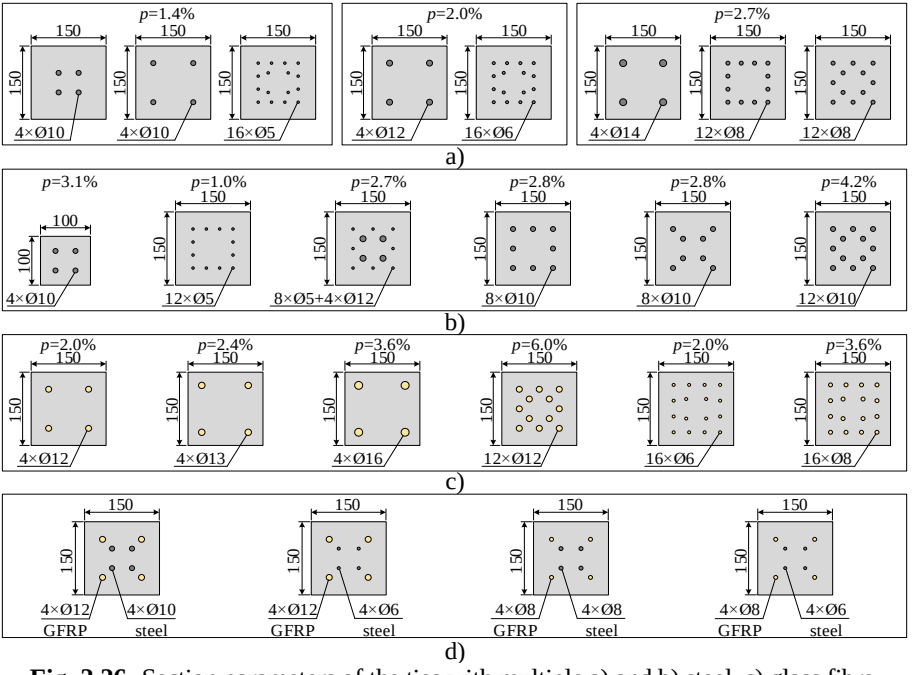

Fig. 2.26. Section parameters of the ties with multiple a) and b) steel, c) glass fibre reinforced polymer, and d) steel + glass fibre reinforced polymer bars (all dimensions in mm)

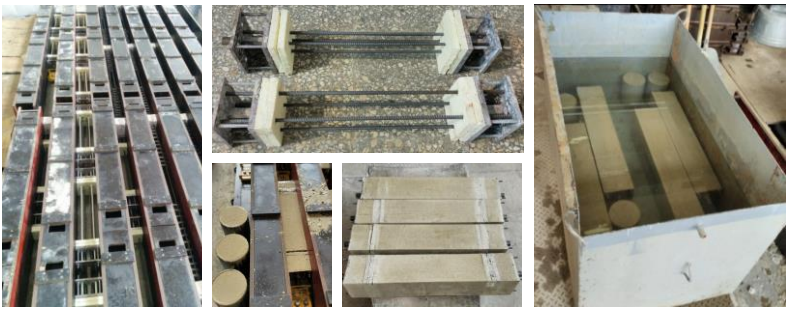

Fig. 2.27. Production and treatment of test specimens

Mechanical properties and surface characteristics of the reinforcement bars are presented in Table 2.1 and Figure 2.1, main characteristics of the ties – in the Table 2.10. The first two columns of Table 2.10 refer to the name of the tie and the material of the reinforcement. Other parameters presented in the table are the cover (c), the reinforcement ratio (p), the average compressive strength of the concrete at 28 days (f_{cm}). The last two columns give the nominal length of the concrete prisms and the amount of the specimens. Nomenclature of the ties characterizes composition of the reinforcement, including the number, material (the letter "G" defines GFRP, while "S" represents steel) and diameter of the bars. Prisms referred as to "1", "2", etc. represent each reinforcement layout, e.g., the prism referred to as *4S10-1* represents the first specimen of the section type reinforced with 4 steel 10 mm bars. The notation "A" in the tie name defines 100×100 mm section specimens, "L" – 1230 mm length ties and "C" – elements with 50 mm concrete cover. The campaign also includes some prisms reinforced with the same amount, but different arrangement of the bars: with a cross (noted as "X") and a rectangular (noted as "R") shape distribution of the bars (e.g. 8S10X and 8S10R, respectively). Nomenclature of the prisms reinforced with combination of different bars consists of two components separated by the slash symbol ("/").

Initially, the tests were carried out using electromechanical testing machine of 100 kN capacity (Rimkus & Vileniskyte 2015). However, due to the limitation of the maximum load and, most importantly, the length of the concrete prism (≈380 mm), the major part of the tests was performed using a servohydraulic machine of 600 kN capacity under displacement control with 0.2 mm/min loading. The reaction was measured with the electronic load cells of the testing machines. The axial deformations were monitored using linear variable displacement transducers (LVDT), which were attached to the reinforcement bars and to the concrete surface as shown in Fig. 2.28.

In order to observe the development of the cracks, the front surface of the ties was exposed to a DIC system (Fig. 2.29). Detail description of this system is pro-

vided in Subsection 2.3.1. The cracking schemes were identified using a procedure developed by Rimkus *et al.* (2015). At characteristic loading levels, the crack widths of selected ties were measured using digital microscope CK102 (with 40× magnification and 0–8 mm measuring range) as shown in Fig. 2.30.

The most design codes are referring with application of steel bars. In order to verify the adequacy of the predictions by design codes (Model Code 2010 and Eurocode 2), the test results presented in this section are limited to the ties with steel reinforcement. Deformation and cracking results of such elements are presented in Subsection 2.4.2, while the results of the ties reinforced with GFRP bars and hybrid combination of GFRP and steel bars reinforcement are analysed in Subsections 3.4.5 and 3.4.6, respectively.

Table 2.10. Main characteristics of the ties

Tie	Reinforcement material	c, mm	p, %	$Ø/p$, mm	f_{cm}, MPa	Nominal length, mm	Number of specimens
4S10A	Steel	25	3.1	323	38.0	500	2
4S10		30	1.4	714	39.1	380	2
4S10		30	1.4	714	47.1	500	6
4S10L		30	1.4	714	40.9	1230	1
4S10C		50	1.4	714	45.3	500	2
4S12		30	2.0	600	54.0	500	2
4S14		30	2.7	519	43.5	500	3
8S10R		30	2.8	357	43.4	500	2
8S10X		30	2.8	357	39.8	500	3
12S5		30	1.0	500	43.7	500	2
12S8R		30	2.7	296	43.7	500	2
12S8X		30	2.7	296	43.3	500	3
12S10		30	4.2	238	45.1	500	5
8S5/4S12		30	2.7	–	43.7	500	2
16S5		30	1.4	357	39.1	380	2
16S5		30	1.4	357	46.7	500	2
16S6		30	2.0	300	54.0	500	2
4G12	GFRP	30	2.0	600	54.0	500	2
4G12L		30	2.0	600	40.9	1230	1
4G13		25	2.4	542	47.6	500	2
4G16		25	3.6	444	38.0	500	2
12G12		30	6.0	200	54.0	500	2
16G6		25	2.0	300	47.6	500	2
16G8		25	3.6	222	38.0	500	2
4G12/4S10	Hybrid (steel+GFRP)	30	2.1*	–	49.3	500	2
4G12/4S6		30	1.1*	–	49.3	500	2
4G8/4S8		30	1.2*	–	49.3	500	2
4G8/4S6		30	0.8*	–	49.3	500	2

*The equivalent reinforcement ratio $p_{s,eq}=[A_s+A_f\cdot(E_f/E_s)]/A$

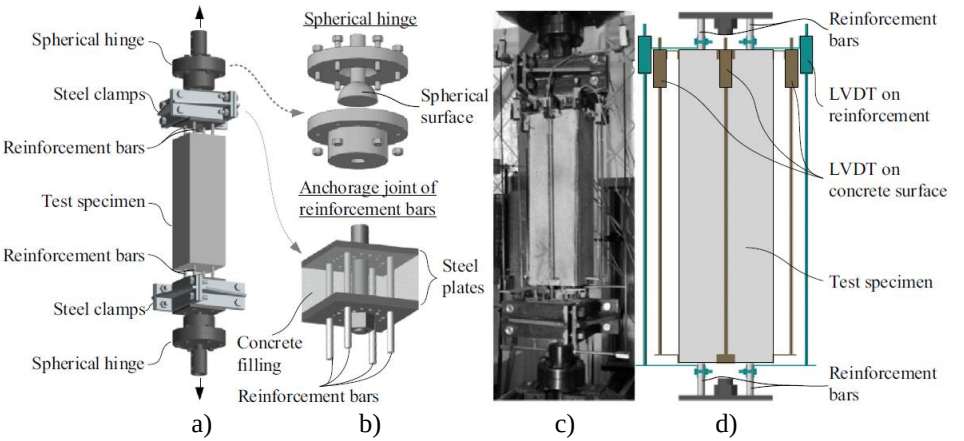

Fig. 2.28. Test of concrete prism with multiple bars: a) composition of the specimen, b) spherical hinge and anchorage joint components, and c) and d) test instrumentation

Fig. 2.29. Surface strain monitoring using digital image correlation (DIC) system: a) test setup, b) scientific grade cameras, c) actual crack pattern of reinforced concrete tie, and d) surface strain map obtained using digital image correlation system

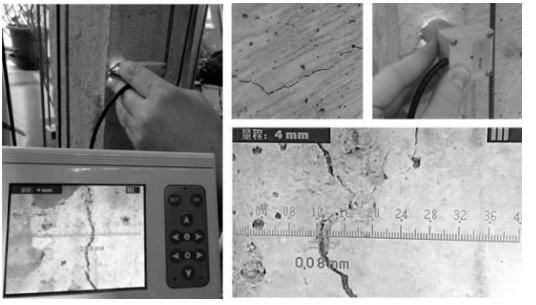

Fig. 2.30. Crack width measurement using optical microscope

2.4.2. Discussion of the Test Results

In addition to the serviceability analysis, adequacy verification of the cracking predictions by design codes (Model Code 2010 and Eurocode 2) has also been addressed within this subsection. Test results of 27 selected concrete ties reinforced with steel bars are presented. All considered ties are grouped regarding reinforcement ratio (1.4%, 2.0% and 2.7%), consisting different reinforcement layouts: 4-bars reference and 16-bars (or 12-bars) alternative (Fig. 2.26a).

2.4.2.1. Deformation Behaviour

The average strain diagrams of the reinforcement bars and concrete surface of selected ties are shown in Figs. 2.31 and 2.32, respectively. The differences between the diagrams are evident taking the bare bar response as the reference. The sources of this dissonance are briefly described in the Subsection 2.3.2.

The deformation results are analysed regarding two different though interrelated aspects: variation of the number of the bars and difference between the strains of reinforcement and concrete surface. The respective results are presented in Figs. 2.33 and 2.34 assuming the average strain of reinforcement as the reference.

An important observation from Fig. 2.33 is that the alternative reinforcement distribution schemes (with 12/16 reinforcement bars) are capable at securing practically indistinguishable deformation behaviour of the identical ties, while a significant scatter is characteristic of the reference ties reinforced with four bars (Fig. 2.30). Scatter of the results, evident at the early cracking stage in the ties with relatively low reinforcement ratios (p = 1.4% and 2.0%), could be attributed to formation of an increased number of internal cracks due to increased bonding area and number of ribs that makes more uniform deformation behaviour of the ties reinforced with 16 bars.

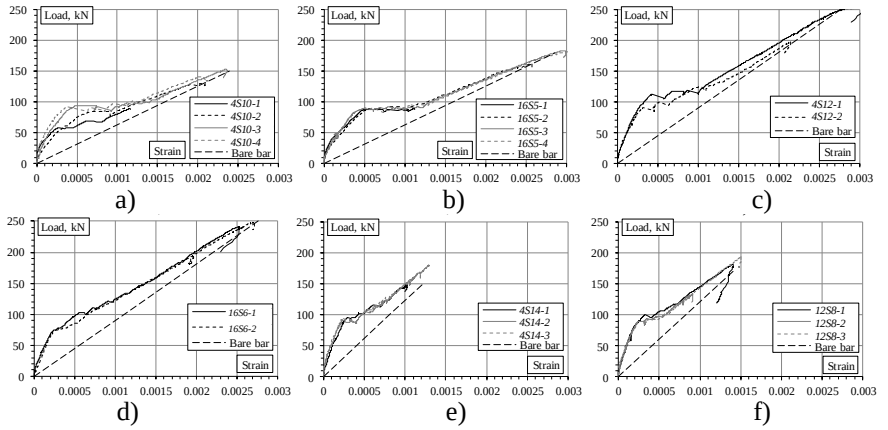

Fig. 2.31. Load-average strain diagrams determined using reinforcement deformation monitoring results: reinforcement ratio a) and b) 1.4%, c) and d) 2.0%, and e) and f) 2.7%

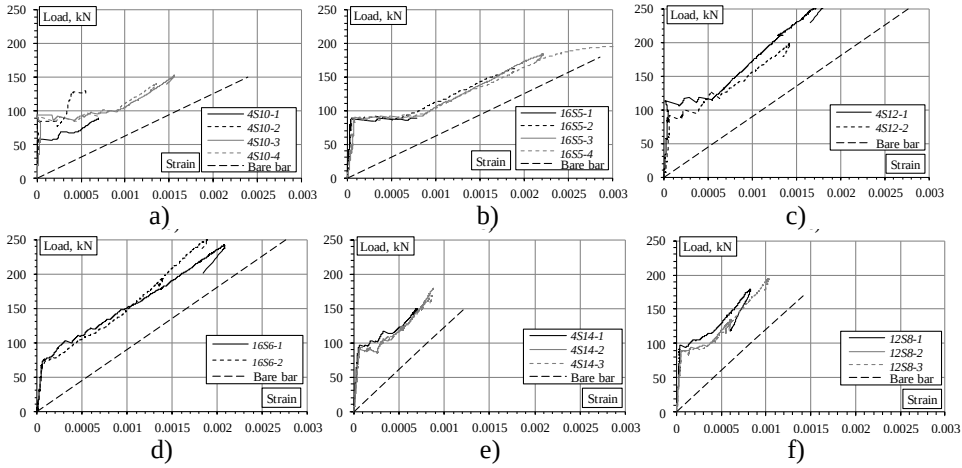

Fig. 2.32. Load-average strain diagrams determined using concrete surface deformation monitoring results: reinforcement ratio a) and b) 1.4%, c) and d) 2.0%, and e) and f) 2.7%

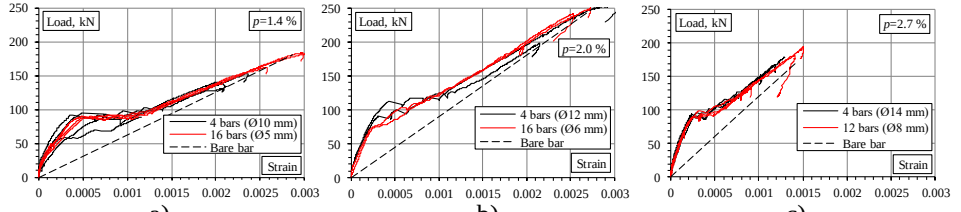

Fig. 2.33. Average strains of reinforcement in the ties with ratio *p* a) 1.4%, b) 2.0%, c) 2.7%

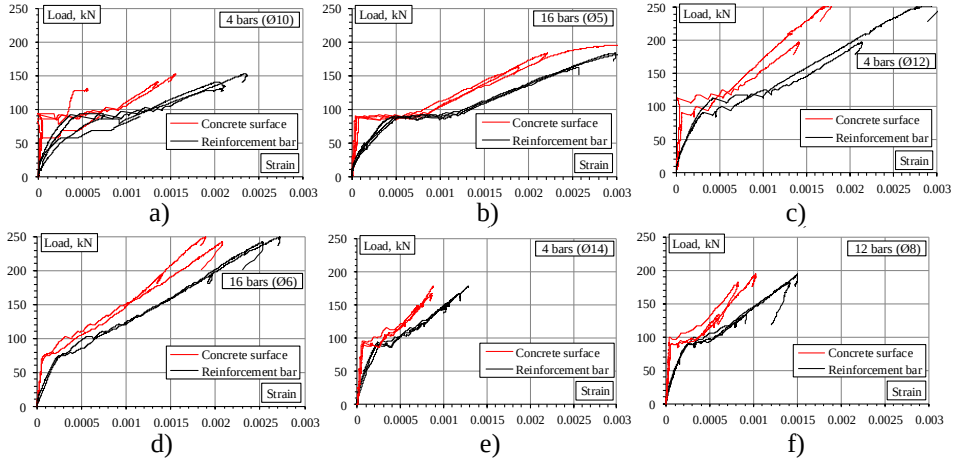

Fig. 2.34. Deformation differences in ties with ratio *p* a) and b) 1.4%, c) and d) 2.0%, and e) and f) 2.7%

Another inference is related to the strain difference of the reinforcement and concrete surface of RC ties. The differences between the diagrams shown in Figs. 2.33 and 2.34 can be related to the strain gradient in the concrete by the means of finite element simulation presented in Subsection 2.3.2. The strain difference is proportional to the distance between the bars and concrete cover. The mitigation of such differences may reduce the scatter of the deformation responses. This statement is supported by the results presented in Figs. 2.33a and 2.33b that indicate a more uniform distribution of the deformations within the concrete of the ties reinforced with 16 bars than that of the counterpart reference.

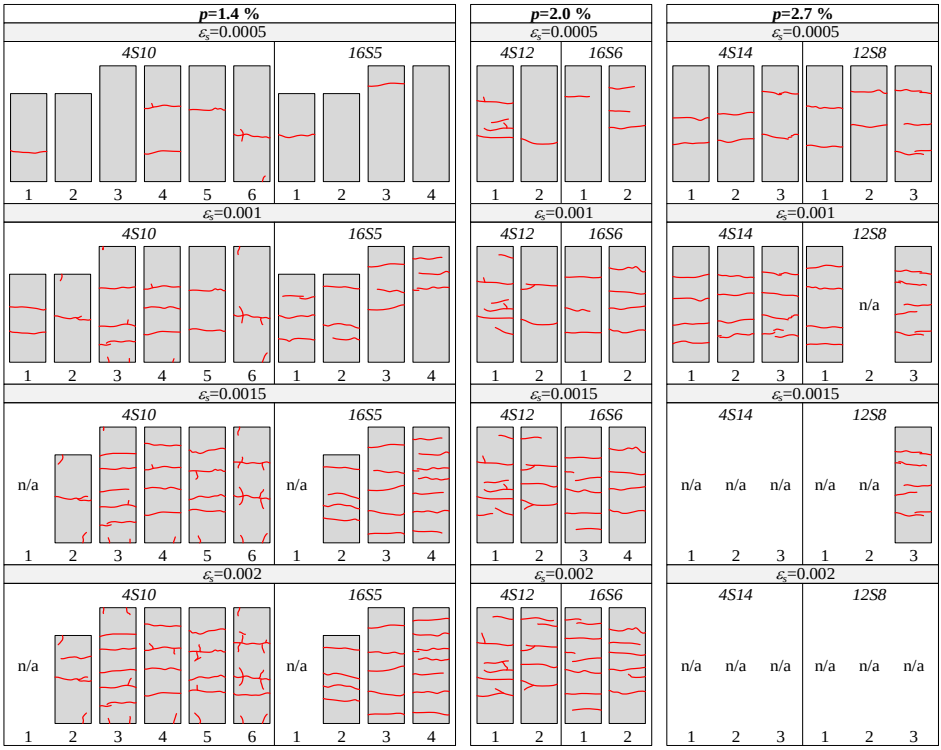

Fig. 2.35. Crack development identified by the digital image correlation system ("n/a" = not applicable)

2.4.2.2. Cracking Behaviour

The cracking schemes obtained by using the relative deformation maps of the surface recognised by the DIC are presented in Fig. 2.35. The schemes are related to the reference average deformations of the reinforcement measured during the experiments. The final crack patterns of the ties are shown in Fig. 2.36. Considering 500 mm length specimens, the different number of cracks is characteristic of the

final patterns of the ties reinforced with 4 and 12/16 bars (Fig. 2.36). However, as shown in Fig. 2.35, these differences become less significant by comparing the cracking schemes related to the reference deformations of the reinforcement. As it was indicated in Subsection 2.3.3, the scatter of individual crack monitoring results obtained using an optical microscope reduces the reliability of the analysis. Hence, the cumulative surface displacements identified by the DIC system are used for comparative analysis of the cracking behaviour of RC ties.

Figure 2.33 indicates that the scatter of the average strains of reinforcement, evident in the ties with relative low reinforcement ratio (p = 1.4% and 2.0%), decreases with increase of the reinforcement area. This may be related to the increase of the reinforcement stiffness making the cracking process less steep. In order to investigate influence of the bar arrangement to the aforementioned effect, concrete ties with relative reinforcement ratio (p = 1.4% and 2.0%) and different bar arrangement are considered for further analysis of the cracking behaviour of RC ties. The displacement profiles of selected ties are shown in Fig. 2.37, where the surface cuts are associated with the position of the reinforcement bars. The cumulative deformations are related with the area determined by the relative elongation curve (Fig. 2.37). This area is calculated at each loading stage by numerical integration of the respective elongation profile.

Hence, the cumulative deformation is considered as an equivalent of the crack opening. The corresponding results of the selected ties are presented in Table 2.11. It can be observed that the cumulative deformation correlates with number of the bars. The cracking analysis, however, must be related with deformation behaviour of the ties evaluated in the previous part ("*Deformation Behaviour*") of this section.

The serviceability analysis described by the Code methods is intended for the stabilized cracking stage (Balázs *et al.* 2013). Figure 2.38 illustrates this issue by relating the cracking schemes (identified by the DIC) to the diagrams of the average bar strains. The strain diagrams also include the stabilized cracking strain limits assessed by the MC 2010. An important observation is that the cracking of the shortest (380 mm) prisms is not stabilized – new cracks were identified by the DIC – though the load-strain diagrams reveal no changes of the stiffness. Alternatively, the cracking of the 500 mm prisms has evidently been stabilized: both the cracking schemes and the average strain diagrams do not demonstrate any changes.

Table 2.11. Cumulative surface deformations of the selected ties, mm

Tie	p, %	Reference strain of the reinforcement ε_s, ‰			
		0.5	1.0	1.5	2.0
4S10-3	1.4	0.07	0.08	0.35	0.77
16S5-4		0.22	0.30	0.61	0.86
4S12-2	2.0	0.25	0.26	0.46	0.68
16S6-1		0.40	0.67	0.86	1.17

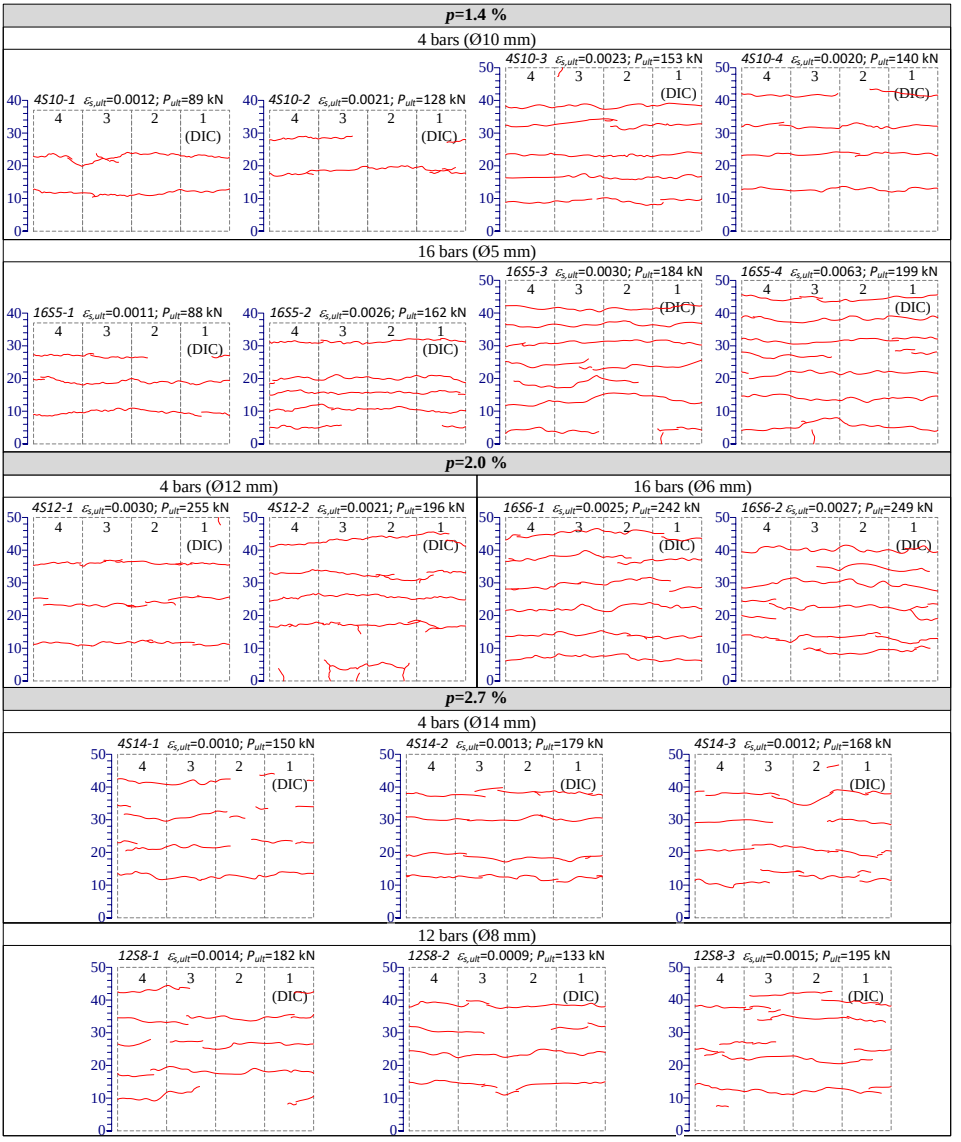

Fig. 2.36. Final crack pattern of the ties

To assess adequacy of the cracking results of the relatively short specimens (380–500 mm), the long 1230 mm tie *4S10L* (Table 2.10) was additionally tested using a lever-arm system developed for a sustained loading (Gudonis *et al.* 2015). Due to limited capability of the DIC system, cracking of the long tie was observed and fixed using an optical microscope. In Fig. 2.39, the final crack pattern of the

tie *4S10L* is compared with the cracking maps of the equivalent short ties determined by the DIC system at the same deformation level of the reinforcement as the final crack pattern of the long tie: the comparison is related to the measured average strain ε_s = 1.4‰. The resultant averaged crack distances in the short and long ties are equal to 100.0 mm and 102.5 mm, respectively.

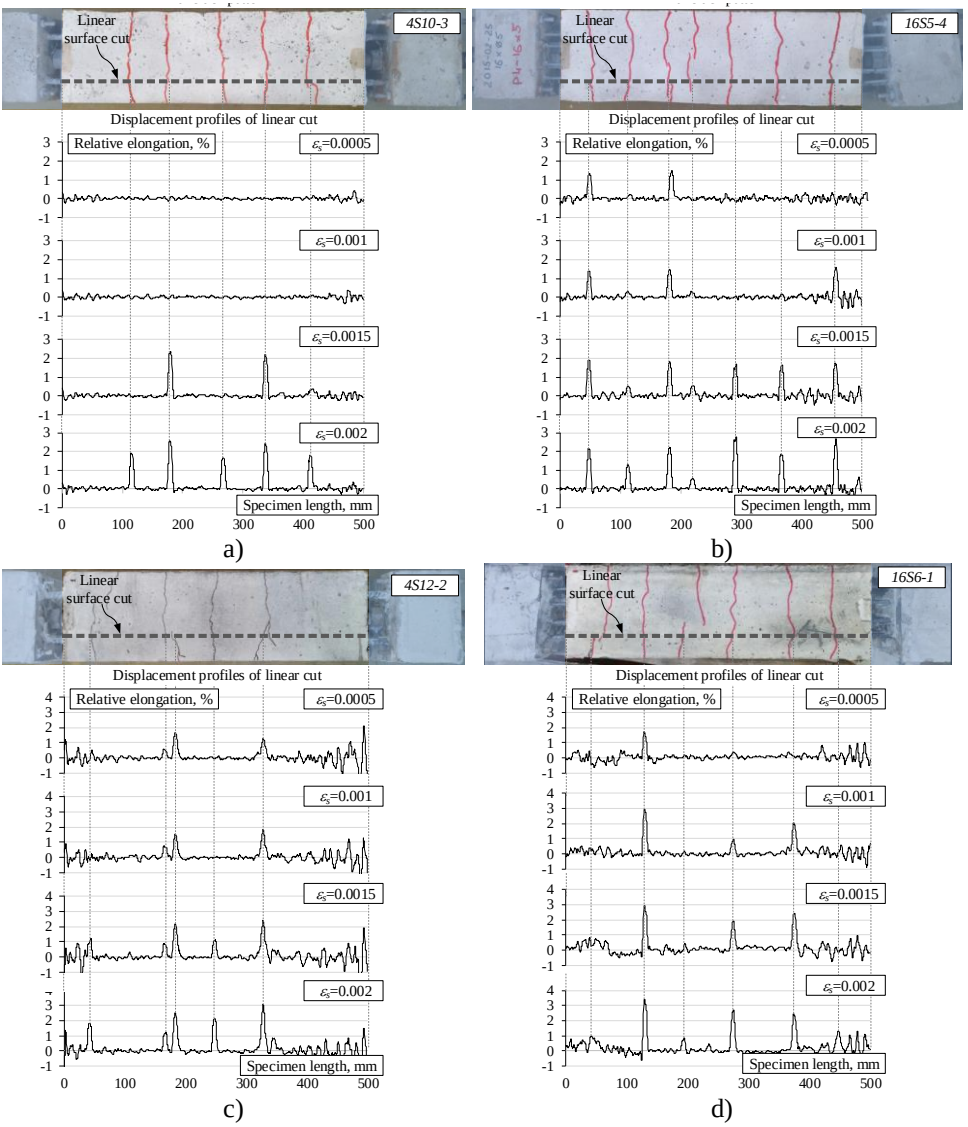

Fig. 2.37. Distribution of relative displacement of the surface of ties a) *4S10-3*, b) *16S5-4*, c) *4S12-2* and d) *16S6-1* identified by the digital image correlation system

Successful results of the aforementioned comparison enable the 500 mm ties to be used for adequacy verification of approaches adopted in design codes. The theoretical strain limit associated with beginning of the stabilized cracking stage was assessed by following the MC 2010 approach:

$$\varepsilon_{sm} = \sigma_{sr}\frac{1-\beta}{E_s} + \varepsilon_{cm}; \quad \sigma_{sr} = \frac{f_{ctm}}{p}\left(1+\alpha_e \cdot p\right), \quad \varepsilon_{cm} = \beta\frac{f_{ctm}}{E_c}, \qquad (2.4)$$

where ε_{sm} and ε_{cm} are the average strain of reinforcement and concrete, σ_{sr} is the maximum stress in the reinforcement in a crack, β (=0.6) is the coefficient that accounts for type of the loading, f_{ctm} is the tensile strength of the concrete (calculated by MC 2010), α_e (= E_s/E_c) is the modular ratio. Figure 2.38 clearly shows that the strain ε_{st} is too radical to identify the stabilized cracking stage if the average deformation of the reinforcement is used as the reference. The opposite results, however, could be obtained in the analysis based on the average deformation of the concrete surface (Fig. 2.32). In fact, none of the experimentally observed deformations represents the average deformation behaviour of the tie. It can be only approximately assessed with the help of these monitoring results.

By accounting for the aforementioned inferences, verification of design code predictions is based on the test results of 500 mm ties. Due to a limited number of the measured crack widths, the verification is limited to the crack spacing. The stabilized cracking stage is associated with the average strain of the reinforcement $\varepsilon_s \approx$ 1.5‰ and 1.0‰ for the ties with $p \leq 2.0\%$ and $p = 2.7\%$, respectively. These values are more than three times the cracking limit assessed by Eqn. (2.4). The respective parameters of 15 representative ties (see Fig. 2.35 for the reference) are given in Table 2.12. The cracking results (the maximum and average crack distances) of the ties are also presented in Table 3. The maximum spacing was assessed by MC 2010 and EC 2. Two main observations can be made from these results:

1. While design codes predict that maximum crack spacing is dependent on the $Ø/p$ ratio, the test results are practically independent on the reinforcement characteristics. As can be observed in Table 2.12, an increase in $Ø/p$ from 300 to 714 causes the corresponding changes of $s_{r,max}$ predicted by the MC 2010 and EC 2 from about 140 mm to 260 mm and from 200 mm to 350 mm, respectively. The test results, however, show the average increase of the maximum distance from 100 mm up to 120 mm and the average spacing from almost 90 mm to 100 mm only.
2. The ratio of the experimental maximum-to-average crack spacing (s_{max} / s_m) is practically constant and on average equal to 1.27. Only one tie demonstrates this ratio greater than 1.70 (grey filled cell in Table 2.12). Such results agree well with the relation identified by Beeby & Forth (2014). Fantilli and Chiaia (2012) suggested a similar value as a basic parameter for scaling crack patterns.

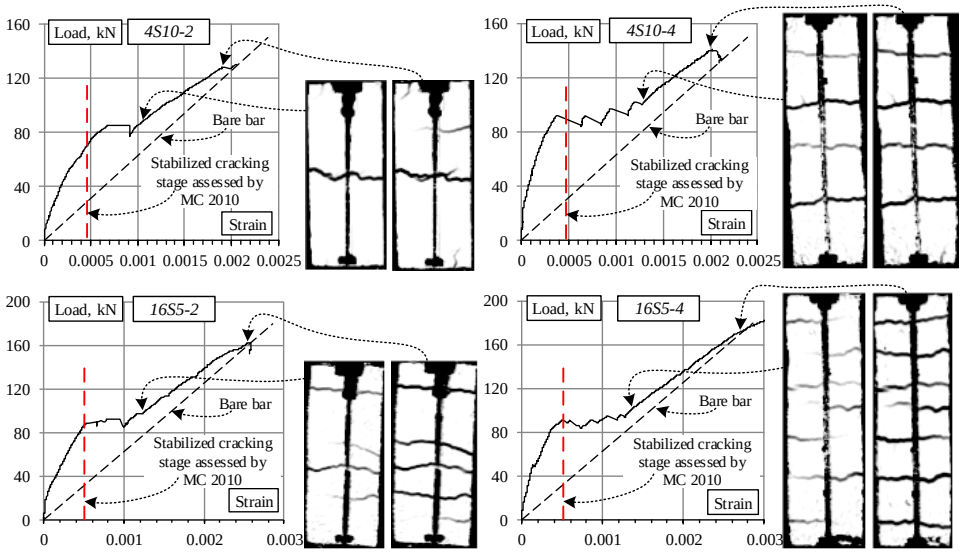

Fig. 2.38. The location of the stabilized cracking stage

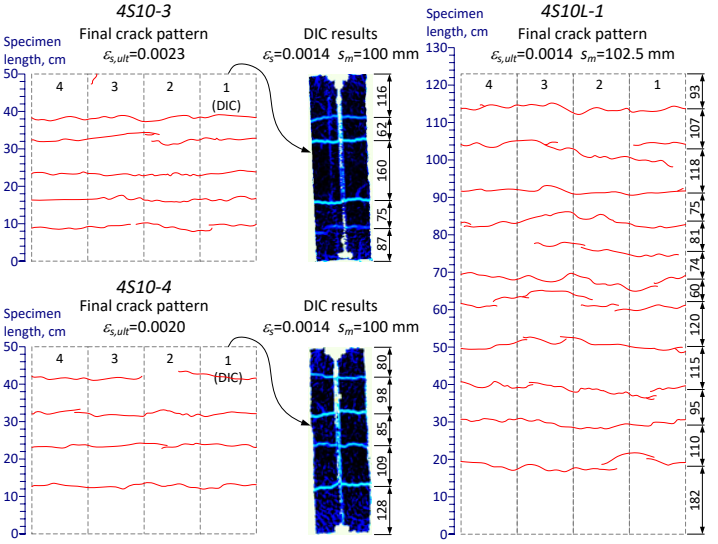

Fig. 2.39. Cracking results of the ties with different length
(*the maximum deformation allowed by the lever-arm equipment)

By investigating structure of the cracking data in Fig. 2.35 and Table 2.12, the following aspects are identified. The cracking process of the tie *4S10-6* has not evidently been stabilized. A chaotic cracking pattern is characteristic of the tie

4S12-1 that has demonstrated an exceptionally high s_{max} / s_m ratio. Consequently, both aforementioned ties were omitted when analysing the cracking tendencies. Figure 2.40 relates the maximum distances with the Ø/*p* ratio. The trend line defined using the test data implicitly indicates a tendency different from the Code approaches. Evident overestimation of the crack distances by both Codes are associated to the ties reinforced with four bars: the EC 2 predictions provide more than twofold overestimation, while the MC 2010 demonstrates results that are more accurate. The adequacy of the predictions improves with the decrease of Ø/*p*: the precise predictions by MC 2010 are characteristic of the ties with the minimum Ø/*p* ratio. On the one hand, the observed inaccuracy might be related to the relatively thin (30 mm) cover uncommon to laboratory ties (a prism reinforced with a centre bar). On the other hand, an important limitation can be related to the application of common laboratory specimens (relatively short concrete prisms reinforced with a centre bar) in the constitutive analysis: refer to Subsection 3.3.2.

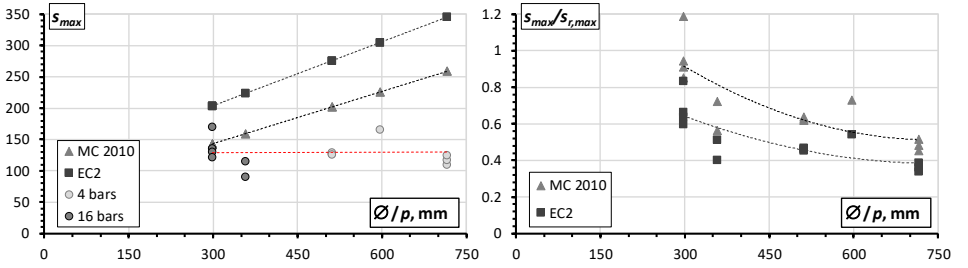

Fig. 2.40. The location of the stabilized cracking stage

Table 2.12. Crack distances sorted by the ratio Ø/*p*

Tie	*p*, %	Ø/*p*, mm	ε_{sm}, ‰	Predicted $s_{r,max}$, mm		Test results		s_{max}/s_m
				MC 2010	EC 2	s_{max}, mm	s_m, mm	
12S8-1	2.7	296	0.283	143	203	170	100	1.70
12S8-3	2.7	296	0.287	143	203	122	100	1.22
16S6-1	2.0	300	0.446	143	203	135	83	1.62
16S6-2	2.0	300	0.446	143	203	130	100	1.30
16S5-3	1.4	357	0.497	159	224	115	83	1.38
16S5-4	1.4	357	0.497	159	224	90	63	1.44
4S14-1	2.7	519	0.275	202	276	127	100	1.27
4S14-2	2.7	519	0.271	202	276	129	100	1.29
4S14-3	2.7	519	0.272	202	276	125	100	1.25
4S12-1	2.0	600	0.447	226	305	130	71	1.82
4S12-2	2.0	600	0.447	226	305	165	100	1.65
4S10-3	1.4	714	0.500	259	346	117	83	1.40
4S10-4	1.4	714	0.500	259	346	125	100	1.25
4S10-5	1.4	714	0.478	259	346	134	100	1.34
4S10-6	1.4	714	0.478	259	346	196	167	1.18

2.4.3. Concluding Remarks

An investigation of cracking and deformation behaviour of concrete ties with multiple bar reinforcement has been carried out. Although the performed investigation was covered a broad test program that includes ties with steel, GFRP and hybrid combination of GFRP and steel bar reinforcement, this section focuses on the test results of 27 concrete prisms reinforced with different number and diameter of steel bars. Three section types (with reinforcement ratio equal to 1.4%, 2.0% and 2.7%) are considered. Each of them consists of different reinforcement schemes: 4-bars reference and 16-bars (or 12-bars) alternative. Most of the ties were made with 30 mm cover. Special equipment has been developed for the tests. Average strains of the reinforcement and concrete surface were used for the deformation analysis. In order to assess the adequacy of the current design codes (Model Code 2010 and Eurocode 2), the predicted crack distances were compared to the experimental results. The investigation reveals that:

- While the design dodes predict that maximum crack spacing is dependent on the $Ø/p$ ratio, the test results (both maximum and average crack spacings) are practically independent of the reinforcement characteristics. For the limited number of the tested ties, the ratio of the maximum-to-average crack spacing varied between 1.2 and 1.8, on average being 1.27. Only one tie demonstrates a ratio greater than 1.70 that is well agreed with the crack assessment criterion suggested in the literature.
- At the stabilized cracking stage, predictions of the maximum crack distance were on the safe side. For the reference ties, the Eurocode 2 predictions were overestimated by 120% on average; the Model Code 2010 demonstrated results that are more precise (with 70% safety on average). The adequacy of the predictions increases with a decrease of the $Ø/p$ ratio. For the alternative reinforcement schemes, the respective predictions demonstrated a more rational safety margin, i.e. 80% and 20%. On the one hand, the observed inaccuracy might be related to the relatively thin (30 mm) cover uncommon for laboratory ties (a square prism reinforced with a single bar). On the other hand, an important limitation can be related to application of a laboratory tie in the constitutive analysis: the common tests do not allow separating effects related with the correlated variables, i.e. bar diameter, cover, and reinforcement ratio.
- The alternative reinforcement schemes are capable at securing practically indistinguishable deformation behaviour of the identical ties, while a significant scatter is characteristic of the reference ties reinforced with four bars. The scatter is particularly evident at the early cracking stage in the ties with relatively low reinforcement ratios (1.4% and 2.0%). It could

be attributed to the release of fracture energy (during the crack formation) that is evidently more uniform in the ties reinforced with 16 bars than in the reference counterparts reinforced with 4 bars.

– Significant differences between the average strains of concrete surface and reinforcement reveal the unreliable character of the deformation assessments based on the surface monitoring results. The similar results were also obtained in the previous test program (Subsection 2.3.4). In the present case (tension load applied directly to the bar reinforcement), the strain gradient is proportional to the distance between the bars and concrete cover. A reduction of the strain gradient reduces the overall scatter of the deformation response. In the current study, a reduction of the strain gradient was achieved in the ties reinforced with 16 bars. These results indicate the importance of the correct evaluation of the strain gradient (that might be significant in relatively short ties having a thick cover) for adequate assessment of the structural behaviour.

2.5. Conclusions of Chapter 2

1. The flexural elements were reinforced using steel and GFRP bars with two principal configurations: conventional layout – when the bars are distributed in a single layer and alternative layout – when the bars are distributed in three layers. Analysis of the flexural test data reveals that:
   1.1. The number of the reinforcement layers correlates with the flexural stiffness.
   1.2. The cracking results do not reveal a clear correlation between crack widths and the crack spacing when the reinforcement layout changes. Furthermore, the maximum crack opening is not necessarily adjacent to the maximum distance between cracks or located between two consecutive uncracked blocks of maximum total length. In this study, 11 of the considered 18 cracked schemes characteristic for the stabilized cracking stage (i.e. 61% of the cases) are in accordance with the conventional assumption of direct relation between the maximum crack width and maximum crack distance.
   1.3. One of predominant effects, governing deformation predictions of flexural elements, is related to the equivalent area of concrete effective in tension. The definition of the effective depth of the beam is a key issue due to the complexity of the internal stress distribution prior to and after cracking. Therefore, analysis of a simplified structure (reinforced concrete prism in tension) with possibly the most straightforward deformation behaviour should be considered.

2. Despite the seeming simplicity of the tensile test layout, a variety of cracking sources are responsible for the noticeable scatter of the test results. To solve this problem, a representativeness condition has been introduced. In the context of the present study, the representativeness is considered as a property of the test specimen isolating uncontrolled effects from the average deformation results. Analysis of the test results of more than 50 representative ties with different geometry and loading setup the study reveals that:
   2.1. The strain gradient in the concrete varies not only along the bar, but also within the cover.
   2.2. The proposed experimental procedure enables the localization of the end effect by iterative reduction of the gauge length.
   2.3. A new testing layout is necessary for separating from one another of the effects related with key-parameters of the section (i.e. concrete cover, reinforcement ratio, and diameter/number of the reinforcement bars).
3. The specific equipment for tensile tests of concrete prisms with multiple bar reinforcement has been developed. It was applied for test of 27 prisms reinforced with different number and diameter of steel bars. Three reinforcement ratios (1.4%, 2.0%, and 2.7%) were considered. Each of them corresponds of two reinforcement layouts: 4-bars reference and 16-bars (or 12-bars) alternative. The investigation revealed that:
   3.1. Maximum and average crack spacing is practically independent of the reinforcement characteristics, while design codes predicts that maximum crack spacing is dependent on the Ø/p ratio.
   3.2. At the stabilized cracking stage, predictions of the maximum crack distance were on the safe side. For the reference ties, the Eurocode 2 predictions were overestimated by 120% on average; the Model Code 2010 demonstrated results that are more precise (with 70% safety on average). For the alternative reinforcement schemes, the respective predictions demonstrated a more rational safety margin, i.e. 80% and 20%. The adequacy of the predictions increases with a decrease of the Ø/p ratio.
   3.3. The alternative reinforcement schemes are capable at securing practically indistinguishable deformation behaviour of the identical ties, while a significant scatter is characteristic of the reference ties reinforced with four bars. The scatter is particularly evident at the early cracking stage in the ties with relatively low reinforcement ratios (1.4% and 2.0%).

3

Serviceability Performance: Predominant Characteristics of Reinforced Concrete Elements

Experimental results presented in previous chapters cover a wide range of phenomena related with serviceability behaviour of reinforced concrete members. It was determined, that the concrete cover, reinforcement ratio and diameter of the reinforcement bars are the key parameters for adequate prediction of the deformations and cracking behaviour. The results of the beam-tests presented in Section 2.2 do not reveal a clear correlation between reinforcement layout and crack width, though the flexural stiffness is closely related with number of the reinforcement layers. Meanwhile Section 2.4 indicated that arrangement of the reinforcement has much more significant influence on the cracking behaviour of tensile elements. Clear understanding of contribution of the predominant characteristics to the serviceability performance, might help formulate principles of the behaviour-oriented design. There are several ways to ensure this aim. A certain concrete cover, suitable reinforcement bar diameter, proper reinforcement ratio, well-balanced stiffness and appropriate surface characteristics of the reinforcement bars, rational combinations of reinforcement materials can solve the serviceability problems. It is important to note, however, that there are existing numerous alternative solutions. This section presents several examples, which might be considered as modal layouts for further analysis. The particular attention is dedicated to

the effect of arrangement of reinforcement bars in tension concrete. Results of the numerical modelling and verification procedures with the help of experimental results are presented. On a basis of experimental results of flexural and tensile elements presented in previous sections, this chapter provides some examples of effective reinforcement for concrete elements. Particular effects of individual characteristics as well are illustrated by using four practical examples. This chapter includes the material presented in journal publications Meškėnas *et al.* (2017) and Rimkus & Gribniak (2017b), and conference proceedings Rimkus *et al.* (2016), Kaklauskas *et al.* (2013), Gribniak *et al.* (2017b) and Rimkus *et al.* (2017).

3.1. Effect of Bar Arrangement

The governed characteristics of the deformation and cracking performance of RC members have been identified in the previous sections. Experimental evidence presented in Section 2.3 have indicated that the cover, reinforcement ratio, and diameter of the reinforcement bar are the principal parameters of serviceability behaviour of RC ties. Findings of Section 2.2 show that the bar arrangement in the tensile zone directly interacts with flexural stiffness of RC beams, but it does not possess a clear correlation with the cracking performance. Conversely, results provided in Section 2.4 indicate that reinforcement layout has a considerable effect on the cracking behaviour, but marginal influence on the axial stiffness of the tensile elements. Meskenenas *et al.* (2017) and Gribniak *et al.* (2013) carried on tests of deformation and cracking behaviour of steel fibre reinforced concrete elements with bar reinforcement. It was indicated that the change in the volume of fibres from 0.3% to 0.6% (from 23.5 kg/m^3 to 47.1 kg/m^3) has no influence on the flexural stiffness as well as the crack behaviour of the beams reinforced with steel bars. In the contrast to the beams with steel reinforcement, the minimum amount of fibres (i.e. 23.5 kg/m^3) was effective increasing the serviceability properties of the beams with GFRP bar reinforcement (Gribniak *et al.* 2013). In fact, this effect is a consequence of two interrelated mechanisms associated with high deformability of such elements. On the one hand, the relatively high deformability of GFRP bars causes wider opening of the cracks, consequently increases the crack bridging effect of the fibres. On the other hand, the fibres ensure uniformity on the compressive zone by preventing cruching failure of the compressive concrete. However, the fibre effect on the serviceability properties of elements made using relatively low content of steel fibres (less than 50 kg/m^3) reinforced with steel bars can be neglected. The increase of the fibre content up to 1% by volume (78.5 kg/m^3) increases flexural stiffness of the beams (Gribniak *et al.* 2013). This increase is very similar to the effect of the bar arrangement in three layers (see Section 2.2). The multiple reinforcement distributed in the tensile zone (Fig. 2.2) evidently ensures uniform distribution of the tensile stresses in the concrete preventing localization of extremal cracks in similar manner as the moderate content (78.5 kg/m^3) of fibres.

Two important inferences were made in Section 2.4. The alternative reinforcement schemes (with 16 bars) are capable at securing practically indistinguishable deformation behaviour of the identical ties, while a significant scatter is characteristic of the reference ties reinforced with four bars. The scatter is particularly evident at the early cracking stage in the ties with relatively low (1.4% and 2.0%) reinforcement ratios. Another inference is related to the strain difference of the reinforcement and concrete surface of RC ties. The strain difference might be proportional to the distance between the bars and concrete cover. The mitigation of such differences may reduce the scatter of the deformation responses.

Test results of the beams reinforced with bars distributed in three layers in the tensile zone (Subsections 2.2.3 and 3.1.2) demonstrated that the adequacy of the "concrete area effective in tension" concept has serious doubts. In order to investigate these aspects, a simplified structure with a more straightforward deformation behaviour should be analysed. The observed differences in the deformation behaviour of RC beams and ties could be related to the load application manner. In case of the conventional tension tests, the load applied to the reinforcement is transferred to the surrounding concrete through the bond, while the opposite effect is characteristic of most of structural cases (including traditional beam tests) – the deformed concrete acts to the reinforcement. Thus, the cracking behaviour of the concrete is also diverse. For this purpose, following section is composed regarding both aforementioned element types separately.

3.1.1. Flexural Elements

Experimental study of deformation response of RC ties presented in Section 2.4 demonstrated, that elements with high concentration of the bars (four bars in the section) possess significantly higher scatter of the test outcomes than that is characteristic of the counterparts with higher number of the reinforcement bar. One of the most straightforward way to illustrate importance of this inference for the flexural behaviour is the numerical modelling with the help of the layered section model (Section 1.3). This model enables predicting the deformation response of flexural members with particular material laws and sectional characteristics.

In order to illustrate different scatter of deformation response of reference and alternative flexural elements (reinforced with 4 and 16 bars, respectively) numerical simulation of I-shape beams was performed. Two types of doubly reinforced beams with identical geometry and different bar distribution subjected to an external bending moment were considered (Fig. 3.1). The geometry of the beams was selected ensuring that the area of concrete effective in tension correspond to the area of the ties with multiple bar reinforcement (Fig. 2.26). The simulations are based on the stress-strain diagrams obtained by using the experimental diagrams of the ties show in Fig. 2.31. In this way six beams reinforced with four 10 mm bars (correspondent to the ties *4S10-1*, *4S10-2*, *4S10-3*, *4S10-4*, *4S10-5*,

4S10-6) and four beams reinforced with sixteen 5 mm bars (correspondent to the ties *16S5-1*, *16S5-2*, *16S5-3*, *16S5-4*) were simulated. Compressive strength of the concrete and modulus of elasticity of steel reinforcement were assumed the same as was determined for the correspondent ties (Table 2.10).

The calculated moment-curvature diagrams of the theoretical beams are shown in Fig. 3.1c. The scatter of the predicted deformation response is particularly evident at the early cracking stage. Coefficient of variation of the deformation response at the service load (defined as 55% of the ultimate bending moment) of the beams with four bars is equal to 67%, while beams with 16 bars showed only 7.7% variance.

Results presented in the Subsection 2.2.2 have shown that the tension-stiffening effect might increase in the beams with several layers of closely spaced reinforcement bars in the tension zone. The increase in flexural stiffness might be taken into account by modifying the effective depth *d* (Barris *et al.* 2013).

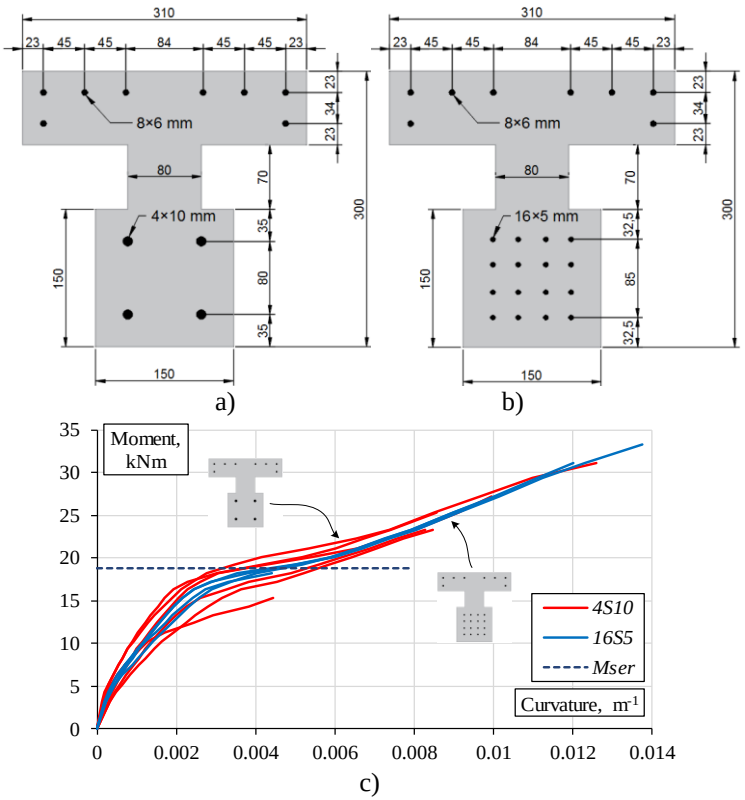

Fig. 3.1. Numerical simulation of I-shaped flexural elements: a) and b) theoretical cross-section of beams reinforced with four and 16 bars, respectively, and c) the predicted moment-curvature diagrams

For the illustration purpose, the effective depth was fitted to achieve best agreement between the theoretical and the experimental moment-curvature relationships (Fig. 2.6). Beams described in Section 2.2 with reinforcement bars distributed in three layers in the tension zone were used for this purpose. All beams had identical concrete cross-sections with a similar concrete strength and two different reinforcement ratios p (0.6 and 1.0%). The modified depth can be obtained as following:

$$d_{mod} = d \cdot \left(1.13 - 0.078 \frac{p_{ef}}{n} \right). \tag{3.1}$$

Here d is the effective depth; p_{ef} is the effective reinforcement ratio described by the Model Code 2010 (*fib* 2013); n is the modular ratio E_s/E_c.

Figure 3.2 compares the theoretical predictions (by *MC 2010*) with test results of the beams with reinforcement bars distributed in several layers. The curvature predictions were made using the actual and modified d values. The modified relative predictions $\Delta\kappa$ [from Equation (2.2)] are presented in Table 3.1. As can be observed by comparing results of Tables 2.4 and 3.1, this modification improves predictions securing a rational safety margins for the service load interval: the average prediction error decreases from –24% to –7% with the ultimate error reduction from –32% to –22%.

To analyse variation of the prediction errors with load, Figure 3.3 scatters the relative predictions $\Delta\kappa$ along the normalized loading level M' determined as

$$M' = \frac{M - M_{cr}}{M_u - M_{cr}}. \tag{3.2}$$

Here M_u is the theoretical ultimate bending moment (assuming the strength limit of the reinforcement equal to 500 MPa); M_{cr} is the theoretical cracking moment. According to Equation (3.2), $M' = 0$ and $M' = 1$ correspond to the cracking and ultimate moment, respectively.

Along the predictions $\Delta\kappa$, Figure 3.3 shows the corresponding trends determined by the means of moving average (with period of 10 points). It can be observed that accurate prediction results were obtained at the advanced loading stages with M' ranging from 0.5 to 1.0. However, at the earlier cracking stages ($0.1 < M' < 0.5$), the predicted curvatures remained significantly overestimated. In other words, the considered beams with several layers of bar reinforcement resisted early development of the cracks. The same tendencies can be observed analysing the cracking schemes shown in Figure 2.10. However, it should be recalled that the present analysis is limited to the test results (202 curvature points) of only four beams with different layouts of the tensile reinforcement; therefore, a more elaborate experimental study is needed to further quantify the empirical relationship (3.1).

Table 3.1. Modified curvature prediction percentage, $\Delta\kappa$ (the loads shown in Figure 2.6)

Beam	Loading level				
	1 (0.32–0.33 M_u)	2 (0.36–0.39 M_u)	3 (0.48–0.54 M_u)	4 (0.58–0.63 M_u)	M_{ser} (0.55 M_u)
S1-1	–13,9	–3.3	4.6	5.6	5.1
S1-6	1.9	4.1	–24.1	–19.4	–21.5
S2-1	–111.9	–119.4	–12.0	6.4	–1.2
S2-5nm	–15.0	–75.1	–36.3	4.4	–10.3

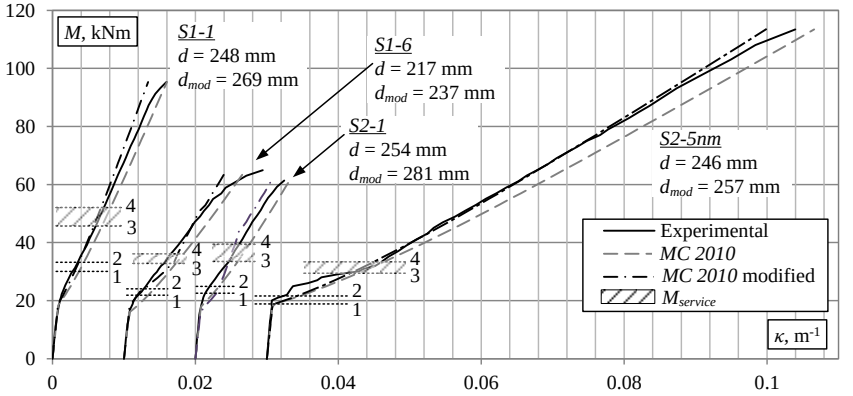

Fig. 3.2. The improved moment-curvature prediction results

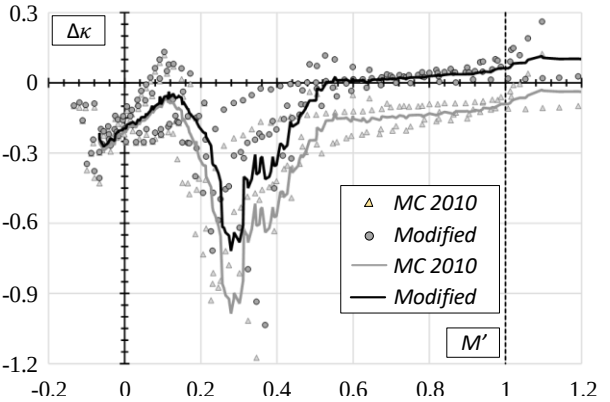

Fig. 3.3. Relative curvature predictions, $\Delta\kappa$, of beams with several reinforcement layers

3.1.2. Tensile Elements

The results presented in Subsection 2.4.2 demonstrate differences of deformation behaviour of the concrete in ties related with various number of reinforced bars. Figure 3.4 shows deformation results of the selected ties with the same total reinforcement area but different number of the bars. (The same ties are considered in

Table 2.11.) Although the average strains of the reinforcement are independent on the number of bars (Fig. 3.4a), noticeable differences of the average strains of the reinforcement and concrete surface are evident from Fig. 3.4b, where the reference deformation levels (ε_s = 0.5‰ and 2.0‰) correspond to the cracking patterns shown in Fig. 2.35. The differences decrease with increase of the reinforcement ratio *p*.

Different surface deformations of the concrete at the same strain of the reinforcement might be associated with different cover and bond performance (related to the diameter of the bars). Section 2.4 revealed no dependence of the experimental cracking distances on the Ø/*p* ratio, while design codes are indicating this ratio as a key factor for assessment of the cracking behaviour. These, in some sense, contradicting results have motivated further investigation of influence of bar diameter on the deformations and cracking behaviour of RC ties.

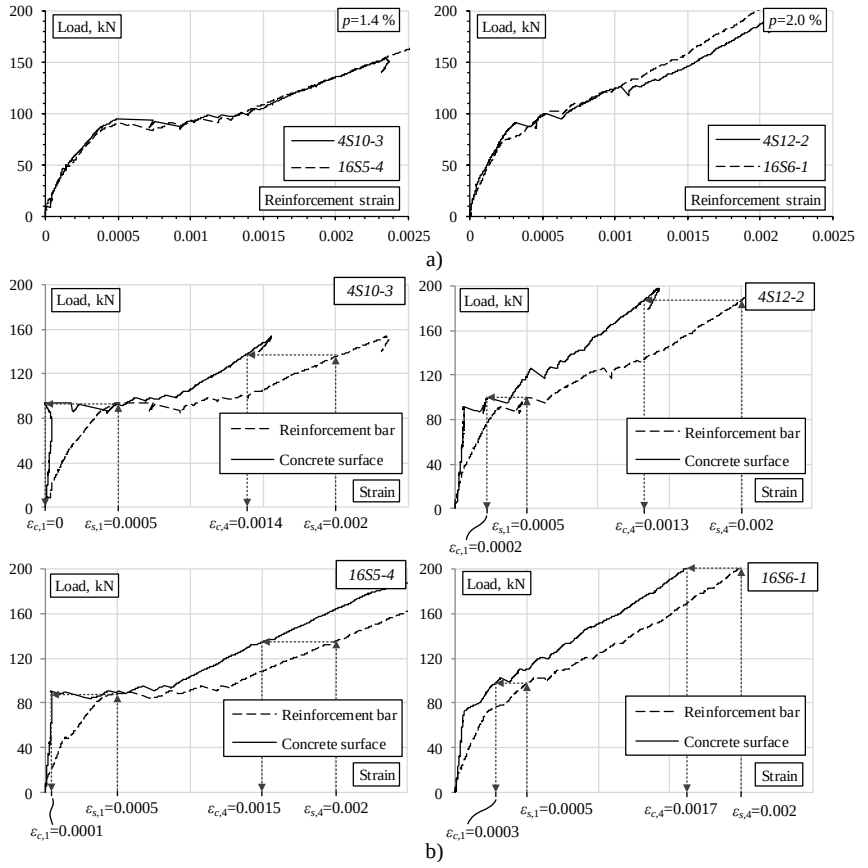

Fig. 3.4. Load-average strain diagrams of a) the selected specimens with reinforcement ratio 1.4% and 2.0%, and b) differences of the strains determined at the concrete surface and reinforcement (the reference strains, ε_s, correspond to the crack patterns in Fig. 2.35)

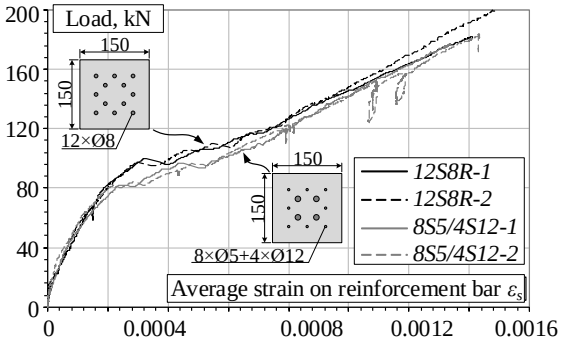

Fig. 3.5. Load-average strain of the reinforcement of the specimens *12S8R* and *8S5/4S12*

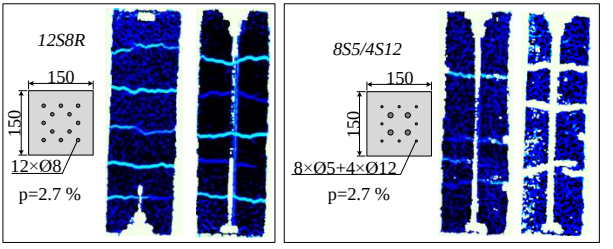

Fig. 3.6. Crack patterns of the specimens *12S8R* and *8S5/4S12* at the stabilized cracking stage (average strain of the reinforcement ε_s=1.4‰)

Two series of reinforced concrete prisms with 150×150 mm cross-section and 30 mm cover (Fig. 2.26a and b) are considered. In total, four ties reinforced with 12 bars of different diameter were tested. The first series designated as *12S8R* is consisted of the ties reinforced with twelve Ø8 mm bars, while the second series designated as *8S5/4S12* represents combination of eight Ø5 mm and four Ø12 mm bars. Both series have provided the same reinforcement ratio p = 2.7%. Deformations and cracking process of the ties were monitored using technique described in Subsection 2.4.1. The test results are presented in Figures 3.5 and 3.6. Crack patterns of the specimens are shown at the stabilized cracking stage (corresponding to the average strain of the reinforcement ε_s = 1.4‰).

From Figure 3.5, it is evident that the average deformations of the bars are almost identical, since the total area of the reinforcement is the same. However, cracking behaviour is different: 5 cracks are appeared in the specimens *12S8R* , while 3 cracks are characteristic of the alternative ties *8S5/4S12*. This might be a consequence of intricate cracking process in the inner part of the specimens. Different interfacial area between concrete and reinforcement leads to a different bond performance: total perimeter of the bars is equal to 301.4 mm and 276.3 mm of the specimens *12S8R* and *8S5/4S12*, respectively.

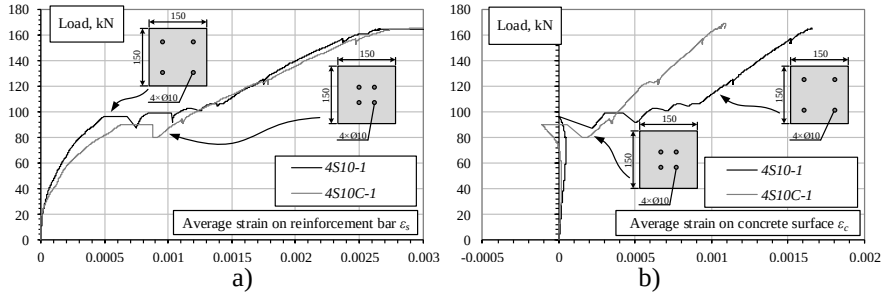

Fig. 3.7. Load-average strain diagrams of the specimens with concrete cover 30 mm and 50 mm: a) strain of the reinforcement bars, and b) strain of the concrete surface

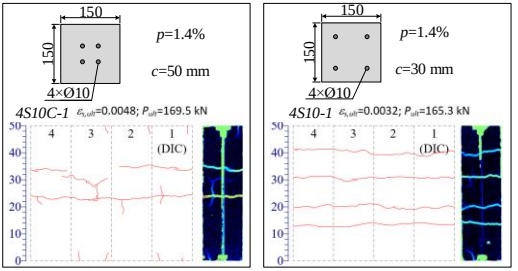

Fig. 3.8. Crack patterns of the specimens with concrete cover a) 50 mm and b) 30 mm (average strain of the reinforcement 4.8‰ and 3.2‰, respectively)

Furthermore, different axial stiffness and surface parameters (Fig. 2.1) might also contribute to different character of the internal cracking. Section 2.3.2 indicates that difference between strains of reinforcement and concrete surface might be proportional to the cover (Fig. 2.19). To illustrate this effect, two series of concrete prisms with the same reinforcement, but different covers are considered (Fig. 2.26a): the reference ties (*4S10-1*) with 30 mm cover that is typical for most structural applications (Aslani *et al.* 2015) and alternative ties (*4S10C-1*) with 50 mm cover characteristic of laboratory specimens. All ties were reinforced with four 10 mm bars that corresponds to the reinforcement ratio of 1.4%. Figures 3.7 and 3.8 show deformation and cracking behaviour of the ties.

Figure 3.7b evidences the cover effect on the surface deformation of the concrete. The enlarged cover induces a "negative" deformation of the surface under the load close to the cracking moment. Figure 3.7a does not represent any extraordinary behaviour of the bar reinforcement, while the cracking schemes in Figure 3.8 shows the opposite result. The final pattern of the alternative specimen (*4S10C-1*) clearly demonstrates the diverse behaviour (length) of the external and internal concrete blocks formed, respectively, between the transverse cracks and

at extremities of the prisms. Thus, the mean crack distance assessed by averaging the lengths of all uncracked segments will be inadequate. This problem might be solved by increasing the length of the prism and by excluding the external blocks from the consideration. The cracking tendencies of the reference (30 mm cover) and the alternative (50 mm cover) ties are also different (Fig. 3.9): slow development of the surface cracks is characteristic of the ties with the enlarged cover.

In the same manner as Figure 2.19, Figure 3.10 illustrates ability of the finite element model to predict cracking behaviour of the concrete in ties with different cover. (The numerical modelling details are described in Section 3.2.) Figure 3.10 associates the numerically identified strain distributions in the concrete with the cracking schemes of four ties with 30 mm cover and two alternative counterparts (with 50 mm cover) observed experimentally. Sufficient agreement between numerical and experimental cracking schemes is obtained.

This example demonstrates that well treated numerical model (i.e. calibrated with carefully collected test data of representative specimens) is capable to predict cracking behaviour of RC ties. Output of numerical simulation might be useful assessing the bar arrangement effect to the internal cracking. Obtained results indicate the importance of correct evaluation of the strain gradient in the concrete for adequate assessment of the structural behaviour of tensile members. This effect is also vital in identifying the area of concrete effective in tension as well as in assessing the tension-stiffening effect.

3.2. Numerical Modelling of Ties with Multiple Bars

Previous section evidenced that the effect of bar arrangement on deformations and cracking of RC ties might be related with the strain gradient in the concrete. Sections 2.3.2 and 3.1.2 displayed that the strain gradient increases with the cover. Enlarged cover might isolate development of the internal cracks preventing formation of the surface cracks. Unfortunately, experimental investigation of the internal cracking effect is extremely complex problem (Goto *et al.* 1971). Thus, this section applies a finite element technique for analysis of the cracking behaviour. This approach enables to predict strain and cracking behaviour of the concrete ties with various arrangement of the reinforcement bars. Such examples are presented in Subsections 2.3.2 and 3.1.2 (Figs. 2.19 and 3.10, respectively). In order to attain numerical result adequate to actual behaviour of the element, a proper calibration of the model is mandatory. This section proposes a methodology of tailoring the numerical models. For the illustration purpose, the numerical model presented in Subsection 2.4.1 is extended for the analysis of concrete ties reinforced with multiple bars. In order to predict deformation and cracking behaviour of the concrete members reinforced with multiple bars, numerical model of concrete prism was constructed.

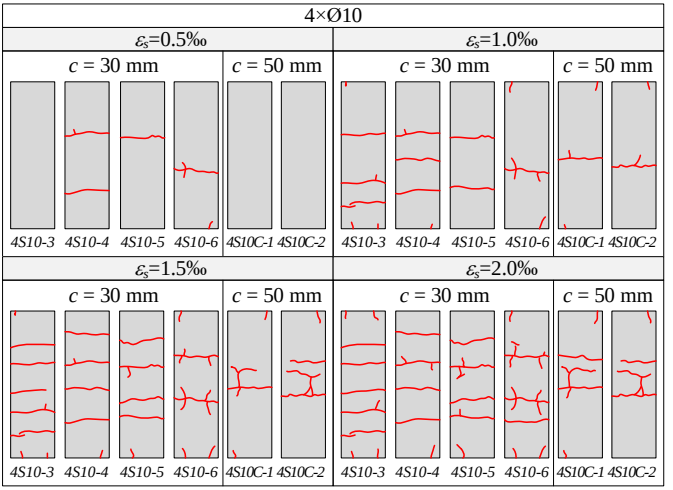

Fig. 3.9. Crack development identified by the digital image correlation system of the ties with different cover

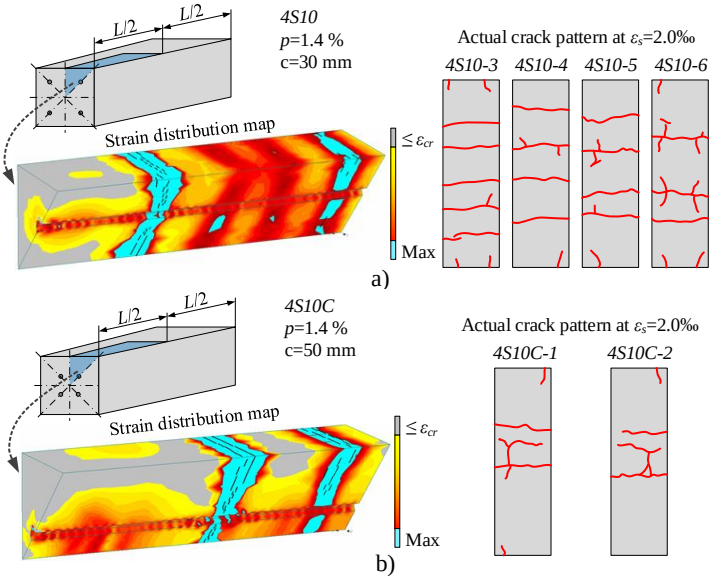

Fig. 3.10. Numerically predicted strain distribution in concrete (deformation of the reinforcement ε_s = 2.0‰) and experimental crack patterns identified by the digital image correlation system of the ties a) *4S10* and b) *4S10C*

As the reference, specimens with 150×150 mm cross-section and 500 mm length reinforced with Ø10 mm deformed steel bars were chosen. Parameters of

the selected specimens (*4S10, 4S10C, 8S10R, 8S10X* and *12S10X*) are presented in Figure 2.41 and Table 2.10. The choice of the modal samples is related with ability of applying the regular bond model proposed by Michou *et al.* (2015) for 10 mm deformed steel bar. This simplification of the bar topology allows to significantly reduce the calculation demands. The bar is modelled as a cylindrical macroelement; the interface of the concrete and reinforcement is modelled as a sequence of cylinders (of same diameter) with periodic field of regular bond parameters. Although such approach does not enable representing the radial bond-stress component, it was successfully validated by using test results of the concrete prisms reinforced with a single bar (Subsection 2.4.1). Recent numerical studies by Gribniak *et al.* (2016) indicate that this approach is acceptable for modelling reinforcement bars of a relatively small diameter (≤10 mm), since the neglected radial stress component increases significantly with the bar diameter.

The deformation problem is solved numerically within the 3D formulation. Following the symmetry conditions, the 1/16 part of the specimen was numerically simulated as shown in Figure 3.11 that also clarifies the boundary conditions. The load was modelled as prescribed displacement attributed to the inner surface of the reinforcement bar.

To create the numerical model, commercial finite element (FE) software ATENA was used (Cervenka 2002). Isoparametric tetrahedral finite elements with 10 degrees of freedom (DOF) and four integration points were used. The average FE size assumed in the analysis was equal to 15 mm with five times refinement at the reinforcement and concrete interface. For concrete, the model SBETA offered by ATENA was utilized. Reinforcement was modelled as linear elastic material. As mentioned previously, the ribbed contact between the reinforcement and concrete was modelled using a regular bond model proposed by Michou *et al.* (2015): the interface of the concrete and reinforcement is modelled as a sequence of cylinders with periodic bond parameters. The bond strength at the ribs is assumed τ_{max} = 175 MPa, whereas between the ribs τ_{max} = 3.0 MPa (see Fig. 3.12). The best-fit principle was used to calibrate the bond model. The experimental values of the compressive strength of the concrete and the modulus of elasticity of the reinforcement (Subsection 2.4.1) were used in the model. The remaining parameters were assumed as default values described by ATENA.

Refined discretization can be used for improving convergence of the numerical analysis. However, too fine discretization is impractical and might be inadequate at representing mezo-structural behaviour of the concrete with relatively large aggregates. Another important aspect is compatibility of meshes at the boundary of macro elements (Cervenka 2017). In this section, two finite element models are considered. *Model-1* has been developed by taking into account the mesh compatibility requirements: separate macroelements of the concrete were generated corresponding the rib location (the width of the macroelements was 2 mm and 5 mm, respectively). *Model-2* was created securing uniform mesh

within the concrete macroelement without consideration of the mesh compatibility criteria. Both models are shown in Fig. 3.13.

As described in Section 2.4, average deformations of the reinforcement and concrete surface were monitored during the tie tests. In Figure 3.14, the simulated diagrams of load-average strain of concrete surface and reinforcement are compared with the experimentally obtained results (Subsection 2.4.2). As can be observed in Figure 3.14a, *Model-1* adequately predicts both, concrete and reinforcement, deformations, while *Model-2* (Fig. 3.14b) is not as accurate. This outcome may be related with neglecting of the strain compatibility criteria.

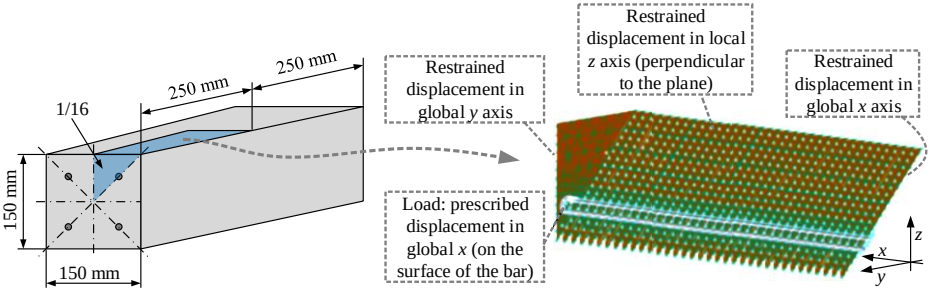

Fig. 3.11. Test specimen and symmetry conditions assumed in the finite element analysis

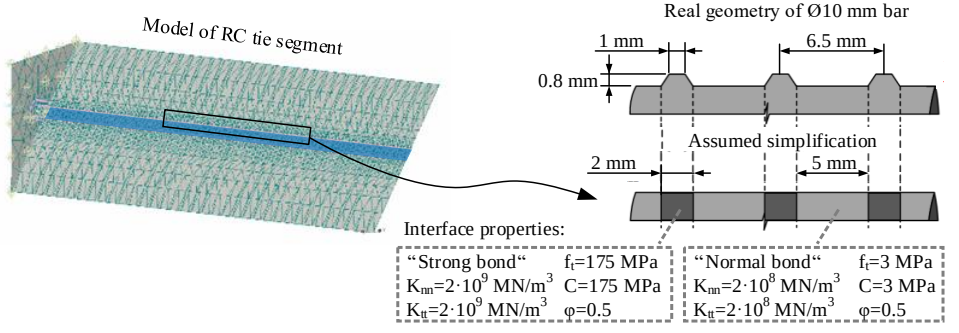

Fig. 3.12. Simplified modelling of the reinforcement ribs using interface elements

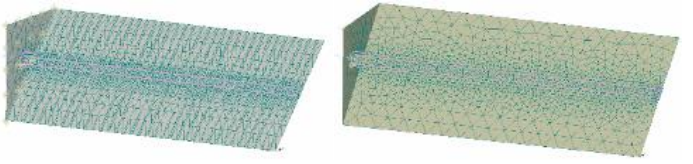

a) b)

Fig. 3.13. Two modelling approaches: a) *Model-1* with compatible mesh at the interface, and b) *Model-2* with uniform mesh of the concrete macroelement

Figure 3.15 shows the predicted strain distribution in the concrete. The strain distribution is related to the same load level (average strain of reinforcement $\varepsilon_{s,avg}$=0.0013). Grey areas indicates strain less than the theoretical cracking limit (ε_{cr}=0.0000825). The sky-blue colour indicates the strains above 0.004 (accounting for the assumed FE size, it approximately corresponds to 0.02 mm crack opening in *Model-1* and 0.06 mm in *Model-2*).

Since the same fracture energy was assumed for all finite elements, artificial mesh of *Model-1* "localizes" the cracking within relatively thick layers. Localization of these cracks is evident in Figure 3.15a. Although the deformation predictions by *Model-1* were accurate (Fig. 3.14a), the strain distribution predicted by *Model-1* seems unrealistic. The opposite results are characteristic of *Model-2* that predicts a more uniform internal strain distribution (Fig. 3.15b). Numerical modelling may be particularly efficient ensuring the "true" distribution of strains in the concrete. Figure 3.16a gives a typical deformed shape of RC tie, whereas Figure 3.16b shows the complex internal strain distribution in concrete. Another beneficial aspect of numerical modelling is ability to evaluate complex load transfer and internal cracking phenomena in RC ties.

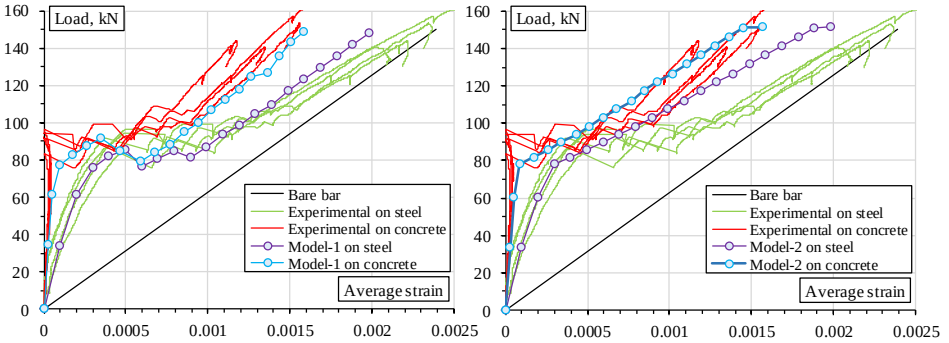

Fig. 3.14. Load-average strain diagrams of the concrete surface and reinforcement of the specimen *4S10* obtained using a) *Model-1* and b) *Model-2*

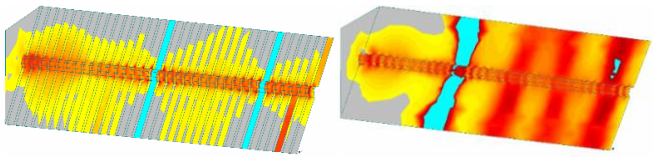

Fig. 3.15. Simulated concrete strain ε_x distribution using two models at the same load level (average strain of reinforcement ε_{avg} = 0.0013): a) *Model-1*, b) *Model-2*
(Note: grey areas indicates strain less than the theoretical cracking limit ε_{cr} = 0.0000825. The sky-blue color indicates the strains above 0.004)

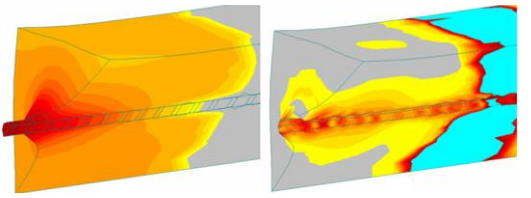

a) b)

Fig. 3.16. Typical behavior of RC tensile elements: a) deformed shaped of *4S10* tie, and b) concrete strain distribution in *4S10* tie

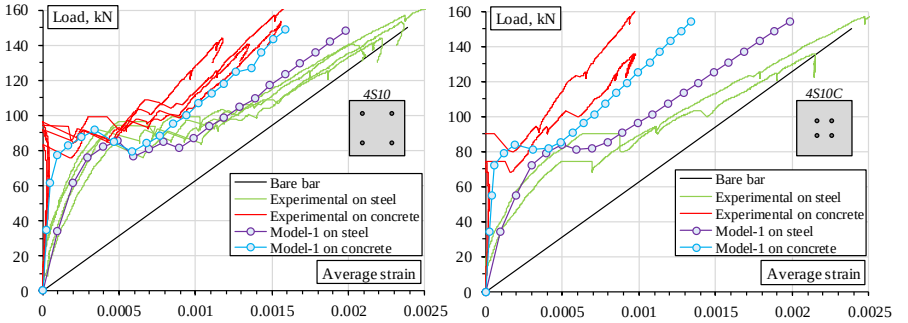

a) b)

Fig. 3.17. Load-average strain diagrams of a) *4S10* and b) *4S10C* specimens with concrete cover of 30 and 50 mm, respectively

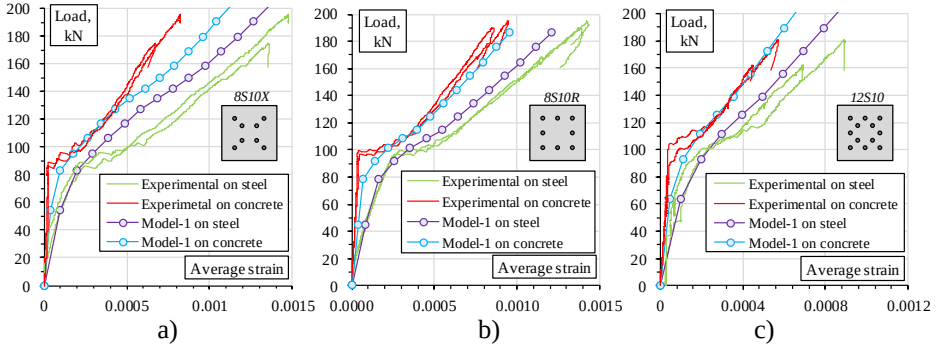

a) b) c)

Fig. 3.18. Load-average strain diagrams of a) *8S10X*, b) *S810R*, and c) *12S10* specimens with different reinforcement layouts

The cracking results identified by the DIC system for the considered ties are compared with the numerical predictions of the strain gradient in the concrete obtained by using *Model-2*, which was previously identified as more suitable for this purpose (than *Model-1*). The results are presented in Figure 3.10. A sufficient

agreement between numerical and experimental cracking result is evident. The average deformation response of the experimental ties was predicted by using *Model-1*. Figure 3.17 shows the load-average strain diagrams of the ties *4S10* and *4S10C*. It is clear that *Model-1* is capable to predict deformation behaviour of the concrete ties with multiple bars. In order to illustrate the abilities of the numerical model, specimens *8S10X*, *8S10R* and *12S10* with more complex bar layout (Fig. 2.26b) were considered as well. Load and average strain diagrams of these ties are shown in Fig. 3.18. As can be observed, agreement between numerical and experimental deformations is quite evident.

The presented numerical results have shown that of the proposed finite element models are suitable for the analysis of the ties with multiple bars. The numerical approach provides the ability to assess effects, which are too complex as to be evaluated experimentally (i.e. end effect, load transfer length, and strain distribution in the concrete). Such numerical models, however, not only must satisfy the representativeness condition (Section 2.3) but also they must be adequately validated. Hence, the test programs must be designed for assuring an additional information useful for the model verification purposes. In the current test program (Section 2.4) this requirement was satisfied by simultaneous monitoring of the average deformations of the bar reinforcement and concrete surface.

3.3. Case Studies

This chapter provides examples of effective reinforcement for concrete elements. Particular effects of individual characteristics are illustrated by using six practical examples. The first numerical example describes methodology for assessment of average deformation of the concrete in RC ties. The second example considers auto-correlation of variables of the traditional tie tests. The third example describes representative layout for tensile tests. The fourth design example is dedicated to the reducing scatter of deformation responses of RC plates. The last two examples cover the effect of the bars stiffness in different combinations on deformation and cracking characteristics of RC ties.

3.3.1. Average Concrete Deformations

Section 3.2 has demonstrated that numerical modelling might be helpful for assessing effects, which are too intricate for experimental analysis. Test results presented in Subsections 2.3.2 and 3.1.2 have indicated that the concept of "concrete area effective in tension" might be misleading and limited to the concrete cover, loading conditions, stress-strain state, and configuration of the unreinforced area. This section presents numerical example of such limitation.

Following the commonly accepted concept of "concrete area effective in tension", the total area in the tie is assumed to be effective in tension. Hence, tensile specimens containing equal amount of reinforcement and same cross-section area of the concrete should theoretically generate the same deformation response.

Figures 3.17 and 3.18 demonstrates a good agreement between the numerical predictions and experimental evidence of deformations of the reinforcement and concrete surface. Therefore, the finite element simulation can be used as a reference for validating the "effective area" concept. For this purpose, two RC ties with identical 150×150 mm cross-section and the same bar reinforcement but different cover are considered. The ties are reinforced with four 10 mm steel bars with 30 mm (reference) and 50 mm (alternative) concrete cover. Parameters of the considered specimens (*4S10* and *4S10C*) are presented in Figure 2.41 and Table 2.10. The numerical simulation procedure is described in Section 3.2. Since the ties posses almost identical deformations of the reinforcement, the present analysis is limited to the deformation behaviour of the concrete. The predicted strain distribution in the concrete is shown in Figure 3.10: the difference in the strain gradient in the concrete is evident. In order to quantify an actual (average) deformation response of the concrete, the numerically predicted average strain of the concrete was approximated by using 15 monitoring points shown in Figure 3.19. For both ties, position of the monitoring points was the same. The average strain of the concrete was obtained by averaging all monitorpointed results. The obtained load-average strain diagrams of the concrete surface and the "averaged" results are presented in Figure 3.20. The presented results reveal two important effects: 1) although the considered ties have theoretically identical characteristics, deformation behaviour of the concrete of the alternatve tie is significantly stiffer than the reference counterpart; 2) the alternative distribution of the reinforcement increases difference between the average and surface deformations of the cracked tie.

Although, specimens *4S10* and *4S10C* contains the same bar reinforcement, average concrete deformations at the service load (determined as 60% of the ultimate load bearing capacity) are significantly different. Figure 3.10 evidences complex distribution of concrete deformations and raise doubts for adequate definition of so called "concrete area effective in tension". Increase of the cover from 30 mm to 50 mm reduces the average deformations of 500 mm ties by 24%.

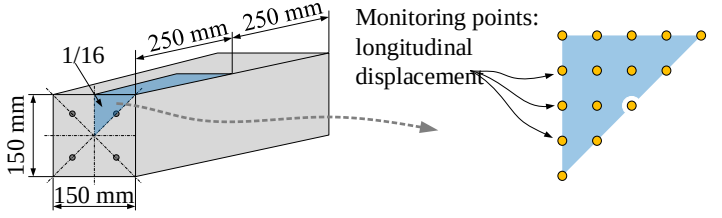

Fig. 3.19. Evaluation of average concrete strain

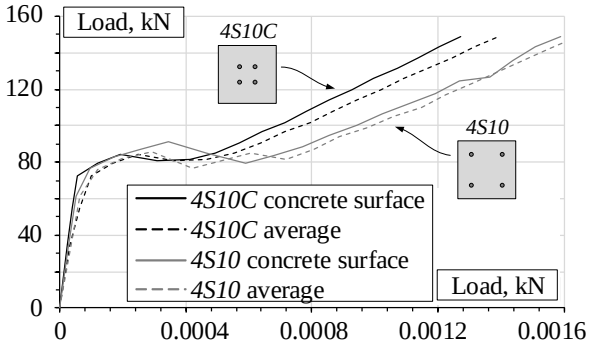

Fig. 3.20. Load-average strain diagrams of test specimens with different concrete cover

3.3.2. Auto-Correlation Effect of Variables of Tie Tests

Section 2.3 indicated that concrete cover, reinforcement ratio and diameter of reinforcement bars are the governing parameters for the cracking behaviour of RC ties. Similar characteristics are considered for the predictions of the maximum crack spacing by design codes (Eurocode 2 and Model Code 2010). However, Subsection 2.4.2 indicated that experimental results of maximum distances between the cracks of RC ties contradicts to design code predictions (see Fig. 2.40 and Table 2.12). An increase in $\varnothing/p$ from 300 to 714 causes the corresponding changes of $s_{r,max}$ predicted by the MC 2010 and EC 2 from about 140 mm to 260 mm and from 200 mm to 350 mm, respectively. The test results, however, show the average increase of the maximum distance s_{max} from 100 mm up to 120 mm only.

The observed inaccuracy might be related to the relatively thin (30 mm) cover uncommon to laboratory ties (a square prism reinforced with a centre bar). On the other hand, both codes imply a similar expression for $s_{r,max}$ assuming it to be a linear combination of two components related to the cover c and the ratio of the bar diameter to the reinforcement ratio $\varnothing/p$:

$$s_{r,\max} = k_1 \cdot c + k_2 \cdot \frac{\varnothing}{p}, \tag{3.3}$$

where k_1 and k_2 are coefficients dependent on various factors (concrete strength, bond quality, loading type, etc.). Considering a simple laboratory tie (square prism with a centre bar), the parameters c, $\varnothing$, and p become correlated:

$$c = \frac{b-\varnothing}{2} \approx \frac{b}{2}; \quad p = \frac{A_s}{A_c} = \frac{\pi \cdot \varnothing^2/4}{b^2 - \pi \cdot \varnothing^2/4} \approx \frac{\pi \cdot \varnothing^2/4}{b^2}, \tag{3.4}$$

where b is side length of the square section. Thus, Eqn. (3.3) can be rearranged as

$$s_{r,\max} = k_1 \cdot \frac{b - \varnothing}{2} + k_2 \cdot \left(\frac{4b^2}{\pi \cdot \varnothing} - \varnothing \right) \approx k_1' \cdot b + k_2' \cdot \frac{b^2}{\varnothing} \tag{3.5}$$

with coefficients k'_1 and k'_2, which now include constants 1/2 and 4/π. This simplification is acceptable if the ratio Ø/*b* is small enough. The common tests, dealing with 100×100 mm cross-section of the prism (i.e. *b*=100 mm), allow to account only for the effect of the bar diameter. This important limitation should be related to the use of simple specimens in constitutive modelling. The current design approaches, however, were empirically deducted by neglecting that limitation. A number of previous studies, e.g., Elfgren & Noghabai 2002, Beeby 2004, Eckfeldt & Schroder 2008, Balázs *et al.* 2013, Debernardi & Taliano 2016, recognised this problem.

It is important to note, that the general idea of the Codes is to formulate a mathematical model (consistent with experimental evidence) that provides a reasonable reliability of the predictions of the maximum crack spacing that can potentially occur. Thus, in order to investigate influence of reinforcement and cross-section characteristics to cracking behaviour or RC ties, application of proper test layout is extremely important to the adequacy of the research. As shown in Section 2.4, the proposed specific equipment for producing and testing concrete ties reinforced with multiple bars allows to design RC ties with independently controlled cross-sectional parameters. In other words, the concrete cover, reinforcement ratio, and diameter of reinforcement bars can be varied in the test specimens independently each other.

3.3.3. Representative Cracking Parameters

Subsection 2.3.3 has indicated the crack monitoring technique as a souce of inadequate interpretation of the cracking results. As shown in Figure 2.24, a crack width may vary along its length that causes scatter of the measurement results. As an alternative of the commonly uesd crack monitoring with an optical microscope, cumulative surface deformation characterization procedure (Subsection 2.3.3) can be considered. The cumulative deformations are independent characteristics, which allow performing adequate estimations for cracking extent and can be related with deformation behaviour of the ties.

In order to determine relation between the number of cracks and the deformation behaviour (tension-stiffening effect) of RC ties, nine concrete prisms are considered. All samples are reffered to the *Specimen A*, *B* and *C* (Fig. 2.12 and Table 2.9). Crack pattern, concrete surface strain distribution, and relative displacement determined at the service load (60% of the ultimate theoretical load) of the selected ties are presented in Fig. 2.23. The green area under the relative displacement profiles in the figure represents the cumulative deformations. This parameter was calculated at each loading stage by integrating the respective relative displacement profiles (Fig. 2.23), i.e. the curve of relative displacement profile is

integrated to the abscissa axis. The load-cumulative deformations diagrams of the ties are presented in Fig. 3.21a. The substantial scatter of the results illustrates the inappropriate way of the cracking analysis. As shown in Subsection 2.3.2, the observed inconsistency of the cracking results could be related with the end effect. From the previous analysis (Subsection 2.3.2), the end effect was found localized within the 40 mm zone near the notches in the *Specimen B* and from the boundary of the *Specimen A*. While, the end effect is found significant within the 30 mm zone in the *Specimen C*. (To determine the end effect for the *Specimen C*, *Specimen B* was considered as the reference.)

To improve representativeness of the ties, the following approach is proposed: 1) the surface exposed for the DIC is reduced as indicated in the adjustment schemes of the *Specimens A*, *B* and *C* (Fig. 3.21b); 2) the cumulative deformations are normalized relating them to the length of the exposed area (characterized by abscissa of the diagrams shown in Fig. 2.23). The modified load-cumulative deformation diagrams are presented in Fig. 3.21c indicating decrease in the scatter. The modified diagrams indicate almost the same deformation behaviour of the cracked ties. This example demonstrates that application of representative layout for tensile tests enables to determine relation between the cracking parameters (e.g. number of cracks, cumulative defromation) and the deformation behaviour of RC ties. This relation is possible to use for identifying the tension-stiffening effect.

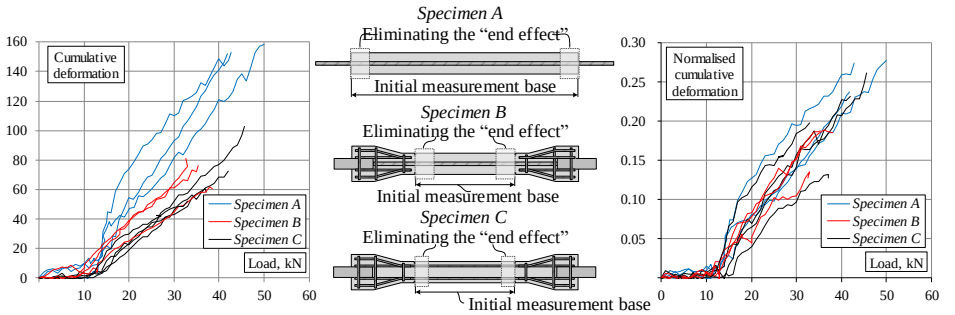

a) b) c)

Fig. 3.21. Load-cumulative displacement relations a) and c) of the selected ties, and b) zones with the localized end effect

3.3.4. Tension Tests of Concrete Prisms with Glass Fibre Reinforced Polymer and Hybrid Reinforcement Bars

The most important benefit of the developed testing equipment is that it allows testing concrete prisms reinforced with various combinations of bars made of any materials. It is imperative for verification of the current models for application of the innovative structural materials and solutions.

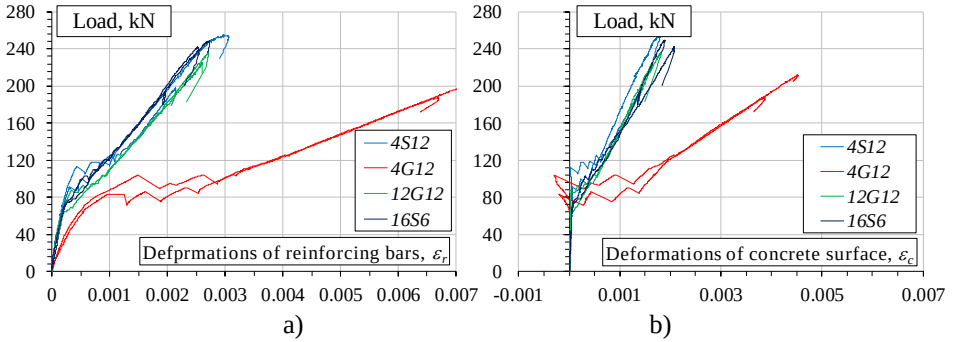

Fig. 3.22. Average deformations of a) the reinforcement and b) concrete surface of the ties with steel and glass fibre reinforced polymer bar reinforcement

To assess deformation and cracking behaviour of the ties reinforced with GFRP and hybrid (steel + GFRP) bars, cross-sections shown in Figures 2.26c and 2.26d were considered. For each of the sections, two identical ties were made of concrete mixture with target compressive strength class of C30/37. The main parameters of the specimens are presented in Table 2.10. As GFRP reinforcement, *ComBAR* by *Schöck* and *Aslan 100* by *Hughes Brothers* bars were used, while S500 steel grade bars and *ComBAR* GFRP bars combined in a single section were used as the hybrid reinforcement (Fig. 2.1). For taking into consideration the existence of different materials in the hybrid reinforcement configurations, the concept of equivalent steel reinforcement ratio, $p_{s,eq}$ (=$[A_s+A_f\cdot(E_f/E_s)]/A$, where A_s, A_f and E_s, E_f are area and modulus of elasticity of steel and GFRP reinforcement, respectively; A – total area of reinforcement), is used. The calculated ratio $p_{s,eq}$ is given in Table 2.10. The tests were performed in a same manner as described in Subsection 2.4.1. The determined load-average strain diagrams of the ties with multiple GFRP bar reinforcement were compared with the steel ties (Fig. 3.22) with either same distribution of bars or equivalent axial stiffness (see Subsection 2.4.2). Average deformations of the reinforcement and concrete surface of the ties with hybrid reinforcement are shown in Fig. 3.23. The nomenclature of the ties presented in Figs. 3.22 and 3.23 is explained in Subsection 2.4.1.

Differences between the deformations of reinforcement and concrete surface are significant. A portion of "negative" deformations of the concrete surface is observed in the ties reinforced with four GFRP bars (Fig. 3.22b). The same results were observed in the ties reinforced with four 10 mm steel bars and 50 mm cover (Fig. 3.7b). This effect might be caused by a low deformation modulus of GFRP bars and thick (50 mm) cover, which induce the strain gradient within the concrete of the boundary zones under the load applied to the reinforcement.

Figure 3.23 indicates that the hybrid combination of the reinforcement bars allows efficiently exploiting the steel reinforcement within the post-yielding

stage. The respective diagrams indicate the hardening behaviour of the specimens after the yielding of the steel bars. In the presence of an additional FRP reinforcement, yielding of the steel only changes the overall stiffness of the tie. Figure 3.23a illustrates this inference by adding the theoretical "bare bar" response (assessed following the material properties presented in Table 2.1).

The final crack patterns of the ties with GFRP bar and hybrid reinforcement are presented in Figs. 3.24 and 3.25, respectively. To assess adequacy of the cracking results of the relatively short 500 mm specimens, "long" (1230 mm) tie with GFRP bar reinforcement was additionally tested using a lever-arm system developed for a sustained loading (Gudonis *et al.* 2015). In order to monitor the development of the cracks, front surface of the short ties was exposed to a DIC system. This system allows to compare the crack patterns at corresponding deformations of reinforcement bars. Due to limited field of view of DIC system, cracking of the long tie was observed and fixed using an optical microscope. The test results are presented in Fig. 3.26. As can be observed, the cracking schemes of the ties with GFRP reinforcement differ significantly. The average crack distances determined at the same deformation levels are also diverse. Seemingly, the cracking process was not stabilized. The opposite results are characteristic of the ties reinforced with steel bars (Fig. 2.39).

Due to different ultimate strain of analysed ties, various number of cracks is characteristic for the final crack patterns. In order to analyse cracking performance of the ties with steel, GFRP and hybrid reinforcement, ties with similar concrete cover, axial stiffness and various arrangement of the bars were selected for further analysis. Cracking schemes of the specimens at corresponding deformation levels are presented in Fig. 3.27. Ties with different reinforcement material, but same cover and axial stiffness demonstrates similar cracking results. To relate the cracking parameters (crack spacing) observed for the ties with GFRP reinforcement with the results shown in Fig. 2.40, the crack patterns were related to the reference deformations of the reinforcement $\varepsilon_r \approx 1.5‰$ (see Subsection 2.4.2).

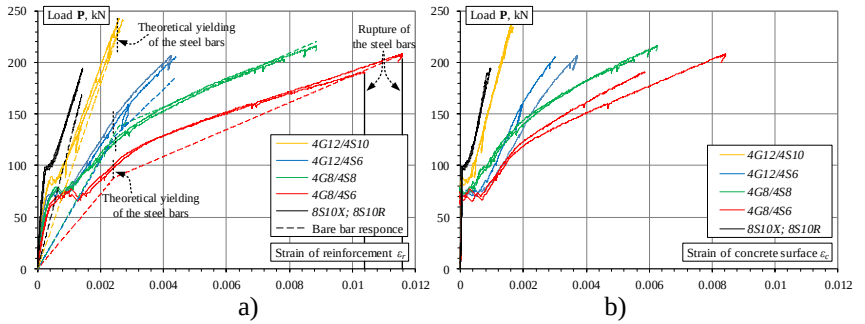

Fig. 3.23. Average deformations of a) the reinforcement and b) concrete surface of the ties with hybrid reinforcement

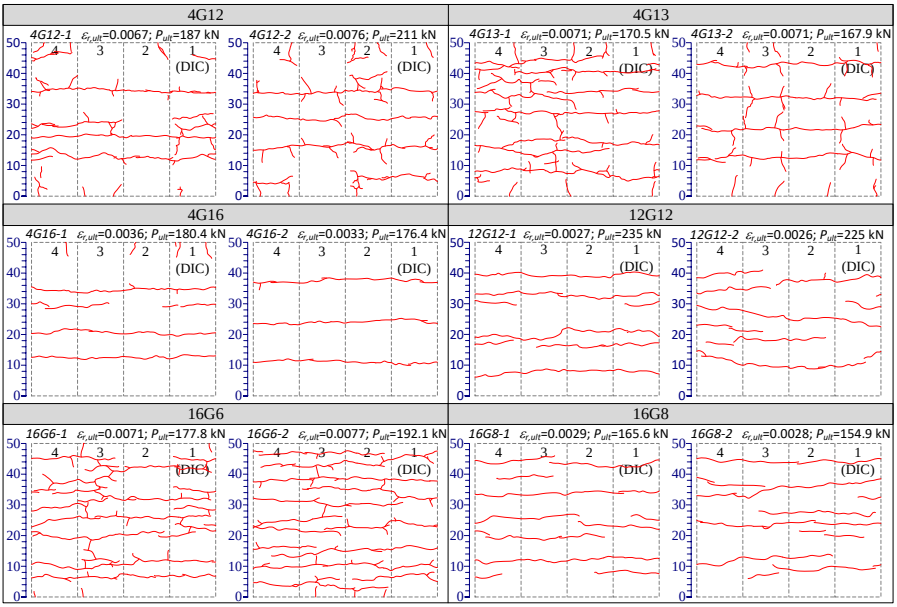

Fig. 3.24. Final crack patterns of the ties with glass fibre reinforced polymer bars

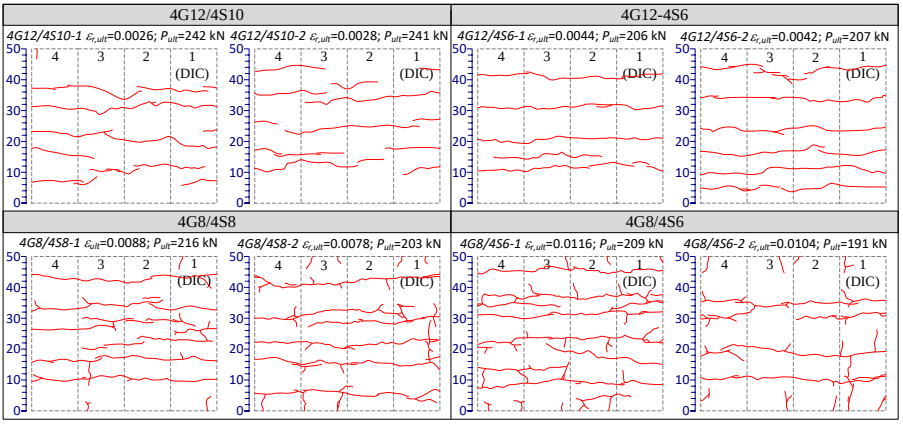

Fig. 3.25. Final crack patterns of the ties with hybrid reinforcement

Due to relatively low modulus of elasticity of GFRP reinforcement, GFRP reinforced ties attain higher deformation levels and postpone stabilised cracking stage. Most part of the investigated ties reinforced with GFRP bars did not arrive at stabilised cracking at the reference deformations of the reinforcement. Therefore, in the further analysis only the ties, which reach stabilised cracking stage at reference deformations, are considered.

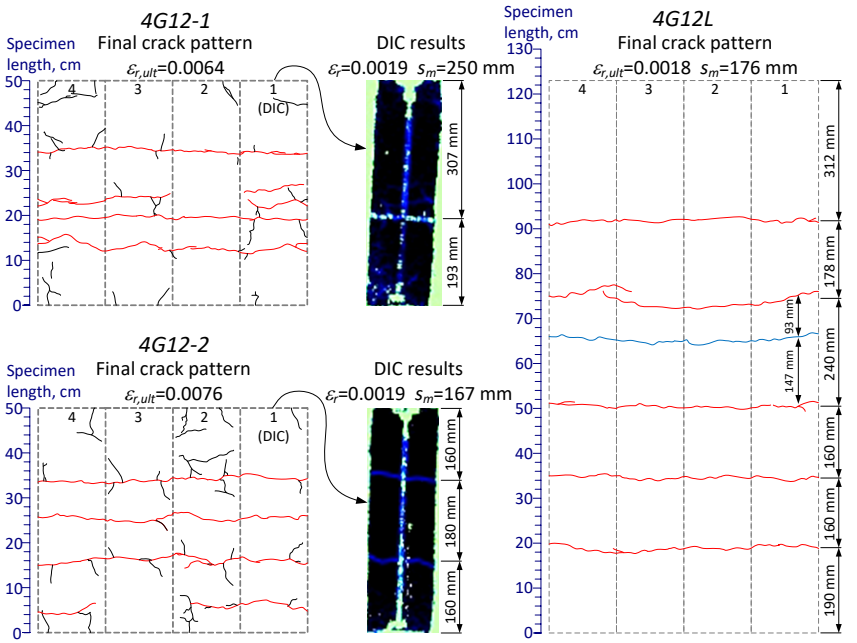

Fig. 3.26. The final crack patterns of the long (1230 mm) tie and cracking maps of the short (500 mm) ties that correspond to the same average deformations of glass fibre reinforced polymer bars

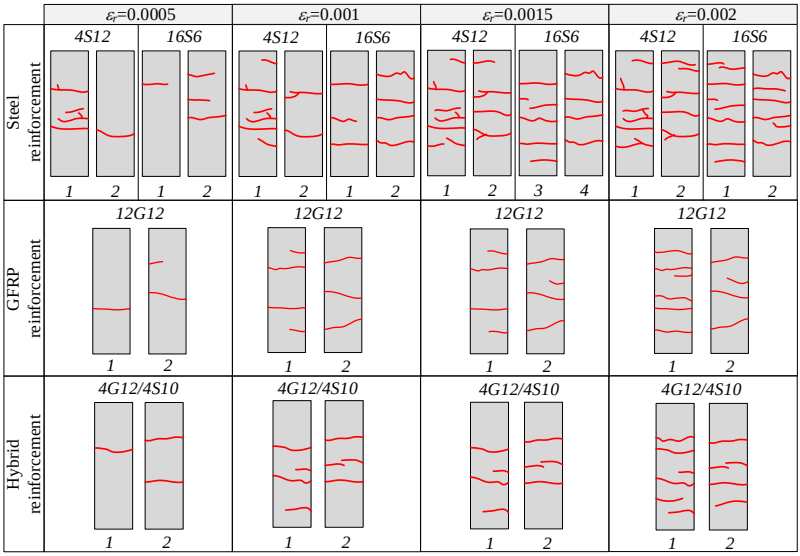

Fig. 3.27. Cracking schemes obtained by the digital image correlation system at corresponding deformations

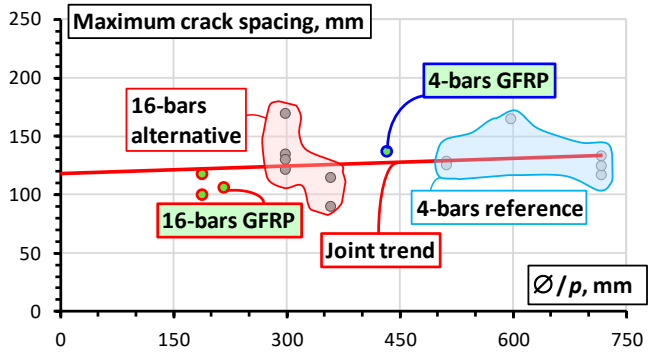

Fig. 3.28. Relationship between the maximum crack spacing and Ø/p ratio of the ties with steel and glass fibre reinforced polymer bar reinforcement

This analysis is limited by results of the ties with GFRP reinforcement, since the hybrid combination of the bars does not enable identification of the Ø/*p* ratio. It is important to note that Fig. 3.28 shows the same results as Fig. 2.40 with inclusion of the crack distances of four ties reinforced with GFRP bars. These ties has the stiffness compatible to the ties with steel reinforcement. Ties with GFRP bars also demonstrate the stabilized cracking stage. The joint trend-line of maximum crack spacing and Ø/*p* relationship indicates almost constant maximum distance between the cracks. This result supports (proves) experimental output presented in Subsection 2.4.2 and enables to formulate a hypothesis that the crack distances are mainly dependent on the geometry of the concrete prism and, particularly, concrete cover. The limited number of the specimens (only four ties with GFRP bars were additionally introduced into the analysis), however, requires additional verification of this hypothesis.

3.4. Conclusions of Chapter 3

This chapter presents experimental and numerical results of reinforced concrete members with particular attention to effects of reinforcement bars arrangement in tension concrete. The chapter considers flexural and tensile elements with various cross-section parameters and loading layouts. On a basis of experimental results of flexural and tensile elements presented in previous sections, this chapter provides some examples of effective reinforcement for concrete elements. Particular effects of individual characteristics as well are illustrated by using six practical examples. This chapter reveals that:

1. The predictions (by *MC 2010*) of the beams with reinforcement bars distributed in three layers demonstrates sufficient accuracy at the advanced

loading stages ($0.5 < M' < 1.0$), while at the earlier cracking stages ($0.1 < M' < 0.5$) the predicted curvatures remains significantly overestimated. However, it should be recalled that these results were obtained from only four beams; therefore, a more elaborate experimental study is needed to further quantify the empirical relationship.

2. Well treated numerical model (i.e. calibrated with carefully collected experimental data of representative specimens) using the regular bond interface between concrete and reinforcement is capable to predict deformations and cracking behaviour of RC ties with different cover, reinforcement ratio and diameter of reinforcement bars. The key parameter to the adequate assessment of the structural behaviour of tensile members is correct evaluation of the strain gradient in the concrete.
3. RC ties with theoretically identical characteristics (i.e. reinforcement ratio and diameter of reinforcement bar), demonstrates significantly different deformation behaviour of the concrete – specimens with 50 mm concrete cover is significantly stiffer than the specimens with 30 mm cover. Increase of the concrete cover from 30 mm to 50 mm reduces the average deformations of 500 mm ties by 24% at the service load (determined as 60% of the ultimate load bearing capacity).
4. The common tie tests, e.g. dealing with 100×100 mm cross-section prism, allow to account only for the effect of the bar diameter. In order to investigate influence of reinforcement and cross-section characteristics to cracking behaviour or RC ties, application of proper test layout is extremely important to the adequacy of the research. The proposed specific equipment for producing and testing concrete ties reinforced with multiple bars allows designing RC ties with independently controlled cross-sectional parameters.
5. The application of representative layout for tensile tests enables to determine relation between the cracking parameters (e.g. number of cracks, cumulative defromation) and the deformation behaviour of RC ties. Moreover, this relation is possible to use for identifying the tension-stiffening effect.
6. The experimental results of concrete ties reinforced with multiple steel and GFRP bars (with similar axial stiffness) indicate almost identical maximum distance between the cracks in the stabilized cracking stage. This result enables stating that the crack distances are predominantly dependent on the geometry of the concrete prism and, particularly, concrete cover.

General Conclusions

1. Based on the literature review, the following conclusions can be drawn:
   1.1. Heterogenity of concrete, external and internal cracks, bond behaviour are responsible for the scatter of test results of reinforced concrete (RC) members. Proper selection of the testing layout might significantly increase the adequacy of interpretation of the structural response.
   1.2. A simplified model of the concrete effective in tension (i.e. the concrete considerably influenced by the bond-stress transfer), is applied for predicting serviceability properties of tensile and flexural elements.
   1.3. Bond behaviour is an important factor of "effectiveness" of the concrete; however, presence of multiple bar reinforcement (in the tension zone) complicates behaviour of the concrete. Therefore, the effect of arrangement of the bars on overall stiffness and cracking behaviour of the tensile zone must be investigated. Deformation monitoring of the concrete surface and bar reinforcement is essential for this purpose.
   1.4. A numerical approach provides the ability to evaluate intricate load transfer and internal cracking phenomena and assess effects, which are too complex as to be evaluated experimentally.
2. The experimental study of effects of the arrangement of tensile reinforcement on the flexural stiffness and cracking of concrete beams deals with two groups of the beams reinforced with steel or GFRP bars. The reference group of the

specimens had a conventional reinforcement layout – the bars distributed in a single layer with minimum cover. The alternative group contains specimens with the same reinforcement ratio (as in the reference beams), but with tensile reinforcement arranged in three layers. The tests revealed that:

2.1. The number of the reinforcement bar layers correlates with the flexural stiffness. At the service load (55% of the theoretical ultimate bending moment), the deflection (curvature) predictions by the Model Code were on the safe side for the beams with three reinforcement layers (the prediction safety varied from 14% to 32%), whereas the predictions for the reference beams were deficient by 7–15%.

2.2. Although the crack spacing predictions by the Model Code for the beams with the bars distributed in several layers were quite accurate, the results for the conventionally reinforced elements differed significantly with the experimental values being about 50% larger than the calculated ones.

2.3. The experimental cracking results do not reveal a clear correlation between crack widths and the crack spacing when the reinforcement layout changes. Although the observed crack distances for the stabilized cracking stage of the beams with three layers of bars were larger, their maximum crack openings were smaller than in the reference specimens with the same reinforcement ratio.

2.4. The maximum crack is not necessarily adjacent to the maximum distance between cracks or located between two consecutive uncracked blocks of maximum total length. In this study, 11 of the considered 18 cracked schemes (i.e. 61% of the cases) are in accordance with the conventional assumption of direct relation between the maximum crack width and maximum crack distance.

3. An intricate nature of flexural elements limits ability of assessing the effects of reinforcement arrangement to the serviceability properties. The direct way of isolating such uncertainty is related with the analysis of RC members subjected to tension. A representativeness condition and corresponding experimental procedure has been proposed for isolating the average deformations of the concrete from uncontrolled effects. The test results of more than 50 typical ties and bone-shaped specimens with different geometry and loading setup revealed that:

3.1. The typical tie tests, e.g. dealing with 100×100 mm cross-section prism, allow to account only for the effect of the bar diameter. In order to investigate influence of reinforcement and cross-section characteristics to cracking behaviour or RC ties, application of proper test layout is vital ensuring adequacy of the result interpretation.

3.2. The difference in the crack pattern (crack spacing) of the nominally identical ties (i.e. identical reinforcement ratio and size of the concrete cross-

section) can be attributed to the differences in the concrete cover and variation of bonded surface of the bars with different diameter.

3.3. The representative layout of tensile tests enables of clarifying the relation between the average deformations and the cracking parameters (e.g. number of cracks, crack width).

4. Specific test equipment for independent variation of the section parameters (concrete cover, reinforcement ratio, and diameter of the reinforcement bars) has been developed. It was used for the test campaign consisted of 64 concrete prisms. The obtained results clarify that:

4.1. Maximum and average crack spacing is practically independent of the reinforcement characteristics, while design codes predicts that maximum crack spacing as dependent on the $Ø/p$ ratio.

4.2. The reinforcement schemes with increased number of reinforcement bars are capable at securing practically indistinguishable deformation behaviour of the identical ties, while a significant scatter is characteristic of the reference ties reinforced with four bars. The scatter is particularly evident at the early cracking stage in the ties with relatively low reinforcement ratios (1.4% and 2.0%).

4.3. RC ties with nominally identical characteristics (i.e. reinforcement ratio and diameter of reinforcement bar), demonstrates significantly different deformation behaviour of the concrete. Increase of the concrete cover from 30 mm to 50 mm reduces the average deformations of 500 mm ties by 24% at the service load.

5. The thesis also includes several examples, which might be considered as modal layouts for the further analysis. The presented results revealed that:

5.1. A well-treated numerical model (i.e. calibrated with carefully collected experimental data of representative specimens) based on the fracture mechanics principles and the regular bond model of reinforcement reported in the literature is capable predicting deformation and cracking behaviour of RC elements with different cover and reinforcement ratio. Adequacy of the assessment of deformation behaviour of RC ties is closely related with evaluation of the strain gradient in the concrete.

5.2. The experimental results of concrete ties reinforced with multiple steel and GFRP bars (with similar axial stiffness) indicate almost identical maximum distance between the cracks in the stabilized cracking stage. This result enables stating that the crack distances are predominantly dependent on the geometry of the concrete prism and, particularly, concrete cover.

References

ACI Committee 408. 2003. *Bond and Development of Straight Reinforcing Bars in Tension* (*ACI 408R-03*). Detroit, MI: American Concrete Institute, 49 p.

ACI Committee 440. 1996. *State of the Art Report on FRP for Concrete Structures*. Detroit, MI: American Concrete Institute, 57 p.

Alexander, K. M., Gilbert, D. J. & Wardlaw, J. 1968. Aggregate-cement bond, cement paste strength and the strength of concrete. *The Structure of Concrete*, London: The Cement and Concrete Association, 59–81.

Ashtiani, M. S., Dhakal, R. P., Scott, A. N. & Bull, D. K. 2013. Cyclic beam bending test for assessment of bond-slip behaviour. *Engineering Structures*, 56, 1684–1697.

Aslani, F., Nejadi, S. & Samali, B. 2015. Instantaneous and time-dependent flexural cracking models of reinforced self-compacting concrete slabs with and without fibres. *Computers and Concrete*, 16(2), 223–243.

Ayudhya, B. I. N. & Ungkoon, Y. 2011. Bond strength of fiber reinforced polymer (FRP) bars in autoclaved aerated concrete (AAC). *Advances in FRP Composites in Civil Engineering*, Berlin: Springer, 585–588.

Baena, M., Torres, L., Turon, A. & Mias, C. 2013. Analysis of cracking behaviour and tension stiffening in FRP reinforced concrete tensile elements. *Composites Part B: Engineering*, 45(1), 1360–1367.

Baena, M., Turon, A., Torres, L. & Miàs, C. 2011. Experimental study and code predictions of fibre reinforced polymer reinforced concrete (FRP RC) tensile members. *Composite structures*, 93(10), 2511–2520.

Balázs, G. L., Bisch, P., Borosnyói, A., Burdet, O., Burns, C., Ceroni, F., Cervenka, V., Chiorino, M. A., Debernardi, P., Eckfeldt, L., El-Badry, M., Fehling, E., Foster, S. J., Ghali, A., Gribniak, V., Guiglia, M., Kaklauskas, G., Lark, R. J., Lenkei, P., Lorrain, M., Marí, A., Ozbolt, J., Pecce, M., Caldentey, A. P., Taliano, M., Tkatcic, D., Torrenti, J. M., Torres, L., Toutlemonde, F., Ueda, T., Vitek, J. L. & Vráblík, L. 2013. Design for SLS according to fib Model Code 2010. *Structural Concrete*, 14(2): 99–123.

Barris C., Torres L., Comas J. & Mias C. 2013. Cracking and deflections in GFRP RC beams: An experimental study. *Composites Part B*: *Engineering*, 55, 580–590.

Barros, J. A., & Fortes, A. S. 2005. Flexural strengthening of concrete beams with CFRP laminates bonded into slits. *Cement and Concrete Composites*, 27(4), 471–480.

Barros, J. A., Taheri, M., & Salehian, H. 2015. A model to simulate the moment–rotation and crack width of FRC members reinforced with longitudinal bars. *Engineering Structures*, 100, 43–56.

Barros, J. A., Taheri, M., Salehian, H., & Mendes, P. J. 2012. A design model for fibre reinforced concrete beams pre-stressed with steel and FRP bars. *Composite Structures*, 94(8), 2494–2512.

Bartlett, F. M. & MacGregor, J. G. 1996. Statistical analysis of the compressive strength of concrete in structures. *ACI Materials Journal*, 93, 158–168.

Base, G. D. & Murray, M. H. 1982. A new look at shrinkage cracking. *Civil Engineering Transactions*, 24(2), 171–176.

Base, G. D., Read, J. B., Beeby, A. W. & Taylor, H. P. 1966. *An Investigation of the Crack Control Characteristics of Various Types of Bar in Reinforced Concrete Beams*. Research Report 18, Part 1, Wexham Springs: Cement and Concrete Association, 45 p.

Bažant, Z. P. & Oh, B. H. 1983. Crack band theory for fracture of concrete. *Materials and Stuctures*, 16(3), 155–177.

Beeby, A. W. 1978. Corrosion of reinforcing steel in concrete and its relation to cracking. *Structural Engineer*, 56(3), 8–23.

Beeby, A. W. 1983. Cracking, cover, and corrostion of reinforcement. *Concrete International*, 5(02), 35–40.

Beeby, A. W. 2004. The influence of the parameter ϕ/ρ eff on crack widths. *Structural Concrete*, 5(2), 71–83.

Bencardino, F. 2013. Mechanical parameters and post-cracking behaviour of HPFRC according to three-point and four-point bending test. *Advances in Civil Engineering*, 2013, Paper ID 12852, 11 p.

Bischoff, P. H. 2001. Effects of shrinkage on tension stiffening and cracking in reinforced concrete. *Canadian Journal of Civil Engineering*, 28(3), 363–374.

Borges, J. F. 1965. *Cracking and deformability of reinforced concrete beams*. Research report. Paris: Laboratório Nacional de Engenharia Civil, 102 p.

Borosnyói, A. & Balázs, G. L. 2005. Models for flexural cracking in concrete: the state of the art. *Structural Concrete*, 6(2), 53–62.

Borosnyói, A. & Snóbli, I. 2010. Crack width variation within the concrete cover of reinforced concrete members. *Építöanyag*, 10(3), 70–81.

Broms, B. B. & Lutz, L. A. 1965. Effects of arrangement of reinforcement on crack width and spacing of reinforced concrete members. *ACI Journal Proceedings*, 62(11), 1395–1410.

Broms, B. B. & Lutz, L. A. 1965. Effects of arrangement of reinforcement on crack width and spacing of reinforced concrete members. *ACI Journal Proceedings*, 62(11), 1395–1410.

Broms, B. B. 1965. Crack width and crack spacing in reinforced concrete members. *ACI Journal Proceedings*, 62(10), 1237–1256.

Cairns, J. & Abdullah, R. B. 1996. Bond strength of black and epoxy-coated reinforcement-a theoretical approach. *Materials Journal*, 93(4), 362–369.

Caldentey, A. P. & Peiretti, H. C. 1999. Medida experimental de las deformaciones a largo plazo en dos vigas hiperestáticas postesas. *Hormigón y Acero*, 211(1), 2–29.

Caldentey, A. P., Cembranos, J. M. & Peiretti, H. C. 2017. Slenderness limits for deflection control: A new formulation for flexural reinforced concrete elements. *Structural Concrete*, 18(1), 118–127.

Caldentey, A. P., Peiretti, H. P., Iribarren, J. P. & Soto, A. G. 2013. Cracking of RC members revisited: influence of cover, $\phi/\rho_{s,ef}$ and stirrup spacing – an experimental and theoretical study. *Structural concrete*, 14(1), 69–78.

Calderón, E. & Fernández, J. 2010. Investigación experimental sobre los modelos normativos de fisuración en piezas de hormigón armado sometidas a flexión pura. *Informes de la Construcción*, 62(518), 43–56 (in Spanish).

Carino, N. J. & Clifton, J. R. 1995. *Prediction of cracking in reinforced concrete structures*. Report No. 5634. Detriot: NISTIR, 235 p.

Castro, P. F. & Carino, N. J. 1998. Tensile and nondestructive testing of FRP bars. *Journal of Composites for Construction*, 2(1), 17–27.

CEN (Comité Européen de Normalisation). 2004. *Eurocode 2: Design of Concrete Structures – Part 1: General Rules and Rules for Buildings, EN 1992-1-1:2004,*. Brussels: CEN, 234 p.

Cervenka V. 2017. *ATENA Program Documentation. Part 2-2. User's Manual for ATENA 3D*, Prague: Cervenka Co., 356 p.

Cervenka, V. 2002. Computer simulation of failure of concrete structures for practice. *Proceedings of the First fib Congress*, 289–304.

Chan, S. H. C. 2012. *Bond and Cracking of Reinforced Concrete*. Doctoral dissertation, Cardiff: Cardiff University, 125 p.

Cheng, Y., Hagan, P. C., Mitra, R. & Wang, S. 2015. Defects Visualization Using Acoustic Emission Tomography Technique. *ACI Materials Journal*, 112(6), 125–131.

Darwin, D., McCane, S. L., Idun, E. K. & Schoenekase, S. P. 1992. Development length criteria: bars not confined by transverse reinforcement. *ACI Structural Journal*, 89(6), 709–720.

Debernardi, P. G. & Taliano, M. 2016. An improvement to Eurocode 2 and fib Model Code 2010 methods for calculating crack width in RC structures. *Structural Concrete*, 17(3), 365–376.

Debernardi, P. G., Guiglia, M. & Taliano, M. 2011. Shear strain in B-regions of beams in service. *Engineering Structures*, 33(2), 368–379.

Debernardi, P. G., Guiglia, M. & Taliano, M. 2013. Effect of secondary cracks for cracking analysis of reinforced concrete tie. *ACI Materials Journal*, 110(2), 126–137.

Deluce, J. R. 2011. *Cracking Behaviour of Steel Fibre Reinforced Concrete Containing Conventional Steel Reinforcement*. Doctoral dissertation, Torino: Torino Politechnica, 205 p.

Dominguez, N., Brancherie, D., Davenne, L. & Ibrahimbegović, A. 2005. Prediction of crack pattern distribution in reinforced concrete by coupling a strong discontinuity model of concrete cracking and a bond-slip of reinforcement model. *Engineering Computations*, 22(5–6), 558–582.

Eckfeldt, L. & Schröder, S. 2008. Random effects inside the cracking data of RC tests. *Proceedings of the Sixth International Probabilistic Workshop*, 183–205.

Elfgren, L. & Noghabai, K. 2002. Tension of reinforced concrete prisms. Bond properties of reinforcement bars embedded in concrete tie elements. Summary of a RILEM round-robin investigation arranged by TC 147-FMB 'Fracture Mechanics to Anchorage and Bond'. *Materials and Structures*, 35(6), 318–325.

EN 10080. 2005. *Steel for the Reinforcement of Concrete–Weldable Reinforcing Steel*, 120 p.

Erdem, S., Kağnıcı, T. & Blankson, M. A. 2015. Investigation of bond between fibre reinforced polymer (FRP) composites rebar and aramid fibre-reinforced concrete. *International Journal of Composite Materials*, 5(6), 148–154.

Fantilli, A. P. & Chiaia, B. 2012. Golden ratio in the crack pattern of reinforced concrete structures. *Journal of Engineering Mechanics*, 139(9), 1178–1184.

fib (International Federation for Structural Concrete). 2000. Bond of reinforcement in concrete: state-of-art report. *fib Bulletin*, 10, 160–167.

fib (International Federation for Structural Concrete). 2013. *Model Code for Concrete Structures 2010*, Berlin: Ernst & Sohn, 245 p.

Forth, J. P. & Beeby, A. W. 2014. Study of composite behavior of reinforcement and concrete in tension. *ACI Structural Journal*, 111(2), 397–407.

Gambarova, P. G. & Rosati, G. 1996. Bond and splitting in reinforced concrete: test results on bar pull-out. *Materials and Structures*, 29(5), 267–276.

Ganesan, N., Indira, P. V. & Sabeena, M. V. 2013. Tension Stiffening and Cracking of Hybrid Fiber-Reinforced Concrete. *ACI Materials Journal*, 110(6), 137–145.

Garg, C., Jain, A., & Kumar, M. S. 2014. Experimental studies on mechanical properties of polypropylene fibre based sustainable concrete. *Proceedings of the International Conference on Sustainable Civil Infrastructure 2014*, 10 p.

Gilbert, R. I. 1992. Shrinkage cracking in fully restrained concrete members. *ACI Structural Journal*, 89(2), 141–149.

Goto, Y. 1971. Cracks formed in concrete around deformed tension bars. *ACI Journal Proceedings*, 68(4), 244–251.

Gribniak, V., Cervenka, V. & Kaklauskas, G. 2013. Deflection prediction of reinforced concrete beams by design codes and computer simulation. *Engineering Structures*, 56, 2175–2186.

Gribniak, V., Kaklauskas, G. & Bacinskas, D. 2009. Experimental investigation of shrinkage influence on tension stiffening of RC beams. *In Proc. of the Eighth International Conference Creep, Shrinkage and Durability of Concrete and Concrete Structures* (CONCREEP 8), 1, 571–577.

Gribniak, V., Kaklauskas, G., Bacinskas, D., Sung, W. P., Sokolov, A. & Ulbinas, D. 2011. Investigation of shrinkage of concrete mixtures used for bridge construction in Lithuania. *The Baltic Journal of Road and Bridge Engineering*, 6(2), 78–83.

Gribniak, V., Kaklauskas, G., Juozapaitis, A., Kliukas, R. & Meskenas, A. 2017. Efficient technique for constitutive analysis of reinforced concrete flexural members. *Inverse Problems in Science and Engineering*, 25(1), 27–40.

Gribniak, V., Kaklauskas, G., Sokolovas, A. & Logunov, A. 2007. Finite element size effect on post-cracking behaviour of reinforced concrete members. *Proceedings of the 9th International Conference Modern Building Materials, Structures and Techniques*, Vilnius: Technika, 563–570.

Gribniak, V., Kaklauskas, G., Torres, L., Daniunas, A., Timinskas, E. & Gudonis, E. 2013. Comparative analysis of deformations and tension-stiffening in concrete beams reinforced with GFRP or steel bars and fibers. *Composites Part B: Engineering*, 50, 158–170.

Gribniak, V., Mang, H. A., Kupliauskas, R. & Kaklauskas, G. 2015. Stochastic tension-stiffening approach for the solution of serviceability problems in reinforced concrete: Constitutive modeling. *Computer-Aided Civil and Infrastructure Engineering*, 30(9), 684–702.

Gribniak, V., Mang, H. A., Kupliauskas, R., Kaklauskas, G. & Juozapaitis, A. 2016. Stochastic tension-stiffening approach for the solution of serviceability problems in reinforced concrete: Exploration of predictive capacity. *Computer-Aided Civil and Infrastructure Engineering*, 31(6), 416–431.

Gribniak, V., Tamulenas, V., Ng, P. L., Arnautov, A. K., Gudonis, E. & Misiunaite, I. 2017. Mechanical behavior of steel fiber-reinforced concrete beams bonded with external carbon fiber sheets. *Materials*, 10(6), 666.

Gudonis, E., Kacianauskas, R., Gribniak, V., Weber, A., Jakubovskis, R. & Kaklauskas, G. 2014. Mechanical properties of the bond between GFRP reinforcing bars and concrete. *Mechanics of Composite Materials*, 50(4), 457–466.

Gudonis, E., Kaklauskas, G., Bacinskas, D., Gribniak, V., Ramanauskas, R. & Tamulenas, V. 2015. Experimental investigation on short-and long-term deformations of cracked reinforced concrete ties. *Proceedongs of the 10th conference CONCREEP*, 958–962.

Hamad, B. S. 1995a. Bond strength improvement of reinforcing bars with specially designed rib geometries. *ACI Structural Journal*, 92(10), 3–23.

Hamad, B. S. 1995b. Comparative bond strength of coated and uncoated bars with different rib geometries. *ACI Materials Journal*, 92(6), 579–590.

Hassoun, M. N. 1985. *Design of Reinforced Concrete Structures*. New York: PWS Engineering, 766 p.

Holschemacher, K., Weiße, D. & Klotz, S. 2005. Bond of reinforcement in ultra high-strength concrete. *ACI Special Publication*, 228, 513–528.

Hordijk, D. A. 1991. *Local Approach to Fatigue of Concrete*. Doctoral dissertation, Delft: Delft University of Technology, 210 p.

Hsu, T. T., Slate, F. O., Sturman, G. M. & Winter, G. 1963. Microcracking of plain concrete and the shape of the stress-strain curve. *ACI Journal Proceedings*, 60(2), 209–224.

Hughes Brothers, Inc. 2011. *Glass Fiber Reinforced Polymer (GFRP) Rebar - Aslan ™ 100 Series*. Data Sheet, Detroit: Hughes Brothers, Inc., 16 p.

Husain, S. L. & Ferguson, P. M. 1968. *Flexural Crack Widths at the Bars in Reinforced Concrete Beams*. Research Report No. 102-1F, University of Texas at Austin, 41 p.

Jakubovskis, R., Kaklauskas, G., Gribniak, V., Weber, A. & Juknys, M. 2014. Serviceability analysis of concrete beams with different arrangements of GFRP bars in the tensile zone. *Journal of Composites for Construction*, 18(5), Paper ID: 04014005, 11 p.

Jiang, D. H., Shah, S. P. & Andonian, A. T. 1984. Study of the transfer of tensile forces by bond. *ACI Journal Proceedings*, 81(3), 251–259.

Jiang, D. H., Shah, S. P., & Andonian, A. T. 1984. Study of the transfer of tensile forces by bond. *ACI Journal Proceedings*, 81(3), 251–259.

Kaklauskas, G. 2017. Crack Model for RC Members Based on Compatibility of Stress-Transfer and Mean-Strain Approaches. *ASCE Journal of Structural Engineering*, 143(9), Paper ID: 12478, 13 p.

Kaufmann, W. 2013. Strength and deformations of structural concrete subjected to in-plane shear and normal forces. *Birkhäuser*, 234, 125 p.

Khadour, A., Baby, F., Herrera, A., Taillade, F., Marchand, P., Rivillon, P. & Toutlemonde, F. 2013. Distributed strain monitoring of reinforcement bars using optical fibers for SHM. *Proceedings of the Seventh International Conference on Concrete under Severe Conditions–Environment and Loading*, 1608–1620.

Kim, J. & Lee, G. P. 2015. Evaluation of mechanical properties of steel-fibre-reinforced concrete exposed to high temperatures by double-punch test. *Construction and Building Materials*, 79, 182–191.

Landis, E. N. & Bolander, J. E. 2009. Explicit representation of physical processes in concrete fracture. *Journal of Physics D: Applied Physics*, 42(21), Paper ID: 214002, 11 p.

Larsen, E. S. & Krenchel, H. 1990. *Durability of FRC-Materials*. Research Report, MRS Online Proceedings Library Archive, 211 p.

Lárusson, L., Fischer, G. & Jönsson, J. 2012. Mechanical interaction between concrete and structural reinforcement in the tension stiffening process. *High Performance Fiber Reinforced Cement Composites* 6, 247–254.

Lee, G. Y. & Kim, W. 2009. Cracking and tension stiffening behavior of high-strength concrete tension members subjected to axial load. *Advances in Structural Engineering*, 12(2), 127–137.

Li, Y., Walraven, J. C., Han, N., Braam, C. R., Hoogenboom, P. C. J. & Houben, I. L. 2010. *Predicting of the Stiffness of Cracked Reinforced Concrete Structures*. Final Report, Delft University of Technology, 153 p.

Lima, P. R., Toledo Filho, R. D. & Melo Filho, J. A. 2014. Compressive stress-strain behaviour of cement mortar-composites reinforced with short sisal fibre. *Materials Research*, 17(1), 38–46.

Löfgren, I. 2005. *Fibre-reinforced Concrete for Industrial Construction - A Fracture Mechanics Approach to Material Testing and Structural Analysis*. Research Report, Chalmers University of Technology, 235 p.

Lowes, L. N. 1999. *Finite Element Modeling of Reinforced Concrete Beam-Column Bridge Connections*. Research Report, Berkeley: University of California, 210 p.

Maekawa, K., Okamura, H. & Pimanmas, A. 2003. *Non-Linear Mechanics of Reinforced Concrete*. Boka Raton: CRC Press, 457 p.

Mahmoud, K. & El-Salakawy, E. 2013. Shear strength of GFRP-reinforced concrete continuous beams with minimum transverse reinforcement. *Journal of Composites for Construction*, 18(1), Paper ID: 04013018, 12 p.

Marfisi, E., Burgoyne, C. J., Amin, M. H. G. & Hall, L. D. 2005. Observation of flexural cracks in loaded concrete beams using MRI. *Magazine of Concrete Research*, 57(4), 225–234.

Mehta, P.K. & Monteiro, P.J.M. 1993. *Concrete: Structure, Properties, and Methods*. Englewood Cliffs: Prentice-Hall, Inc., 237 p.

Mesbah, H. A. & Buyle-Bodin, F. 1999. Efficiency of polypropylene and metallic fibres on control of shrinkage and cracking of recycled aggregate mortars. *Construction and building materials*, 13(8), 439–447.

Mias, C., Torres, L., Turon, A. & Barris, C. 2013. Experimental study of immediate and time-dependent deflections of GFRP reinforced concrete beams. *Composite Structures*, 96: 279–285.

Michou, A., Hilaire, A., Benboudjema, F., Nahas, G., Wyniecki, P. & Berthaud, Y. 2015. Reinforcement–concrete bond behavior: Experimentation in drying conditions and meso-scale modeling. *Engineering Structures*, 101, 570–582.

Miglietta, P. C., Grasselli, G. & Bentz, E. C. 2016. Finite/discrete element model of tension stiffening in GFRP reinforced concrete. *Engineering Structures*, 111, 494–504.

Moradian, M. & Shekarchi, M. 2016. Durability and dimensional stability of steel fiber reinforced cementitious mortar in comparison to high performance concrete. *Asian Journal of Civil Engineering*, 17(4), 515–535.

Morita, S. & Kaku, T. 1979. Splitting bond failures of large deformed reinforcing bars. *ACI Journal Proceedings*, 76(5), 93–110.

Mufti, A. A. 2001. *Reinforcing Concrete Structures with Fibre Reinforced Polymers*. MSc Thesis. Ottawa: ISIS, 124 p.

Nmai, C. K., Suchorski, D. M., Bell, L., Khan, T., Rear, K. & Bohan, R. 2006. Reinforcement for concrete–materials and applications. ACI Education Bulletin E2–00 (Reapproved), Committee E-701, Detroit, MI: American Concrete Institute, 69 p.

Ogura, N., Bolander, J. E. & Ichinose, T. 2008. Analysis of bond splitting failure of deformed bars within structural concrete. *Engineering Structures*, 30(2), 428–435.

Østergaard, L. & Olesen, J. F. 2004. Comparative study of fracture mechanical test methods for concrete. *Fracture Mechanics of Concrete Structures*, 455–462.

Otsuka, K. & Ozaka, Y. 1992. Group effects on anchorage strength of deformed bars embedded in massive concrete block. *Proceedings of International Conference on Bond in Concrete—From Research to Practice, Riga Technical University*, 1, 1–38.

Pereira, E. N. B., Fischer, G. & Barros, J. A. 2011. Image-based detection and analysis of crack propagation in cementitious composites. *Proceedings of the International Conference on Advances in Construction Materials through Science and Engineering*, 245–256.

Pilakoutas, K., Guadagnini, M., Neocleous, K. & Matthys, S. 2011. Design guidelines for FRP reinforced concrete structures. *Proceedings of the Institution of Civil Engineers-Structures and Buildings*, 164(4), 255–263.

Pinet, É., Hamel, C., Glišić, B., Inaudi, D. & Miron, N. 2007. Health monitoring with optical fiber sensors: from human body to civil structures. *Health Monitoring of Structural and Biological Systems*, 6532, Paper ID: 653219, 8 p.

Pokorný, P., Kouřil, M., Stoulil, J., Bouška, P., Simon, P. & Juranek, P. 2015. Problems and normative evaluation of bond-strength tests for coated reinforcement and concrete. *Materials and Technology*, 49(6), 847–856.

Purainer, R. 2005. *Last- und Verformungsverhalten von Stahlbetonflächentragwerken unter zweiaxialer Zugbeanspruchung*. PhD Thesis, University of the Federal Armed Forces, Munich, Germany, 235 p. (in German).

Quayyum, S. 2010. *Bond behaviour of fibre reinforced polymer (FRP) rebars in concrete*. Doctoral dissertation, University of British Columbia, 169 p.

RELEM RC-5. 1982. *Bond test for reinforcement steel – 1. Beam test*. Technical Recommendations for the Testing and Use of Construction Materials: RC 5. 213–217.

RILEM RC-6. 1978. *Bond Test for Reinforcement Steel. 2. Pull-out Test.* Technical Recommendations for the Testing and Use of Construction Materials: RC 6. 218–220.

Rizkalla, S. H., & Hwang, L. 1984. Crack prediction for members in uniaxial tension. *ACI Journal Proceedings*, 81(6), 572–579.

Rostásy, F. S., Koch, R., Leonhardt, F., & Patzak, M. 1976. *Zur Mindestbewehrung für Zwang von Außenwänden aus Stahlleichtbeton: Versuche zum Tragverhalten von Druckübergreifungsstößen in Stahlbetonwänden*. Berlin: Ernst und Sohn, 125 p.

Scott, R. H., & Beeby, A. W. 2005. Long-term tension-stiffening effects in concrete. *ACI Structural Journal*, 102(1), 31.

Slate, F. O. & Olsefski, S. 1963. X-rays for study of internal structure and microcracking of concrete. *ACI Journal Proceedings*, 60(5), 575–588.

Soudki, K. A. 2001. *Concrete Problems and Repair Techniques*. Waterloo, Ontario, Department of Civil Engineering, 245 p.

Stramandinoli, R. S., & La Rovere, H. L. 2008. An efficient tension-stiffening model for nonlinear analysis of reinforced concrete members. *Engineering Structures*, 30(7), 2069–2080.

Tam, K. S., & Scanlon, A. 1986. Deflection of two-way slabs subjected to restrained volume change and transverse loads. *ACI Journal Proceedings*, 83(5), 737–744.

Tammo, K. & Thelandersson, S. 2009. Crack behavior near reinforcing bars in concrete structures. *ACI Structural Journal*, 106(3), 259–271.

Tammo, K., & Thelandersson, S. 2006. Crack opening near reinforcement bars in concrete structures. *Structural Concrete*, 7(4), 137–143.

Tepfers, R. 1973. *A theory of bond applied to overlapped tensile reinforcement splices for deformed bars*. Doctoral dissertation, Chalmers University of Technology, 183 p.

Tepfers, R. 1979. Cracking of concrete cover along anchored deformed reinforcing bars. *Magazine of concrete research*, 31(106), 3–12.

Torres, L., Neocleous, K., and Pilakoutas, K. 2012. Design procedure and simplified equations for the flexural capacity of concrete members reinforced with fibre-reinforced polymer bars. *Structural Conc*rete, 13(2): 119–129.

Trigo, A. P. M., & Liborio, J. B. L. 2014. Doping technique in the interfacial transition zone between paste and lateritic aggregate for the production of structural concretes. *Materials Research*, 17(1), 16–22.

Vilanova, I., Torres, L., Baena, M., Kaklauskas, G., & Gribniak, V. 2014. Experimental study of tension stiffening in GFRP RC tensile members under sustained load. *Engineering Structures*, 79, 390–400.

Weerheijm, J. 2013. *Understanding the tensile properties of concrete*. Cambridge: Woodhead Publishing, 365 p.

Williams, A. 1986. *Tests on Large Reinforced Concrete Elements Subjected to Direct Tension*. Report No. 562. Wexham Springs: Cement and Concrete Association, 54 p.

Williams, A. 2003. *Design of reinforced concrete structures*. Austin: Engineering Press, 383 p.

Windisch, A. 2016. Crack control: an advanced calculation model–part I: Review of classic tests. *Concrete Structures*, 41–48.

Windisch, A. 2017. Crack control: an advanced calculation model–part II: The advanced model. *Concrete Structures*, 18–25.

Wu, C., Chen, G., Volz, J. S., Brow, R. K., & Koenigstein, M. L. 2012. Local bond strength of vitreous enamel coated rebar to concrete. *Construction and Building Materials*, 35, 428–439.

Zheng, W., Kwan, A. K. H. & Lee, P. K. K. 2001. Direct tension test of concrete. *ACI Materials Journal*, 98(1), 63–71.

List of Scientific Publications by the Author on the Topic of the Dissertation

Journal Publications

Journals Referred in ISI Web of Science Database (with Impact Factor)

Gribniak, V., Rimkus, A., Torres, L., Jakštaitė, R. 2017a. Deformation analysis of reinforced concrete ties: Representative geometry. *Structural concrete*. Berlin: Ernst & Sohn Verlag. ISSN 1464-4177. eISSN 1751-7648. 18(4), 634–647. [IF: 1.424]

Rimkus, A., & Gribniak, V. 2017a. Experimental investigation of cracking and deformations of concrete ties reinforced with multiple bars. *Construction and building materials*. Oxford: Elsevier Ltd. ISSN 0950-0618. eISSN 1879-0526. 148, 49–61. [IF: 3.169]

Meškėnas, A., Gribniak, V., Kaklauskas, G., Sokolov, A., Gudonis, E., Rimkus, A. 2017. Experimental investigation of cracking behaviour of concrete beams reinforced with steel fibres produced in Lithuania. *The Baltic Journal of Road and Bridge Engineering*. Vilnius: Technika. ISSN 1822-427X. eISSN 1822-4288. 12(2), 82–87. [IF: 0.698]

Gribniak, V., Perez Caldentey, A., Kaklauskas, G., Rimkus, A., Sokolov, A. 2016. Effect of arrangement of tensile reinforcement on flexural stiffness and cracking. *Engineering structures*. Oxford: Elsevier Ltd. ISSN 0141-0296. 124, 418–428. [IF: 2.258]

Rimkus, A., & Gribniak, V. 2016. Discussion: Sustained service load behavior of concrete beams with recycled concrete aggregates, by Adam M. Knaack and Yahya C. Kurama: by Arvydas Rimkus and Viktor Gribniak. *ACI structural journal*. Farmington Hills: American Concrete Institute. ISSN 0889-3241. 113(4), 874–876. [IF: 1.350]

Journals Referred in Other Scientific Databases

Rimkus, A., Gribniak, V. 2017b. Experimental data of deformation and cracking behaviour of concrete ties reinforced with multiple bars. *Data in Brief*. Amsterdam: Elsevier Ltd. ISSN 2352-3409. 13, 223–229.

Publications in Conference Proceedings

Conference Proceedings Referred in ISI Web of Science Database (ISI Proceedings)

Rimkus, A., Jakštaitė, R., Kupliauskas, R., Torres, L., Gribniak, V. 2017. Experimental identification of cracking parameters of concrete ties with different reinforcement and testing layouts. *Procedia Engineering*. Modern Building Materials, Structures and Techniques (MBMST 2016). Amsterdam: Elsevier Ltd. ISSN 1877-7058. 172, 930–936.

Rimkus, A., Podviezko, A., Gribniak, V. 2015. Processing digital images for crack localization in reinforced concrete members. *Procedia Engineering*. Innovative solutions in construction engineering and management. Flexible approach: Operational Research in Sustainable Development and Civil Engineering – meeting of EURO working group and 15th German–Lithuanian–Polish colloquium (ORSDCE 2015). Amsterdam: Elsevier Science Ltd. ISSN 1877-7058. 122, 239–243.

Kaklauskas, G., Gribniak, V., Meškėnas, A., Rimkus, A., Kaklauskas, A., Kupliauskas, R. 2013. Determination of the residual stress-crack opening relationship of SFRC flexural members. *AIP Conference proceedings*. 11th International Conference on Numerical Analysis and Applied Mathematics 2013 (ICNAAM 2013). Melville: AIP Publishing. ISSN 0094-243X. 1558, 2151–2154.

Other Conference Proceedings

Gribniak, V., Rimkus, A., Torres, L. 2017b. Cracking and deformation analysis of concrete ties reinforced with multiple GFRP bars. *Proceedings of the 25th Annual International Conference on Composites/Nano Engineering (ICCE-25)*. July 16–22, 2017, Rome, Italy. 1–2.

Rimkus, A., Gribniak, V., Jakubovskis, R., Torres, L., Jakštaitė, R. 2017. Experimental study of effect of arrangement of GFRP bars on tensile behaviour of concrete elements. *Proceedings of the Third International Conference on Mechanics of Composites (MECHCOMP 3)*. Bologna: Societa' Editrice Esculapio. ISSN 2421-2822. 109–110.

Rimkus, A., & Vilėniškytė, A. 2015. Armatūros strypų išdėstymo įtakos tempiamųjų betoninių elementų deformacijoms bei pleišėjimui eksperimentiniai tyrimai. *Proceedings of the 18th conference for junior researchers „Science – Future of Lithuania“*, Vilnius: Technika. ISBN 9786094578212. 1–4.

Gudonis, E., Rimkus, A., Kaklauskas, G., Gribniak, V., Kupliauskas, R. 2014. Experimental investigation on deformation behavior of RC ties. *Mechanika'2014: proceedings of the 19th international conference*. Kaunas: Technologija. ISSN 1822-2951. 94–99.

Rimkus, A., Meškėnas, A., Tamulėnas, V. 2014. Sumaniųjų tiltų taikymo perspektyvos Lietuvoje. *17-oji Lietuvos jaunųjų mokslininkų konferencija "Mokslas - Lietuvos ateitis" 2014 metų teminė konferencija "Statyba = Civil engneering"*. Vilnius: Technika. ISSN 2029-7149. ISBN 9786094576942. 1–7.

Patents

Gribniak, V., Rimkus, A. 2016. Betoninio konstrukcinio elemento armatūros strypų grupės tvirtinimo įranga: patentas / išradėjai: Viktor Gribniak, Arvydas Rimkus. LT 6275. 2016-06-27. 6 p.

Summary in Lithuanian

Įvadas

Problemos formulavimas

Cementinis betonas apibūdinamas kaip trapi medžiaga, atlaikanti gana didelius gniuždymo įtempius, tačiau turinti nedidelį tempiamąjį stiprį. Todėl statybinių konstrukcijų elementuose, kuriuose gali atsirasti tempimo įtempiai, naudojami armatūros strypai. Dažniausiai naudojami plieniniai strypai, tačiau taikomos ir kitos medžiagos, turinčios didelį tempiamąjį stiprį bei gerai sukimbančios su cemento akmeniu. Statybinių konstrukcijų laikomosios galios nustatymo uždaviniai paprastai nesukelia didesnių sunkumų, kadangi juose yra taikomi fundamentiniai deformuojamo kūno mechanikos principai ir prielaidos. Betono pleišėjimo vertinimas bei šių rezultatų analizė yra vienas sudėtingiausių armuoto betono konstrukcijų tyrimų aspektų.

Darbo aktualumas

Pastaraisiais metais pasaulyje sukuriama daug naujų medžiagų, skirtų betono armavimui, tačiau platesniam jų taikymui būtina išanalizuoti jų elgseną ir užtikrinti patikimus jų mechaninių savybių nustatymo būdus. Eksperimentinių bandymų pagrindu sudaromi skaitiniai ir analiziniai metodai, kurie taikomi konstrukcinių elementų tinkamumui tirti bei vertinti. Ypač stiprių medžiagų taikymas lemia, kad konstrukcijų tinkamumo (deformacijų ir pleišėjimo ribojimo) reikalavimai tampa pagrindiniu projektavimo kriterijumi. Dėl šios priežasties itin svarbu parinkti bandymo metodus ir tinkamai interpretuoti gautus rezultatus.

Šiuo darbu siekiama nustatyti esminius armuotų betoninių elementų skerspjūvio parametrus, lemiančius kompozitinės struktūros irimo pobūdį. Deformacijų pasiskirstymo betono apsauginiame sluoksnyje tyrimas leistų įvertinti vidinio ir išorinio pleišėjimo procesą, teisingai interpretuoti bandymų rezultatus. Darbe pateikti eksperimentiniai rezultatai sudarys matematinio modelio, kuris patikimai leistų prognozuoti įvairių medžiagų strypais armuotų betoninių konstrukcijų elgseną, kūrimo pagrindą. Šiame kontekste patikimumas siejamas su konstrukcinių elementų bandymų rezultatų skaida: patikimumas yra atvirkščiai proporcingas bandymų rezultatų sklaidai.

Tyrimo objektas

Disertacinio tyrimo objektas – strypais armuoti betoniniai elementai, veikiami trumpalaike apkrova. Tiriamos sijos bei tempiamieji betoniniai elementai, su skerspjūvyje skirtingai išdėstyta armatūra. Elementų gniuždomasis betono stipris 38–56 MPa. Atliekant analizę, keičiami elementų parametrai: armatūros skersmuo, mechaninės strypų savybės, armavimo koeficientas, skerspjūvių geometrija ir apsauginio betono sluoksnio storis.

Darbo tikslas

Tiriant tempiamųjų ir lenkiamųjų elementų strypinės armatūros išdėstymo tempiamojoje zonoje įtaką elementų eksploatacinėms savybėms, nustatyti veiksnius, lemiančius elementų deformacijas bei pleišėjimą, įvertinti šių parametrų išsibarstymą.

Darbo uždaviniai

Darbo tikslui pasiekti sprendžiami šie uždaviniai:

1. Nustatyti armuoto betono deformacijas ir pleišėjimą lemiančius parametrus.
2. Atlikti eksperimentinę ir skaitinę armatūros strypų išdėstymo įtakos armuotų betoninių elementų deformacijoms ir pleišėjimui analizę.
3. Patikrinti projektavimo normose pateiktų išraiškų, nusakančių armuotų betoninių elementų deformacijas ir pleišėjimą, adekvatumą.
4. Pasiūlyti alternatyvius armatūros strypų išdėstymo būdus, kurie leistų kontroliuoti (mažinti eksperimentinių rezultatų sklaidą) elementų standumą bei pleišėjimą eksploatacinėmis sąlygomis.

Tyrimų metodika

Tiriamasis darbas pagrįstas ribotos imties kruopščiai atrinktų eksperimentinių bandinių deformacijų ir pleišėjimo kokybine analize. Remiantis literatūros apžvalgoje nustatytais kriterijais, tiriamieji bandiniai (elementų skerspjūvio forma, armavimo parametrai, bandymo būdai ir pan.) buvo parenkami priartėjimo būdu atsižvelgiant į jų tinkamumą nustatyti eksploatacines savybes lemiančius veiksnius. Vadovaujantis eksperimentine patirtimi ir inžinerine intuicija, atliekama gautų rezultatų (charakteringų jų bruožų) aprašomoji analizė. Nustatomi, tiriami bei interpretuojami gautų rezultatų sąryšiai (pvz. kintamųjų koreliacija) atsižvelgiant į teorinę bei fizinę jų kilmę. Atliekant pakartotinus

bandymus buvo užtikrinamas rezultatų patikimumas. Tyrimo metodika leidžia nustatyti strypinės armatūros išdėstymo įtaką betoninių elementų deformacijoms ir pleišėjimui, tačiau dėl riboto šiame darbe nagrinėtų bandinių skaičiaus darbo rezultatai negali tiesiogiai apibūdinti armuoto betono konstrukcijų elgsenos plačiąja prasme.

Mokslinis naujumas

1. Prielaida, kad egzistuoja tiesinė priklausomybė tarp maksimalaus plyšio pločio bei maksimalaus atstumo tarp plyšių, nebūtinai teisinga. Maksimalaus pločio plyšys susiformuoja ne visada greta maksimalaus ilgio nesupleišėjusio betono bloko. Ši prielaida paremta eksperimentiniais devynių armuoto betono sijų pleišėjimo rezultatais.
2. Sukurta įranga, leidžianti gaminti ir bandyti tempiamuosius elementus, kurių pagrindiniai skerpjūvių parametrai (apsauginio betono sluoksnio storis, armavimo koeficientas ir armatūros strypų skersmuo) gali būti vienas nuo kito nepriklausomai keičiami. Tempiamųjų armuoto betono elementų pleišėjimo rezultatai, gauti naudojant sukurtą įrangą, parodė, kad atstumas tarp plyšių nepriklauso nuo elemento armavimo parametrų (armatūros strypų skersmens bei armavimo koeficiento). Išbandytų 64 tempiamųjų elementų pleišėjimo rezultatai nepatvirtina armuotų betoninių konstrukcijų projektavime taikomų prielaidų. Nustatyta, kad labiausiai pleišėjimą įtakojantis parametras yra apsauginis betono sluoksnio storis.
3. Pasiūlyta bandinių reprezentatyvumo sąlyga leidžia izoliuoti tiriamąjį parametrą nuo nekontroliuojamų efektų didinant bandymo rezultatų interpretavimo patikimumą (kuris šiame darbe siejamas su duomenų sklaida). Pavyzdžiui, reprezentatyvi tempiamojo elemento forma (t. y. tam tikras armatūros strypų išdėstymas bei atitinkamas apsauginio betono sluoksnio storis) leidžia sumažinti „krašto efektą“, kuris yra siejamas su skirtingomis armatūros strypų ir betono paviršiaus deformacijomis.
4. Remiantis literatūroje pasiūlytu betono ir armatūros strypų reguliaraus sukibimo modeliu bei betono irimo mechanikos principais, skaitiškai sumodeliuoti tempiamieji betono elementai, armuoti keletu strypų. Toks modeliavimo būdas skaičiavimo laiko sanaudų atžvilgiu yra itin efektyvus bei nereikalauja didelių kompiuterinės įrangos resursų. Be to, šis būdas užtikrina realų (adekvatų fizikinio bandymo rezultatams) deformacijų pasiskirstymą ir armatūroje, ir betone bei rodo pleišėjimo procesą armuoto betono elementuose.
5. Eksperimentiniai ir skaitinio modeliavimo rezultatai rodo, kad armuoto betono elementuose tempiamojo betono deformacijos kinta ne tik išilgine elemento kryptimi, bet ir pačiame betono apsauginiame sluoksnyje. Šie rezultatai patvirtina, kad projektavimo dokumentuose taikoma efektyviojo tempiamojo betono koncepcija, nėra universali. Šios koncepcijos taikymas priklauso nuo elementų apkrovimo sąlygų, įtempių ir deformacijų būvio bei nearmuoto betono konfigūracijos.

Darbo rezultatų praktinė reikšmė

1. Sukurta specifinė tempiamųjų betono elementų, armuotų keletu bet kokios medžiagos strypų, gamybos bei bandymo įranga. Įranga leidžia gaminti tempiamuosius elementus, kurių pagrindiniai skerspjūvio parametrai (apsauginio betono sluoksnio storis, armavimo koeficientas ir armatūros strypų skersmuo) vienas nuo kito nepriklauso ir gali būti keičiami. Sukurta įranga patentuota 2016 metais Lietuvos Respublikos valstybiniame patentų biure (patento numeris LT 6275 B).
2. Pasiūlytas bandymo metodas, leidžiantis stebėti tempiamųjų betoninių elementų, armuotų keletu strypų, betono paviršiaus bei armatūros deformacijas. Šis būdas suteikia galimybę gauti papildomą informaciją apie deformacijų pasiskirstymą betone, kuri yra būtina kuriant eksperimentinius bandymus atitinkančius skaitinius modelius.
3. Sukurta bandymo įranga bei pasiūlyta deformacijų stebėjimo metodika leidžia vertinti projektavimo normose pateiktų armuoto betono elementų pleišėjimą prognozuojančių išraiškų adekvatumą.

Ginamieji teiginiai

1. Siekiant išvengti pagrindinių kintamųjų (apsauginio betono sluoksnio storio, armavimo koeficiento ir armatūros strypų skersmens) koreliacijos tarpusavyje, tradicinė tempiamųjų armuoto betono elementų bandymo įranga turėtų būti patobulinta.
2. Visuotinai pripažintos „efektyviojo tempiamojo betono“ koncepcijos taikymas yra ribotas.
3. Didesnis armatūros strypų skaičius gali pagerinti vidutiniškai armuotų (armavimo koeficientas kinta nuo 1,4 % iki 2,0 %) elementų eksploatacines savybes. Šis efektas akivaizdus ankstyvojoje pleišėjimo stadijoje.
4. Armuoto betono modeliavimas baigtiniais elementais, taikant betono irimo bei armatūros ir betono sukibimo modelius, pateiktus literatūroje, leidžia tirti itin sudėtingus betono elgsenos aspektus, kurie yra pernelyg komplikuoti eksperimentiniam jų vertinimui.

Darbo rezultatų aprobavimas

Disertacijos tyrimams sukurtai armuoto betono tempiamųjų elementų bandymų įrangai gautas Lietuvos Respublikos patentas. Disertacijos tema paskelbta 14 mokslinių publikacijų, iš kurių 5 – žurnaluose turinčiuose cituojamumo rodiklį, o 3 – konferencijų rinkiniuose, referuojamuose *Clarivate Analytics Web of Science* duomenų bazėje. Doktorantūros studijų laikotarpiu (2013–2017) disertacijos rezultatai buvo paskelbti 9 mokslinėse konferencijose:

- 25-oji tarptautinė konferencija *Composites and Nano Engineering*. Roma, Italija, 2017.
- 3-oji tarptautinė konferencija *Mechanics of Composites*. Bolonija, Italija, 2017.

- 12-oji tarptautinė konferencija *Modern Building Materials, Structures and Techniques*. Vilnius, Lietuva, 2016.
- 15-asis Vokietijos, Lietuvos ir Lenkijos kolokviumas ir *EURO* darbo grupės *Sustainable Development and Civil Engineering* susitikimas. Poznanė, Lenkija, 2015.
- 11-oji tarptautinė konferencija *Numerical Analysis and Applied Mathematics*. Rodas, Graikija, 2013.
- 19-oji tarptautinė konferencija *Mechanika*. Kaunas, Lietuva, 2014.
- 18-oji Lietuvos jaunųjų mokslininkų konferencija *Mokslas – Lietuvos ateitis*. Vilnius, Lietuva, 2015.
- 17-oji Lietuvos jaunųjų mokslininkų konferencija *Mokslas – Lietuvos ateitis*. Vilnius, Lietuva, 2014.
- 4-oji jaunųjų mokslininkų konferencija *Fizinių ir technologijos mokslų tarpdalykiniai tyrimai*. Vilnius, Lietuva, 2014.

Disertacijos struktūra

Disertaciją sudaro įvadas, 3 skyriai, bendrosios išvados, literatūros sąrašas (137 šaltinių), autoriaus mokslinių publikacijų disertacijos tema sąrašas (14 publikacijų), LR patentas, santrauka lietuvių kalba bei 3 priedai. Darbo apimtis 143 puslapiai.

Padėka

Disertacinio darbo autorius dėkoja Lietuvos mokslo tarybai už suteiktą konkursinės doktorantūros vietą, finansuojamą pagal Europos Sąjungos struktūrinių fondų projektą „Doktorantūros studijų plėtra“. Autorius nuoširdžiai dėkoja savo mokslinio darbo vadovui, Inovatyviųjų statybinių konstrukcijų laboratorijos vedėjui, dr. Viktor Gribniak už kantrybę, motyvaciją, žinias bei entuziastingus patarimus rengiant disertaciją. Autorius taip pat dėkoja Vilniaus Gedimino technikos universiteto Tiltų ir specialiųjų statinių katedros darbuotojams bei doktorantams už patarimus ir vertingas diskusijas. Autorius ypatingai dėkingas dr. Aleksandr Sokolov už geranorišką pagalbą atliekant eksperimentinius tyrimus ir dr. Pui Lam NG už konstruktyvias pastabas ir komentarus rengiant disertaciją. Už vertingas įžvalgas disertacinio darbo tema autorius dėkoja dr. Andor Windisch, dr. Lluis Torres Llinas, dr. Alejandro Perez Caldentey ir prof. dr. Joaquim Antonio Oliveira Barros, kurių patirtis ir kompetencija padėjo reikšmingai pagerinti disertacinio darbo kokybę. Autorius nuoširdžiai dėkoja savo tėvams, Audronei ir Petrui, sesei Ievai ir mylimai žmonai Dovilei už nuolatinį palaikymą, kantrybę ir paramą rengiant disertaciją.

1. Armuoto betono elementų deformacijos ir pleišėjimas

Pirmajame disertacijos skyriuje atlikta literatūros šaltinių disertacijos tematika analizė. Aptartos betono bei plieno ir polimerinės armatūros charakteringosios savybės. Akcentuota didelė eksperimentiškai nustatomų betono charakteristikų sklaida dėl

struktūrinių betono defektų ir bandymo metodų pasirinkimo bei bandymo įrangos ypatumų. Aprašyti sudėtingi betono ir armatūros strypų tarpusavio sąveikos mechanizmai bei jos mechanines savybes lemiantys veiksniai. Didelę šio skyriaus dalį sudaro įžvalgos apie armuoto betono deformacijas ir pleišėjimą bei šių savybių skaitinio modeliavimo principų aptarimas. Skyriuje taip pat apibūdintos armuoto betono deformavimosi stadijos, atskleistos nagrinėjamų elementų elgsenos stebėjimo galimybės fizikinių eksperimentų metu bei bandymo metodų pasirinkimo svarba. Apžvelgti armuoto betono projektavimo normose pateikti deformacijų bei pleišėjimo prognozavimo metodai.

Parodyta, kad armuoto betono deformacijas bei pleišėjimą lemia betono tempiamasis stipris, armatūros tamprumo modulis, betono ir armatūros sukibimo charakteristikos bei elemento skerspjūvio geometrija. Siekiant įvertinti bendrą armatūros strypų bei aplink esančio betono darbą naudojama „efektyviojo tempiamojo betono“ koncepcija. Parodyta, kad armatūros strypų skaičius tempiamojoje betoninio elemento dalyje reikšmingai įtakoja betono elgseną (deformavimąsi). Dėl šios priežasties strypinės armatūros išdėstymo įtakos bendram elemento standumui bei pleišėjimui tyrimas yra itin svarbus. Atliekant tokius tyrimus eksperimentinis armatūros bei betono paviršiaus deformacijų nustatymas yra būtinas siekiant adekvačiai įvertinti deformacijų pasiskirstymą betone. Remiantis vien eksperimentiniais metodais, tai padaryti yra itin sudėtinga. Vienas paprasčiausių būtų nagrinėti sudėtingus betono elgsenos ypatumus – armuoto betono modeliavimas baigtiniais elementais. Skyriaus pabaigoje apibrėžtas tyrimo objektas bei iškelti darbo uždaviniai.

2. Eksperimentiniai armuoto betono elementų deformacijų ir pleišėjimo tyrimai

Antrajame disertacijos skyriuje nagrinėjama strypinės armatūros išdėstymo įtaka betoninių elementų deformacijoms ir pleišėjimui. Skyriuje pateikiami eksperimentiniai armuoto betono lenkiamųjų ir tempiamųjų elementų rezultatai bei atliekama jų analizė. Dalis eksperimentinių rezultatų pateikta trečiajame skyriuje. Antrajame skyriuje pateiktus duomenis pagal nagrinėjamų elementų tipą galima suskirstyti į tris grupes: lenkiamieji betoniniai elementai, armuoti plieniniais bei GFRP strypais, tipiniai tempiamieji betoniniai elementai, armuoti vienu plieniniu strypu, bei specifiniai tempiamieji betoniniai elementai, armuoti keletu plieninių strypų.

Analizuojant lenkiamųjų elementų pleišėjimą ir deformacijas buvo tiriamos 9 sijos. Nagrinėjami 3000 mm tarpatramio elementai buvo armuoti plieno arba stiklo pluoštu armuoto polimero (GFRP) strypais, išdėstytais vienu ir trimis sluoksniais. Atitinkamai parinktas strypų skersmuo ir kiekis užtikrino vienodą sijų armavimo koeficientą. Sijų skerspjūviai pavaizduoti S2.1 paveiksle. Šiame paveiksle naudojami žymėjimai: p – armavimo koeficientas, c – apsauginio betono sluoksnio storis, $A_{c,ef}$ ir p_{ef} – efektyvaus betono plotas bei armavimo koeficientas (apskaičiuoti pagal armuoto betono elementų projektavimo normų *Eurokodas 2* rekomendacijas), sijų pavadinimuose „*nm*“ – stiklo pluoštu armuoto polimero strypais armuoti elementai.

Palygintas daugiasluoksnio ir tradicinio strypų išdėstymo vienu sluoksniu skerspjūvyje efektyvumas, atsižvelgiant į supleišėjusio betono gebėjimą atlaikyti tempimo įtempius bei varžyti plyšių vystymąsi. Tyrimai parodė, kad armatūros strypų sluoksnių

skaičius lemia elementų lenkiamąjį standumą, kuris nusako sijų deformavimosi bei pleišėjimo pobūdį. Vertinant armatūros sluoksnių skaičiaus įtaką sijų įlinkiams (kreiviams) buvo atliekami teoriniai šio parametro skaičiavimai vadovaujantis *Eurokodo 2* nurodymais. Šios reikšmės buvo priimtos kaip atskaitinės (etaloninės) lyginant sijas, armuotas vienu ir trimis strypų sluoksniais. Pastebėta (S2.1 lentelė), kad apkrovos lygiui pasiekus eksploatacinės apkrovos reikšmę (M_{ser}), kurią sudaro 55 % nuo ribinės apkrovos, sijų, armuotų trimis strypų sluoksniais, kreivis teoriškai nustatomas su 14–32 % atsarga, lyginant su eksperimentų rezultatais. Tuo tarpu įprastai armuotų sijų kreivio teorinė reikšmė įvertinama nepakankamai – apskaičiuojamas 7–15 % mažesnis kreivis.

Siekiant objektyviai įvertinti sijų pleišėjimo parametrus, buvo pasiūlytas atstumo tarp plyšių nustatymo metodas pagal plyšių skaitmeninių nuotraukų duomenis. Šis metodas pagrįstas hierarchiniu klasterio taškų grupavimo principu, kai iš pleišėjimo schemos plyšių koordinačių imties identifikuojami atstumai tarp plyšių bei įvertinamas jų kitimas elemento apkrovimo metu. Pleišėjimo analizės metu gauti rezultatai (S2.2 lentelė) skiriasi nuo aptartų kreivių skirtumų: didžiausias atstumas tarp plyšių nepakankamai įvertinamas elementams, armuotiems trimis armatūros sluoksniais. Naudojant skaitmeninių vaizdų koreliacijos metodiką, šiems elementams užfiksuotas „pavėluotas“ pleišėjimas – plyšiai elemento paviršiuje pastebimi vėliau, nei pasiekta teorinė betono tempiamojo stiprio riba. Toks rezultatas galėtu būti siejamas su „lėtesniu“ vidinių plyšių formavimusi elementuose, kuriuose armatūros strypai išdėstyti trimis sluoksniais, tačiau šią hipotezę sunku įrodyti eksperimentiškai.

Atliekant plyšių išsidėstymo ir jų pločių stebėjimus kintant apkrovai nustatyta, kad didžiausią plotį turintis plyšys nebūtinai atsiveria tarp dviejų nesupleišėjusių betono blokų ar greta didžiausią atstumą tarp plyšių turinčios elemento dalies. Tik 11 iš 18 (61 %) eksperimentų metu gautų pleišėjimo schemų patvirtina šią projektavimo normų prielaidą.

Taip pat verta paminėti, kad „efektyvaus“ tempiamojo betono zonos aukščio nustatymas gali būti siejamas su sija *S1-6* (S2.1 pav.). Specifinis sijos armavimas lėmė, kad trečiasis (arčiausias skerspjūvio svorio centro) armavimo strypų sluoksnis nepatenka į minėtąją efektyviąją betono zoną. Atitinkamai, šis sluoksnis pagal normų reikalavimus neturi būti įtraukiamas į pleišėjimo parametrų vertinimą, tačiau tokie skaičiavimo rezultatai prieštarauja eksperimentiškai nustatytoms plyšio pločio ir atstumo tarp plyšių reikšmėms. Neatitikimas pašalintas, įvertinus visus armatūros sluoksnius, priešingai nei nurodyta *Eurokode 2*. Tai įrodo „išskirstyto“ strypų išdėstymo efektyvumą. Panašūs rezultatai (didesnis standumas bei atsparumas pleišėjimui) gauti nagrinėjant sijas su strypais, išdėstytais vienu sluoksniu, bet pagamintas iš dispersiškai armuoto betono.

Siekiant įvertinti „efektyviojo tempiamojo betono“ zonos neapibrėžtumą, kuris pasireiškia lenkiamuose elementuose, toliau šiame skyriuje nagrinėti tipiniai tempimo bandymai (naudojant vienu strypu armuotą betoninę prizmę S2.2 pav.). Tokie bandymai leidžia fiksuoti vidutines armatūros strypo ir betono paviršiaus deformacijas. Pleišėjimo ir deformacijų pasiskirstymo stebėjimui bandinių paviršiuje buvo naudojami didelės raiškos vaizdo fiksavimo įrenginiai bei jų sinchronizavimo įranga, kurios veikimas paremtas skaitmeninių vaizdų koreliacijos (angl. DIC – Digital Image Correlation) metodika.

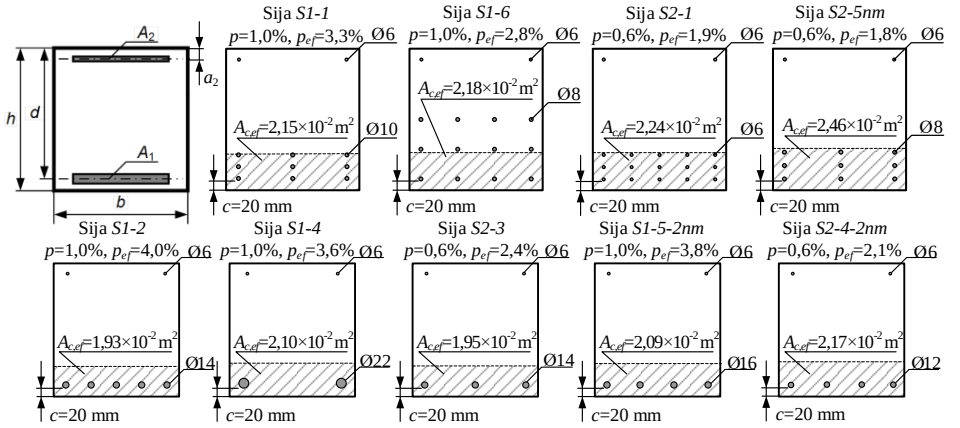

S2.1 pav. Eksperimentinių sijų skerspjūviai (užbrūkšniuotas plotas atitinka efektyvaus betono plotą, nustatytą pagal *Eurokodo 2* rekomendacijas)

S2.1 lentelė. Sijų eksperimentiškai ir teoriškai nustatytų kreivių skirtumai (Δκ*, %) skirtinguose apkrovos lygiuose

Grupė	Sija	M_u, kNm	Apkrovimo lygis				
			1 0,32–0,33·M_u	2 0,36–0,39·M_u	3 0,48–0,54·M_u	4 0,58–0,63·M_u	M_{ser} 0,55·M_u
I	*S1-1*	92,24	–36,3	–23,7	–14,2	–13,0	–13,6
	S1-6	59,95	–92,9	–71,9	–34,6	–30,2	–32,2
	S2-1	60,56	–62,3	–84,6	–35,3	–25,8	–29,7
	S2-5nm	52,74	–15,2	–85,9	–49,2	–4,7	–20,7
II	*S1-2*	122,89	3,0	8,6	10,4	11,1	10,8
	S1-4	103,52	3,7	4,6	6,4	6,9	6,7
	S1-5-2nm	101,48	18,6	16,7	12,3	12,2	12,2
	S2-3	75,71	–2,1	1,4	7,6	7,9	7,8
	S2-4-2nm	58,77	57,1	41,5	18,3	11,9	14,9

S2.2 lentelė. Sijų eksperimentiškai ir teoriškai nustatytų didžiausių atstumų tarp plyšių skirtumai kai $M=M_{ser}$

Grupė	Sija	Ø, mm	p_{ef}, %	h_{ef}, mm		$s_{r,max}$, mm		Δs, %
				2,5(*h*-*d*)	(*h*-*x*)/3	Eksperimentinė	Apskaičiuotoji	
I	*S1-1*	9×Ø10	3,3	–	76,3	137,5	124,6	9,4
	S1-6	12×Ø8	2,8	–	80,4	194,1	120,3	38,0
	S2-1	15×Ø6	1,9	–	80,5	168,3	128,2	23,9
	S2-5nm	9×Ø8	1,8	–	89,4	151,4	161,0	-6,3
II	*S1-2*	5×Ø14	4,0	68,0	–	141,7	137,7	2,8
	S1-4	2×Ø22	3,6	–	75.2	125,1	209,0	-67,1
	S1-5-2nm	4×Ø16	3,8	75,6	–	105,7	155,7	-47,3
	S2-3	3×Ø14	2,4	69,0	–	134,1	203,9	-52,0
	S2-4-2nm	4×Ø12	2,1	78,5	–	122,3	199,8	-63,4

Lyginant elementų su skirtingu apsauginiu betono sluoksniu pleišėjimą nustatyta, kad apsauginio betono sluoksnio storis yra vienas reikšmingiausių skerspjūvio parametrų. Siekiant parodyti apsauginio sluoksnio įtaką elemento deformacijoms, baigtinių elementų programa ATENA buvo atlikta skaitinė analizė, kurios metu nagrinėti 10 mm skersmens plieniniu strypu armuotos 60×60 mm ir 100×100 mm skerspjūvio betoninės prizmės (apsauginis betono sluoksnis buvo atitinkamai lygus 25 ir 45 mm). Sumodeliuotas betono deformacijų pasiskirstymas nagrinėtuose elementuose pateiktas S2.3 paveiksle. Galima pastebėti, kad deformacijos varijuoja ne tik išilgine elemento kryptimi. Pakankamai storas apsauginis betono sluoksnis gali varžyti pleišėjimo procesą, t. y. izoliuoti plyšių vystymąsi elemento viduje (neleidžiant plyšiams pasiekti elemento išorės). Didelis apsauginis betono sluoksnis sukuria „neefektyvią“ betono zoną, kuri negali būti vienodai vertinama nustatant vidutines betono deformacijas. Dažniausiai laikoma, kad armatūros ir betono vidutinės deformacijos yra vienodos. Šią prielaidą galima laikyti teisinga, analizuojant deformacijų pasiskirstymą 60×60 mm skerspjūvio prizmėje. Kita vertus, nagrinėjant 100×100 mm skerspjūvio elementą, akivaizdu, kad deformacijų pasiskirstymas betone yra netolygus ir minėta prielaida nėra teisinga. Tokių elementų (su dideliu apsauginiu betono sluoksniu) vidutinės betono paviršiaus deformacijos dažniausiai yra ženkliai mažesnės nei armatūros deformacijų reikšmės. Todėl nei vienas šių parametrų analizuojamas atskirai neatspindi tikrosios elemento elgsenos. Dėl šios priežasties pleišėjimo ir deformacijų analizės adekvatumas turi būti siejamas su nagrinėjamų elementų reprezentatyvumu. Nagrinėjamu atveju tempiamųjų elementų geometrija turi būti nustatyta įvertinant vidutinių deformacijų pasiskirstymą betone.

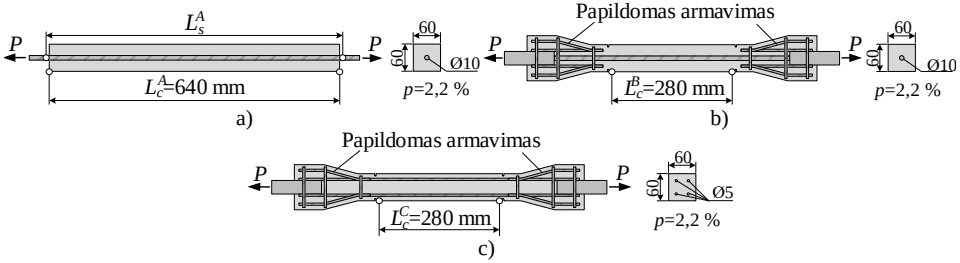

S2.2 pav. Tempiamieji betono elementai armuoti: a) vienu strypu; b) vienu ir c) keturiais strypais

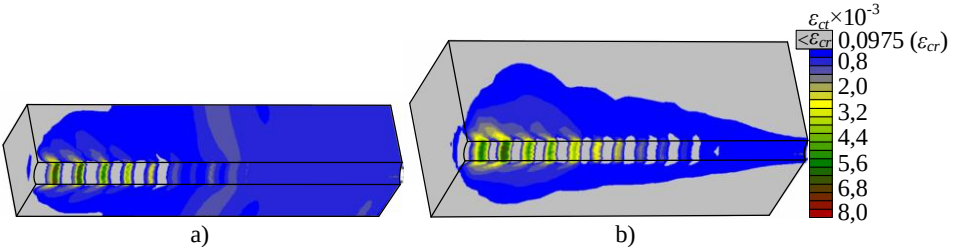

S2.3 pav. Baigtinių elementų programa ATENA nustatytas deformacijų pasiskirstymas tempiamuosiuose elementuose a) 60×60×280 mm ir b) 100×100×280 mm, kai vidutinės armatūros deformacijos lygios 0,77 ‰ (pilkai pažymėtas plotas – betonas iki pleišėjimo deformacijos)

Antrajame skyriuje pasiūlyta iteratyvi betono paviršiaus deformacijų matavimo bazės mažinimo metodika, skirta pakraščio efekto (angl. *end effect*) nustatymui tempiamosiuose elementuose. Ši metodika leidžia nustatyti reprezentatyvius tempiamųjų armuoto betono elementų geometrijos parametrus, kurie būtini siekiant adekvačiai vertinti elementų pleišėjimo elgseną. Taikant šią metodiką nustatyta, kad apsauginio betono sluoksnio storis tiesiogiai proporcingas eksperimentinių armuoto betono elementų rezultatų sklaidai.

Siekiant įvertinti armatūros strypų išdėstymo įtaką tempiamųjų betoninių elementų deformacijoms ir pleišėjimui, sukurta ir užpatentuota bandymo įranga (S2.4 pav.), leidžianti atlikti keletu strypų armuotų elementų tempimo bandymus. Unikali įranga suteikė galimybę sukomponuoti elementų skerspjūvius taip, kad varijuotų tik armatūros strypų skersmuo, išlaikant vienodą apsauginį betono sluoksnį bei armavimo koeficientą. Taikant šią įrangą (S2.5a pav.) buvo nagrinėjamos skirtingo ilgio bei skerspjūvio matmenų tempiamųjų betoninių prizmių su skirtingu armatūros strypų išdėstymu skerspjūvyje deformacijos ir pleišėjimas. Nagrinėti skerspjūviai pateikti S2.5b paveiksle. Bandymų metu matuotos elementų deformacijos armatūros strypuose bei betono paviršiuje, be to, naudojant skaitmeninių vaizdų koreliacijos metodiką buvo analizuojamas pleišėjimo procesas.

Bandiniai pagal armavimo koeficientą buvo suskirstyti į grupes. Kiekvieną grupę sudarė nuo 4 iki 12 elementų, armuotų naudojant skirtingą strypų kiekį – 4 (etaloniniui skerspjūviui) ir 16 arba 12 (alternatyviems skerspjūviams). Daugumos šių elementų betono apsauginis sluoksnis buvo vienodas, c = 30 mm. Remiantis S2.6 paveiksle pateiktais apkrovos ir vidutinių armatūros deformacijų duomenimis pastebėta, kad tos pačios grupės elementų, armuotų 16 (12) strypų, vidutinės armatūros deformacijos yra praktiškai identiškos. Tuo tarpu 4 strypais armuotų elementų deformacijos reikšmingai skiriasi tarpusavyje. Šis reiškinys yra akivaizdus ankstyvoje pleišėjimo stadijoje santykiniai mažai armuotiems elementams (p = 1,4 %).

Nagrinėjant atstumus tarp plyšių, pagal galiojančių projektavimo normų metodus apskaičiuotos reikšmės buvo palygintos su bandymų metu stabilizuoto pleišėjimo stadijoje užfiksuotais rezultatais. Pastebėta, kad pagal *Eurokodą* apskaičiuotas maksimalus atstumas tarp plyšių yra vidutiniškai 120 % didesnis nei eksperimentiškai nustatytas, tuo tarpu *Model Code* normatyvinio reglamento rezultatai eksperimentines reikšmes vidutiniškai viršija tik apie 60 %. Bandymai parodė, kad vidutinių ir maksimalių atstumų tarp plyšių dydis nepriklauso nuo armavimo parametrų (armatūros ploto bei strypų išdėstymo), nors norminiuose projektavimo dokumentuose yra aiškiai išreikšta maksimalių atstumų tarp plyšių priklausomybė nuo strypų skersmens ir armavimo koeficiento santykio (S2.7 pav.).

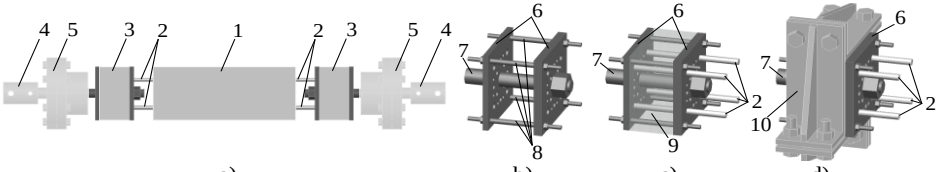

S2.4 pav. Sukurta bandymo įrangą: a) armuoto betono bandinys, b ir c) strypų tvirtinimo mazgai ir d) mazgas su papildoma apspaudimo įranga, kur 1 – nagrinėjamas elementas, 2 – armatūros strypai, 3 – strypų inkaravimo mazgai, 4 – standartinės tempimo mašinos jungtys, 5 – sferiniai lankstai, 6 – inkaravimo mazgo tvirtinimo plokštelės, 7 – mazgo centrinis strypas, 8 – inkaravimo mazgo tvirtinimo plokštelių jungiamieji strypai, 9 – betonas, 10 – papildoma apspaudimo įranga

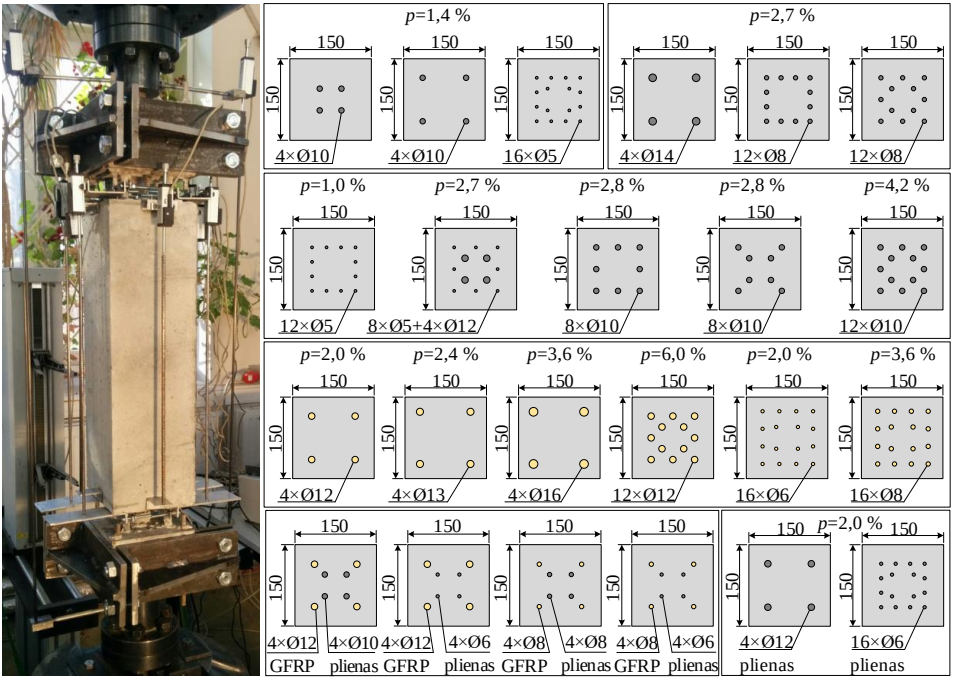

a) b)

S2.5 pav. Tempiamųjų keliais strypais armuotų betoninių elementų a) bandymas ir b) skerspjūviai

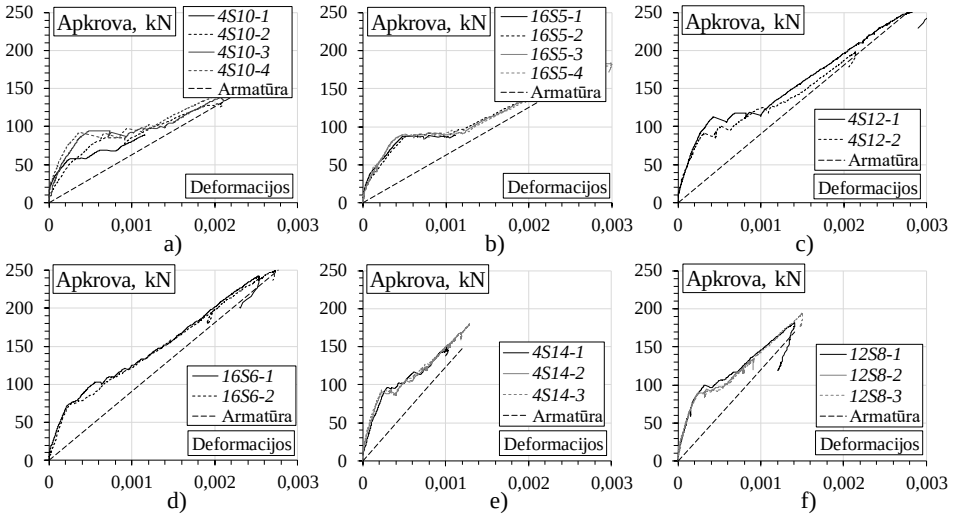

S2.6 pav. Tempiamųjų elementų apkrovos ir deformacijų grafikai: a) ir b) elementams armuotiems 1,4 %, c) ir d) – 2,0 %, e) ir f) – 2,7 %

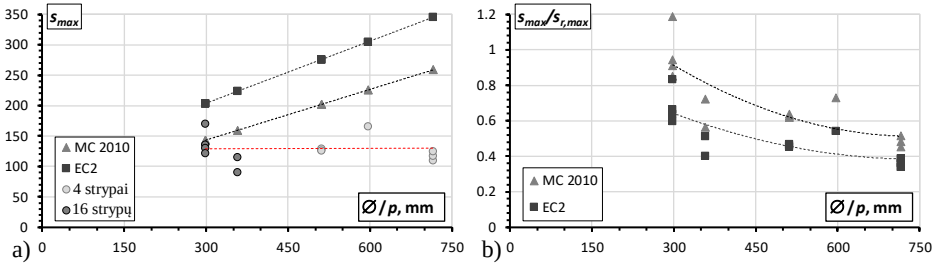

S2.7 pav. Atstumų tarp plyšių nuo Ø/*p* priklausomybė: a) maksimalios ir b) vidutinės reikšmės

3. Eksploatacinės savybės: Armuoto betono elgseną lemiančios charakteristikos

Trečiajame disertacijos skyriuje aptariamos lenkiamųjų bei tempiamųjų armuoto betono elementų eksploatacines savybes įtakojančios charakteristikos. Taip pat pateikiami betoninių elementų, armuotų keletu strypų, skaitinio modeliavimo rezultatai. Siekiant ištirti skirtingos armatūros medžiagos įtaką armuoto betono elementų tinkamumui, analizuojami tempiamieji betoniniai elementai su GFRP ar hibridiniu (plieniniais ir GFRP strypais) armavimu. Pateikiama eksperimentinių ir skaitinių specifinių betoninių elementų armuotų plieniniais ir GFRP strypais rezultatų analizė.

Antrajame disertacijos skyriuje atlikus eksperimentinius specifinių armuoto betono elementų bandymus nustatyta, kad to pačio armatūros ploto išdėstymas naudojant daugiau mažesnio skersmens strypų gali efektyviai varžyti plyšių vystymąsi ankstyvoje armuoto betono elemento pleišėjimo stadijoje. Šis konstrukcinis sprendimas taip pat leidžia sumažinti eksperimentinių rezultatų sklaidą, kuri siejama su projektavimo patikimumu. Pastarąją išvadą siekta patvirtinti skaitiniu armuoto betono sijos pavyzdžiu. Taikant literatūros apžvalgoje pateiktą sluoksnių modelį apskaičiuotos dviejų I-formos sijų, armuotų keturiais ir 16 strypų (S3.1 pav.), lenkimo momentų ir deformacijų reikšmės. S3.2 paveiksle matyti, kad veikiant eksploatacinei apkrovai rezultatų sklaida elemente, armuotame 16 strypų, yra ženkliai mažesnė (7,7 %) nei keturiais strypais armuotoje sijoje (67 %).

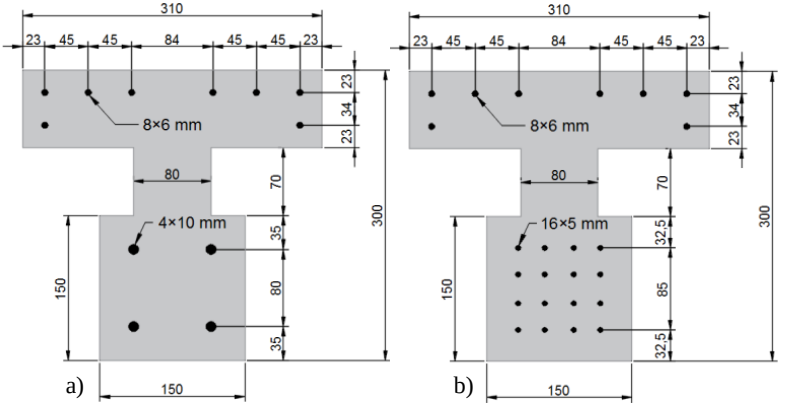

S3.1 pav. Skaitiškai sumodeliuota I-formos sija: a) su keturiais ir b) su 16 strypų

Skyriuje aptariami modeliavimo rezultatai (S3.3 pav.) rodo, kad armuoto betono elementuose tempiamojo betono deformacijos kinta ne tik išilgine elemento kryptimi, bet ir pačiame apsauginiame betono sluoksnyje. Rezultatai patvirtina, kad efektyviojo tempiamojo betono koncepcijos, taikomos projektavimo dokumentuose, adekvatumas yra ribotas. Taikant šią koncepciją turi būti atsižvelgiama į elementų apkrovimo sąlygas, įtempių ir deformacijų būvį bei nearmuoto betono konfigūraciją.

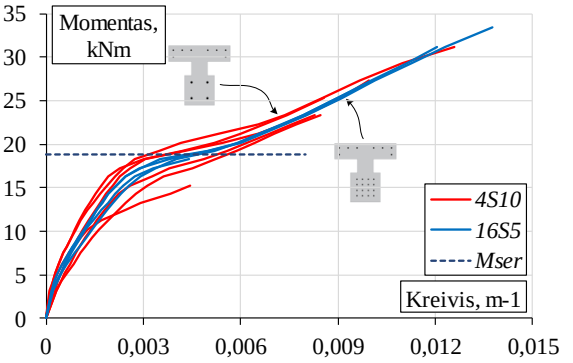

S3.1 pav. Skaitiškai sumodeliuotų sijų prognozuojamų momentų ir kreivių priklausomybės

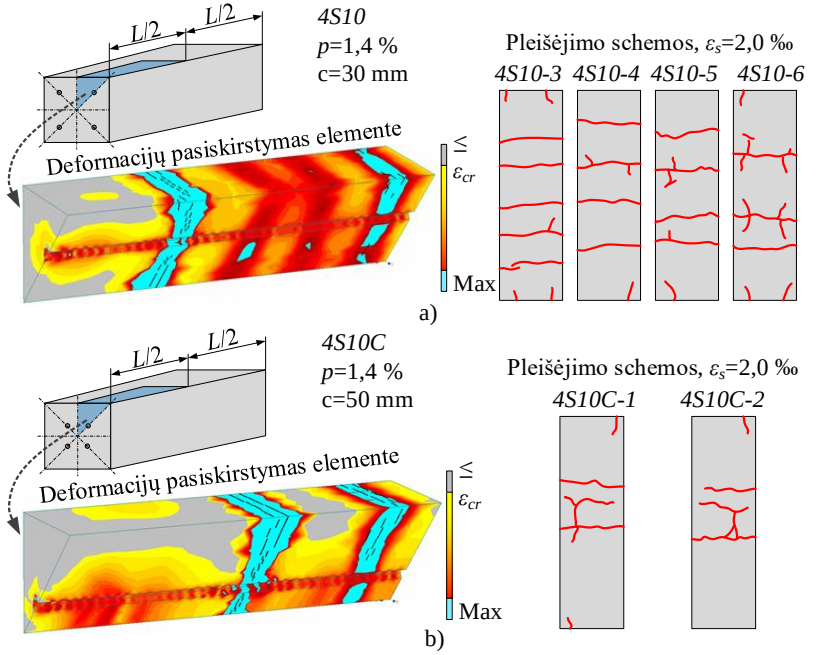

S3.3 pav. Deformacijų pasiskirstymas armuoto betono elementuose (vidutinė armatūros deformacija 2,0‰) nustatytas baigtinių elementų programa ATENA ir eksperimentinės pleišėjimo schemos: a) *4S10* prizmės su apsauginiu sluoksniu *c* = 30 mm ir b) *4S10C* prizmės su *c* = 50 mm

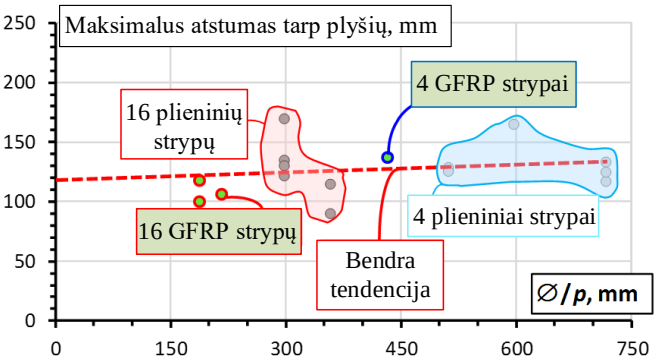

S3.4 pav. Maksimalaus atstumo tarp plyšių ir Ø/*p* santykio pasiskirstymas betoniniams elementams armuotiems plieno ir stiklo pluošto strypais

Taip pat šiame skyriuje atkreipiamas dėmesys į armatūros medžiagos įtaką armuoto betono elementų pleišėjimui. Eksperimentiniai tempiamųjų betoninių elementų, armuotų keletu plieninių bei GFRP strypų (kurių ašinis standumas panašus) rezultatai parodė, kad stabilizuoto pleišėjimo stadijoje abiem atvejais gauti tarpusavyje panašūs maksimalūs atstumai tarp plyšių (S3.4 pav.). Šie rezultatai leidžia teigti, kad atstumas tarp plyšių daugiausia priklauso nuo armuoto betono elemento geometrijos ir betono apsauginio sluoksnio storio.

Bendrosios išvados

1. Apibendrinus literatūros analizės rezultatus, galima teigti, kad:
   1.1. Heterogeninė betono struktūra, vidiniai bei išoriniai plyšiai bei betono ir armatūros sukibimas lemia didelę armuoto betono elementų eksperimentinių rezultatų (deformacijų ir pleišėjimo) sklaidą. Tinkamas armuoto betono elementų bandymo būdo parinkimas leidžia adekvačiai interpretuoti eksperimentinius bandymų rezultatus.
   1.2. Tempiamųjų ir lenkiamųjų armuoto betono elementų bendro armatūros strypų bei aplink juos esančio betono darbo vertinimui naudojama „efektyviojo tempiamojo betono“ koncepcija.
   1.3. Vienas svarbiausių veiksnių lemiančių „efektyviojo tempiamojo betono“ zonos dydį yra armatūros ir betono sukibimas bei betono deformacijos, kurias įtakoja armatūros strypų skaičius tempiamojoje betoninio elemento dalyje. Dėl šios priežasties strypinės armatūros išdėstymo įtakos bendram elemento standumui bei pleišėjimui tyrimas yra itin svarbus.
   1.4. Skaitinis armuoto betono modeliavimas yra vienas tinkamiausių būdų atlikti armuoto betono deformacijų bei pleišėjimo analizę nagrinėjant sudėtingus betono elgsenos aspektus, kurių eksperimentiniai tyrimai yra itin komplikuoti..
2. Eksperimentiškai nagrinėti trumpalaike apkrova veikiamų sijų, kuriuose armatūros strypai (plieno arba GFRP) išdėstyti vienu arba trim sluoksniais, pleišėjimas bei deformacijos. Apibendrinant tyrimų rezultatus galima teigti, kad:

2.1. Nepriklausomai nuo strypinės armatūros medžiagos (plieno arba GFRP), sijų lenkiamasis standumas koreliuoja su armatūros strypų sluoksnių skaičiumi. Nustatyta, kad apkrovos lygiui pasiekus eksploatacinės apkrovos reikšmę (55 % nuo laikomosios sijos galios) sijų, armuotų trimis strypų sluoksniais, kreivis (remiantis Model Code pateiktomis išraiškomis) nustatomas su 14–32 % atsarga, lyginant su eksperimentų rezultatais. Tuo tarpu įprastai armuotų sijų kreivis įvertinamas nepakankamai – apskaičiuojama 7–15 % mažesnė reikšmė.

2.2. Sijų, armuotų naudojant tris strypų sluoksnius, atstumų tarp plyšių skaičiavimai remiantis Model Code pateiktomis išraiškomis yra pakankamai tikslūs, tačiau įprastai armuotoms sijoms eksperimentinės atstumų tarp plyšių reikšmės yra 50% didesnės už apskaičiuotąsias.

2.3. Eksperimentiniai pleišėjimo rezultatai neparodo atstumų tarp plyšių bei plyšio pločio koreliacijos, keičiant armatūros strypų išdėstymą sijos skerspjūvyje. Stabilizavusis pleišėjimo procesui sijose, su trimis strypų sluoksniais, eksperimentiškai nustatytas atstumas tarp plyšių buvo didesnis, o maksimalus plyšio plotis mažesnis, lyginant su įprastai armuotomis sijomis.

2.4. Maksimalaus pločio plyšys susiformuoja ne būtinai greta maksimalaus ilgio nesupleišėjusio betono bloko. Tik 11 iš 18 (61 %) eksperimentinių tyrimų metu gautų pleišėjimo schemų patvirtina prielaidą, kad didžiausias plyšio plotis yra tiesiogiai susijęs su didžiausiu atstumu tarp plyšių ir yra vienas greta kito.

3. Tiriant tempiamojo betono efektyvumą bei siekiant išvegti efektų, siejamų su deformacijų pokyčiais sijų skerspjūvyje, buvo atliekami tipinių elementų (betoninių prizmių armuotų vienu metaliniu strypu) tempimo bandymai. Apibendrinus eksperimentinių tyrimų rezultatus, kurių metu išbandyta daugiau nei 50 įvairios geometrijos ir apkrovimo sąlygų elementų, galima teigti, kad:

3.1. Armuoto betono elementų pleišėjimo analizės metu atliekant tipinius 100×100 mm skersmens elementų tempimo bandymus įmanoma įvertinti tik armatūros skersmens įtaką elemento pleišėjimui. Siekiant išvengti skerspjūvio parametrų tarpusavio koreliacijos būtinas alternatyvus bandymo būdas.

3.2. Skirtingi eksperimentiniai pleišėjimo rezultatai (atstumai tarp plyšių), gauti atlikus teoriškai identiškų (vienodo armavimo koeficiento bei skerspjūvio geometrijos) tempiamųjų elementų bandymus, gali būti siejami su apsauginio betono sluoksnio storio skirtumu bei skirtingu armatūros ir betono sukibimo plotu (bendru strypų perimetru).

3.3. Reprezentatyvaus bandinio (geometrinių parametrų) koncepcijos taikymas tempiamiesiems armuoto betono elementams leidžia susieti pleišėjimo parametrus su elemento deformacijomis.

4. Sukurta specifinė tempiamųjų armuoto betono elementų armuotų keletu strypų bandymo įranga. Apibendrinus specifinių tempiamųjų betoninių elementų eksperimentinius tyrimus, kuriuo sudarė 64 armuoto betono prizmės, galima teigti, kad:

4.1. Maksimalus ir vidutinis atstumas tarp plyšių nepriklauso nuo armuoto betono elemento armavimo parametrų. Tuo tarpu projektavimo normose pateiktos išraiškos maksimalų atstumą tarp plyšių tiesiogiai sieja su skersmens ir armavimo koeficiento (Ø/p) santykiu.

4.2. To pačio armatūros ploto išdėstymas didesniame (mažesnio skersmens) strypų skaičiuje gali efektyviai varžyti plyšių vystymąsi ankstyvoje armuoto betono elemento pleišėjimo stadijoje. Šis efektas būdingas sąlyginai mažai armuotiems elementams (1,4–2,0 %). Taip pat toks armavimo paskirstymas elemente ženkliai mažina pleišėjimo parametrų (atstumo tarp plyšių) išsibarstymą, t. y. didina tokių elementų projektavimo patikimumą.

4.3. Teoriškai identiškų (turinčių vienodą armavimo koeficientą bei armatūros strypų skersmenį) tempiamųjų armuoto betono elementų betono deformacijos ženkliai skiriasi. Betonas elementuose su 50 mm apsauginiu sluoksniu nėra efektyvus. Didesnis betono apsauginis sluoksnis (50 mm) lemia 24 % mažesnes vidutines betono deformacijas veikiant eksploatacinei apkrovai (lyginant su elementais su 30 mm apsauginiu sluoksniu).

5. Pateikti įvairius tinkamumo aspektus iliustruojantys pavyzdžiai. Nagrinėti aspektai nusako galimus konstrukcijų patikimumo užtikrinimo būdus. Apibendrinus pateiktus pavyzdžius, galima pastebėti, kad:

5.1. Tinkamai sukalibruotas (naudojant pakitimus eksperimentinius duomenis) skaitinis armuoto betono modeliavimo būdas paremtas betono irimo mechanikos principais bei armatūros ir betono besikartojančio kintamo standumo sukibimo modeliu, leidžia adekvačiai įvertinti elementų su skirtingu armatūros skersmeniu, betono apsauginiu sluoksniu bei armavimo koeficientu deformacijų ir pleišėjimo elgseną.

5.2. Eksperimentiniai tempiamųjų betoninių elementų, armuotų keletu plieninių arba GFRP strypų (panašaus suminio ašinio standumo), rezultatai parodė, kad stabilizuoto pleišėjimo stadijoje gauti identiški maksimalūs atstumai tarp plyšių. Šie rezultatai leidžia teigti, kad nepriklausomai nuo strypų medžiagos atstumas tarp plyšių priklauso nuo armuoto betono elemento geometrijos, armatūros ašinio standumo bei betono apsauginio sluoksnio storio.

Annexes[1]

Annex A. Declaration of academic integrity

Annex B. The coauthors' agreements to present publications material in the dissertation defence

Annex C. Copies of scientific publications by the author on the topic of the dissertation

[1]The annexes are supplied in the enclosed compact disc

Arvydas RIMKUS

EFFECTS OF BAR REINFORCEMENT ARRANGEMENT ON DEFORMATIONS AND CRACKING OF CONCRETE ELEMENTS

Doctoral Dissertation

Technological Sciences,
Civil Engineering (02T)

Arvydas RIMKUS

STRYPINĖS ARMATŪROS IŠDĖSTYMO ĮTAKA BETONINIŲ ELEMENTŲ DEFORMACIJOMS IR PLEIŠĖJIMUI

Daktaro disertacija

Technologijos mokslai,
Statybos inžinerija (02T)

2017 11 17. 13 sp. l. Tiražas 20 egz.
Vilniaus Gedimino technikos universiteto
leidykla „Technika“,
Saulėtekio al. 11, 10223 Vilnius,
http://leidykla.vgtu.lt
Spausdino UAB „BMK leidykla“,
J. Jasinskio g. 16, 01112 Vilnius